PEPOLE'S DEMOCTRATIC REPUBLIC OF ALGERIA
وزارة التعـليـــم العـــالـــي و البـحث الـعلـــمـي
MINISTRY OF HIGHER EDUCATION AND SCIENTIFIC RESEARCH
جـامعـــة عـمـــار ثـلـيـجـي بالأغواط
UNIVERSITY AMAR THELIDJI OF LAGHOUAT
كلـيـــــة العـلـــــوم
FACULTY OF SCIENCES
قسم البيولوجيا
DEPARTEMENT OF BIOLOGY

In view of obtaining the Master's degree

Field: Natural and Life Sciences
Major: Biological Sciences
Option: Applied Biochemistry

Theme

In Silico study of anticancer activity of some marine alkaloids from marine sources on human osteosarcoma

By:

Tamimount Khouloud

Khelifa Anis

Grinat Mouna

Committee Members :

Dr. Samira NIA	**President**
Dr. Leila BOU-SALAH	**Examinator**
Prf. Khedidja BENAROUS	**Supervisor**
Dr. Abderahmane LINANI	**Co-Supervisor**

Academic year 2022- 2023

Acknowledgments

First and foremost, we extend our heartfelt appreciation to our thesis supervisor, **Professor Khedidja Benarous**, and our helpful co-supervisor, **Dr. Abderahman Linani**. I am immensely thankful for their guidance, encouragement, and unwavering support throughout the entire process of this work. They challenged us with their expertise and provided invaluable insights that shaped our understanding. They taught us everything we needed to know to successfully accomplish this endeavor.

I am especially grateful for their confidence in our abilities. Their belief in us has been a driving force behind this work. Without their support, this rapport would not have been possible. Words cannot adequately convey the depth of my gratitude.

we would like to express my gratitude to the members of the jury for accepting to evaluate this work.

Dedication by Khouloud

To my amazing ***mother****: who has worked towards my success through her love, prayers, and support, despite her absence in my life today (R.I.P).*

To my ***father****: who can be proud and find here the result of many years of his sacrifices.*

To my sister ***Faiza****: you are my greatest wish in this life.*

To my dear brothers ***Abdelhake and Abdelmalek****: thank you for your constant encouragement, and moral support.*

To my friends and sisters with whom I have shared beautiful moments: ***Mouna, Rania, Chourouk****, it has been an honor to live this period of my life with you. Together, we have always been the happiest girls.*

Also, to my countless friend ***Khelifa Anis****.*

I want to thank my supervisor and co-supervisor, ***Khadidja Benarose*** *and* ***Linani Abderahman*** *for their extreme care to obtain the best version of this project and their valuable advice*

Dedication by Anis

Firstly, I thank my self for the hard work that I did in this journey that started long ago.

At the same time, I want to thank my amazing parents and sibling and my whole big family from my grandmother to my cousins, who are like my siblings from a different mother, for their continued support.

Also, to my countless friends and my colleagues in this project **Tamimount Khouloud** *and* **Grinat Mouna**.

I want to thank my supervisor and co-supervisor, **Khadidja Benarose** *and* **Linani Abderahman** *for their extreme care to obtain the best version of this project and their valuable advice.*

Dedication by Mouna

To my beautiful mother for all the sacrifices and for all the beautiful moments of my life

To my dad for the support, love and all your beautiful adventures

To my grandmother for the feelings of curiosity, of magic and wonder that you brought to my childhood and that persist till today

To my brother, for all the nonsense and all the games of life that we have shared

To my little sister **Khadidja** *for every laugh, every hope, every hug i'm here because of you*

*To the little sweetest hope in my life -***Ziad**

to my other half and sweetheart **Khouloud** *thank you for being in my life*

To my bestie **Safa** *for the wonderful thoughts, laughs and everything we shared and we will share together.*

To my cousin **Khadidja** *for all our memories, our dreams and all the laughs and good times*

Abstract

Osteosarcoma, a prevalent form of bone cancer predominantly affecting children and adolescents, has been the subject of extensive research efforts. Recent advances in molecular genetic research have revolutionized our understanding of the disease's origins, leading to the discovery of targeted therapeutic approaches. In this study, our objective is to conduct an *in-silico* investigation on the anti-tumoral properties of seven marine alkaloids against the human osteosarcoma cell line SaOS2, targeting newly identified oncogenic proteins, including four enzymes and one receptor that have participated in major pathways of the tumor cells. The seven marine alkaloids examined in this study are as follows: Coscinamide A (Mol1), Leucettamine B (Mol2), Polyandrocarpamine A (Mol3), Coscinamide B (Mol4), Coscinamide C (Mol5), Dispacamide (Mol6), and Eudistomin Y1 (Mol7). To achieve this goal, we employed several computational methods. Firstly, we performed molecular docking (MD) using Autodock Vina to evaluate the binding affinity of the ligand-protein complexes. Additionally, we obtained the pharmacokinetic properties and toxicity profiles of these alkaloids using ADMET's online servers. We conducted a biological cytotoxicity prediction using the CLC-Pred online server, which confirmed that the antitumoral effect is not limited to osteosarcoma alone but is also applicable to various other types of cancer. We also utilized the STRING database to predict protein-protein interactions and investigate potential pathways and activities. The results of our study indicate that mol5 exhibited the highest affinity for the ER target, while mol7 demonstrated the highest affinity for the PIM-1 and HSP90 targets. For the T311M HDAC8 and BMP-2 targets, Mol4 and Mol1 respectively are the highest score. Detailed information of the best interactions is presented in the results section. Importantly, despite the general toxicity of alkaloids, our investigation revealed that the seven compounds demonstrated a favorable safety profile and exhibited non-toxic characteristics, suggesting their viability for use. These promising results need further validation through *in vitro* and *in vivo* studies to confirm the effectiveness of these marine alkaloids in treating osteosarcoma.

Keywords: osteosarcoma, SaOS2, marine alkaloids, molecular docking, ADMET, CLC-Pred, STRING.

Resumé

L'ostéosarcome, une forme prédominante de cancer des os touchant principalement les enfants et les adolescents, a fait l'objet de nombreux efforts de recherche. Les avancées récentes de la recherche en génétique moléculaire ont révolutionné notre compréhension des origines de la maladie, conduisant à la découverte d'approches thérapeutiques ciblées. Dans cette étude, notre objectif est de mener une investigation *in silico* sur les propriétés anti-tumorales de sept alcaloïdes marins contre la lignée cellulaire de l'ostéosarcome humain SaOS2, en ciblant des protéines oncogènes nouvellement identifiées, comprenant quatre enzymes et un récepteur qui ont participé à des voies majeures des cellules tumorales. Les sept alcaloïdes marins examinés dans cette étude sont les suivants : Coscinamide A (Mol1), Leucettamine B (Mol2), Polyandrocarpamine A (Mol3), Coscinamide B (Mol4), Coscinamide C (Mol5), Dispacamide (Mol6) et Eudistomin Y1 (Mol7). Pour atteindre cet objectif, nous avons utilisé plusieurs méthodes informatiques. Tout d'abord, nous avons effectué un amarage moléculaire (AM) en utilisant Autodock Vina pour évaluer l'affinité de liaison des complexes ligand-protéine. De plus, nous avons obtenu les propriétés pharmacocinétiques et les profils de toxicité de ces alcaloïdes en utilisant les serveurs en ligne d'ADMET. Nous avons effectué une prédiction de la cytotoxicité biologique en utilisant le serveur en ligne CLC-Pred, ce qui a confirmé que l'effet antitumoral n'est pas limité à l'ostéosarcome seul, mais est également applicable à différents types de cancer. Nous avons également utilisé la base de données STRING pour prédire les interactions protéine-protéine et étudier les voies et les activités potentielles. Les résultats de notre étude indiquent que Mol5 présente la plus grande affinité pour la cible ER, tandis que Mol7 démontre la plus grande affinité pour les cibles PIM-1 et HSP90. Pour les cibles HDAC8 et BMP-2, Mol4 et Mol1 respectivement sont les score les plus élevé. Des informations détaillées sur les meilleures interactions sont présentées dans la section des résultats. Il est important de noter que malgré la toxicité générale des alcaloïdes, notre étude a révélé que les sept composés présentaient un profil de sécurité favorable et des caractéristiques non toxiques, suggérant leur viabilité d'utilisation. Ces résultats prometteurs nécessitent une validation supplémentaire par des études in vivo et in vitro pour confirmer l'efficacité de ces alcaloïdes marins dans le traitement de l'ostéosarcome.

Mots clés : ostéosarcome, SaOS2, alcaloïdes marins, docking moléculaire, ADMET, CLC-Pred, STRING.

الملخص

تعتبر الساركوما الشكل السائد من سرطان العظام الذي يؤثر في الغالب على الأطفال والمراهقين ، احد اهم مواضيع البحوث. احدثت التطورات الحديثة في البحوث الجينية الجزيئية ثورة في فهمنا لأصول المرض ، مما أدى إلى اكتشاف الطرق العلاجية الحديثة. في هذه الدراسة ، هدفنا هو إجراء تحقيق باستعمال الوسائل المعلوماتية على الساركوما العظمية خاصة السلالة العظمية المختلطة البشرية سااوس2 ودلك باستعمال سبعة قلويدات بحرية، ودلك باستهداف البروتينات البارزة التي تم تحديدها حديثًا ، هاته المركبات تصنف الى اربعة انزيمات ومستقبل واحد. القلويات البحرية السبعة التي تم تجميعها في هذه الدراسة هي كما يلي: كوسينااميد أ جزيئة1 ، لوسيتامين ب جزيئة2، بولياندروكاربامين أ جزيئة3 ، كوسينااميد ب جزيئة4 ، كوسينااميد س جزيئة5 ، ديسباكاميد جزيئة6، و اخيرا اوديستومين ذ1. لتحقيق هدف الدراسة ، استخدمنا العديد من الوسائل والاساليب. أولاً ، تم إجراء الالتحام الجزيئي (ا ج) باستخدام برنامج اوتودوك فينا التلقائي لتقييم التقارب بين البروتينات المحددة مع القلويدات السبعة. بالإضافة إلى ذلك ، حصلنا على الخصائص الدوائية والسمية لهذه المركبات باستخدام خوادم ا ت ت ا س عبر مواقع في الانترنت. كدلك اجرينا تنبؤًا بالسمية لهاته المركبات على الخلايا باستخدام خادم سلس بريد اونلاين، والذي أكد أن التأثير المضاد للأورام لا يقتصر على ساركوما عظمية وحدها ولكنه ينطبق أيضًا على أنواع أخرى من السرطان. استخدمنا أيضًا قاعدة بيانات سترينج السلسلة للتنبؤ بتفاعلات بين البروتين و البروتين والتحقيق في المسارات والأنشطة المحتملة. تشير نتائج دراستنا إلى أن الجزيء5 اظهر اعلى نتائج ارتباط لمستقبل استروجين ، في حين أظهر جزيء7 أعلى نتائج ارتباط لأهداف انزيم كيناز سيرين/تريونين بيم1 و بروتين الصدمة الحرارية90. اما لانزيم هيستون ديسيتيلاز و انزيم التشكل العظمي2، أظهر الجزيء1 و 4 أعلى درجة ارتباط طاقوي. يتم تقديم معلومات مفصلة بشأن أفضل التفاعلات التي لوحظت خلال الالتحام الجزيئي في قسم النتائج. الأهم من ذلك ، على الرغم من السمية العامة للقلويدات ، كشف تحقيقنا أن المركبات السبعة اظهرت خصائص غير سامة مما يؤدي الى اعتبارها امنة الاستعمال. هذه النتائج الواعدة تحتاج إلى مزيد من التحقق من الصحة من خلال المختبرات وكدلك على جسم الانسان لتاكيد فعالية هذه القلويدات البحرية في علاج ساركوما العظمية.

كلمات مفتاحية : اوستيوساركوما، قلويدات بحرية، الارتباط الجزيئي، سترينج، ا ت ت ا س، سلس بريد اونلاين

List of abbreviations

A		**K**	
ADM	Adriamycin	KI	Inhibitory constant
ADME/Tox	Absorption, Distribution, Metabolism, Excretion, Toxicity	**L**	
ADT	AutoDock Tools	LDH	Lactate Dehydrogenase
ALP	Alkaline Phosphatase	Log P	Lipophilicity
B		LogS	Solubility
BBB	Blood-Brain Barrier	**M**	
BCD	Bleomycin, Cyclophosphamide, Dactinomycin	Md	Molecular Docking
BMP2K	Bone morphogenetic protein 2	MRI	Magnetic Resonance Imaging
C		MSCs	Mesenchymal Stem Cells
CDDP	Cisplatin	MW	Molecular weight
CID	Compound ID	**N**	
CL	total CLearance	NCBI	National Center for Biotechnology Information
CLC-Pred	Cell Line Cytotoxicity Predictor	NPP 20/23	Number of published papers between 2020 /2023
CNS	Central Nervous System	**O**	
CT	Computed Tomography	OS	Osteosarcoma
CYP450	Cytochrome P450 enzymes	**P**	
D		PDB	Protein Data Bank
DOX	Doxorubicin	PDF	Portable Document Format
DSV	Discovery Studio visualizer	PET	Positron Emission Tomography
E		Pim1	Proto-oncogene
EC	Enzyme Class	PK	Pharmacokinetic properties
EPI	Epirubicin	PNG	Portable Network Graphic
ER	Estrogen Reseptor	PPIs	Protein-protein interactions
H		**R**	
HD-MTX	High-dose Methotrexate	RR%	Repetition Rate
hERG	Human Ether-a-go-go Related Gene channel	**S**	
HIA%	Human Intestinal Absorption	SaOS-2	Sarcoma osteogenic 2
HIs	Hydrophobic Interactions	STRING	Search Tool for Recurring Instances of Neighboring Genes
Hsp90	Heat Shock Protein 90	SVG	Scalable Vector Graphics
I		**T**	
IC50	Inhibitory Concentration 50	T1/2	half-life Time
IFO	Ifosfamide	TPSA	Topological Polar Surface Area.
IUPAC	International Union of Pure and Applied Chemestrey		

List of figures

List of tables

List of Appendixes

Table of contents

INTRODUCTION

Osteosarcoma has garnered significant attention within the field of oncology as one of the extensively investigated diseases [1.2.3]. It is a rare but highly aggressive form of bone cancer, predominantly affecting children and adolescents, but can occur in individuals of any age [4.5.6]. Serving as the most prevalent primary malignant bone tumor, osteosarcoma comprises approximately **20%** of all bone tumors [7.8]. It is characterized by the development of abnormal bone tissue within the affected bone, resulting in structural alterations and the potential for metastasis to other organs [2.3.7].

Typically, this disease manifests within the growth plate region of long bones in the body [9], such as the femur, tibia, or humerus, although it can manifest in other bones as well [10.11]. Osteosarcoma is thought to arise from primitive mesenchymal cells responsible for bone formation, with a distinctive hallmark of osteoid production [12.13]. The majority of cases display mutations resulting in the inactivation of TP53 and RB genes within their genomes [14]. While the precise etiology remains poorly understood, specific risk factors have been identified, including prior radiation therapy, genetic predisposition, and certain hereditary disorders [15.16].

Furthermore, our investigation encompassed an exploration of diverse diagnostic methodologies employed for osteosarcoma. This encompassed the utilization of imaging modalities, including X-rays, computed tomography (**CT**), and magnetic resonance imaging (**MRI**), for the purpose of tumor detection and staging [17.18].

The primary therapeutic strategies for human OS patients involve a combination of surgery, chemotherapy [19], and the prognosis of patients greatly depends on the disease's extent at the time of diagnosis and the stage of its development [20.21.22.23]. However, there remains an imperative for the development of novel and more efficacious treatment modalities, particularly in cases where osteosarcoma demonstrates resistance to existing therapies or has metastasized to other locations [24].

The development of novel pharmacological agents that exhibit heightened efficacy, improved safety profiles, and reduced side effects stands as a primary objective. In the pursuit of such a therapeutic solution, we have directed our attention towards exploring marine alkaloids obtained from marine sponges and Ascidiacea [25.26]. These marine sources represent a

largely unexplored reservoir of bioactive compounds that have yet to be comprehensively investigated and that display promising potential for their ability to inhibit human OS [25,26].

Drug discovery and development grew into a wide interdisciplinary field during the last decades. For that reason, we intend to test the *in silico* inhibition effect of seven marine alkaloids against the human oseosarcoma cell line Saos2, targeting new key oncogenic proteins that lead to tumor suppression. This will be accomplished by employing molecular docking techniques using AutoDock Vina and Discovery packages to evaluate their binding potential. Moreover, an ADMET study was conducted to investigate the pharmacokinetic properties (**PK**) of these marine alkaloids. Subsequently, the obtained results will be validated through the performance of a Protein-protein interaction (**PPI**) study, aimed at confirming the relation between all the studied human osteosarcoma targets.

The manuscript comprises four sections:

- The initial section is dedicated to a comprehensive bibliographic review, providing a concise summary of vital information regarding the disease, including its symptoms, diagnosis, and current treatment approaches, as well as highlighting the proteins under study and describing the marine source of alkaloids.
- The second part details the materials and methods employed in this *in silico* study, encompassing a thorough delineation of the various methodologies utilized.
- The third segment encompasses the presentation of all the results and discussions derived.
- Finally, we conclude with a comprehensive conclusion and perspectives.

BIBLIOGRAPHIC REVIEW

1. Osteosarcoma:

Osteosarcoma, also referred to as osteogenic sarcoma, represents the most prevalent primary solid tumor of non-hematopoietic origin that primarily develops within bone [2.3.27]. It is generally recognized as a high-grade malignancy, accounting for approximately **80-90%** of cases, and exhibits an inverse relationship with the extent of metastasis, with approximately 20% of cases displaying metastasis, predominantly to the lungs, followed by other skeletal sites, and rarely involving lymph nodes [3.7.8.28.29].

Osteosarcoma is considered a rare yet exceptionally aggressive form of bone cancer, with an annual incidence rate of **4.7** per million individuals in the pediatric and adolescent population (**aged 5-19 years**) [5.8.29]. Furthermore, it accounts for **8.9%** of cancer-related deaths in children [30.31.32.33]. In older adults **(>65 years old**), osteosarcoma can arise in association with Paget's disease of the bone or as a consequence of radiation therapy for various malignancies [31.33].

Multiple factors are closely linked to the development of osteosarcoma, including age, gender, race, height, genetic predisposition, and congenital bone abnormalities [15.34].

2. Localization of Osteosarcoma within the Human Body

Osteosarcoma represents approximately **20%**, of all bone tumors. While OS can manifest in any bone, it predominantly originates in the long bones of the appendicular skeleton [10.11.35]. Predominantly, it occurs near the knee joint, either in the distal femur (**42%**) or the proximal tibia (**19%**) [10.11.35]. Furthermore, OS may develop in both the proximal and distal humerus (**10%**), along with the scapula near the shoulder joint [36]. while only **1.25%** is found in the ribs [35.37]. It is worth mentioning that OS can also occur in various other bones, including the os coxa (**hip bone**) and the mandible (**jaw bone**) [38], as depicted in **Figure 01.**

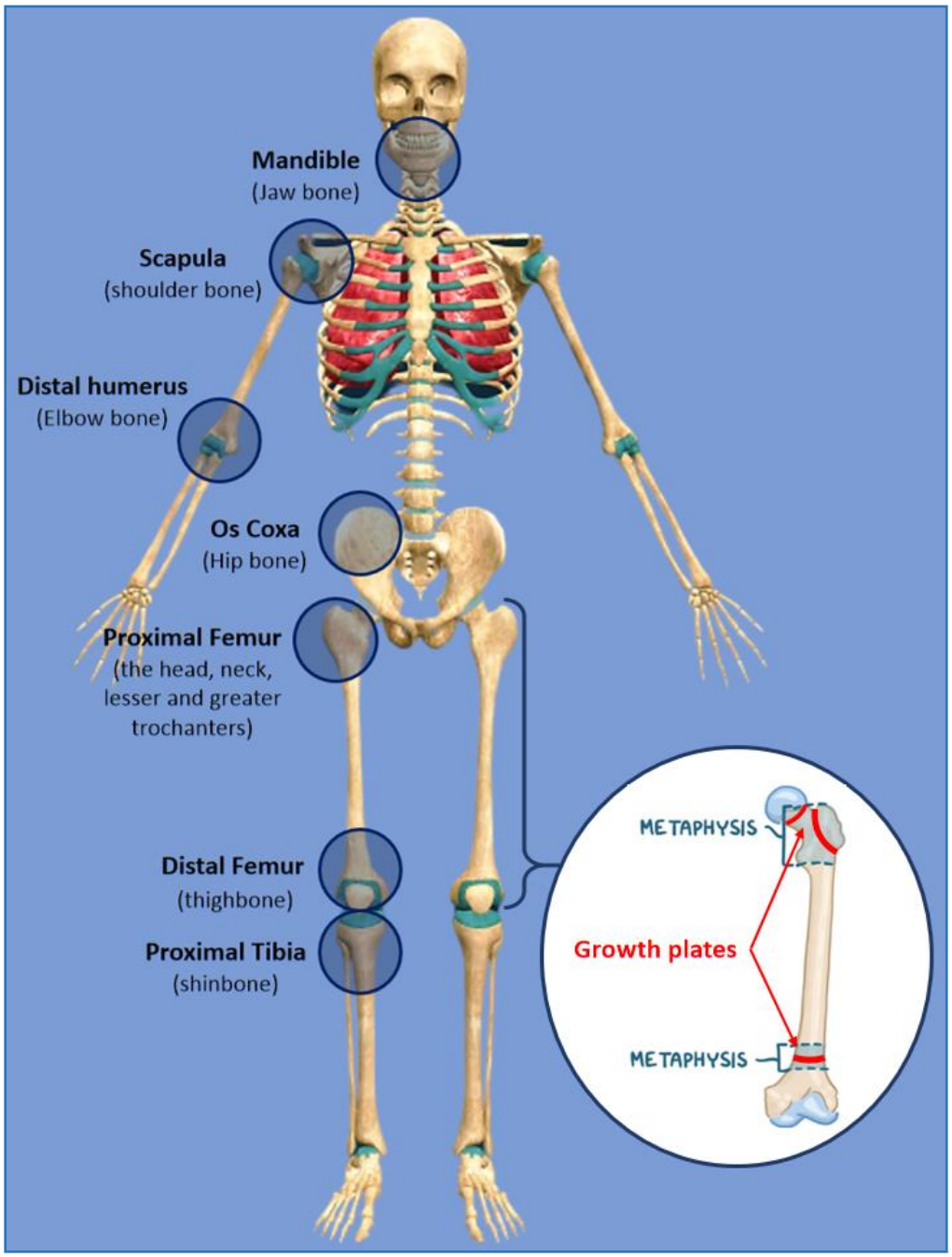

Figure 01: Localization of Osteosarcoma within the Human skeleton [38] depicted using a medical art servier (https://smart.servier.com/).

Osteosarcoma typically originates within the metaphyseal cavity or in close proximity to the growth plates, (areas experiencing the most rapid bone growth) [9.39.40.41]. Notably, in children and adolescents, there is an additional neroportion situated between the epiphysis and the diaphysis (bone shaft) [9.39.40]. In adults, the growth plates are completely ossified and fused with the epi and diaphysis [17.42.43]. Within this general area, three different types of cells are present, but our specific focus is on the osteoblasts **(figure 02).**

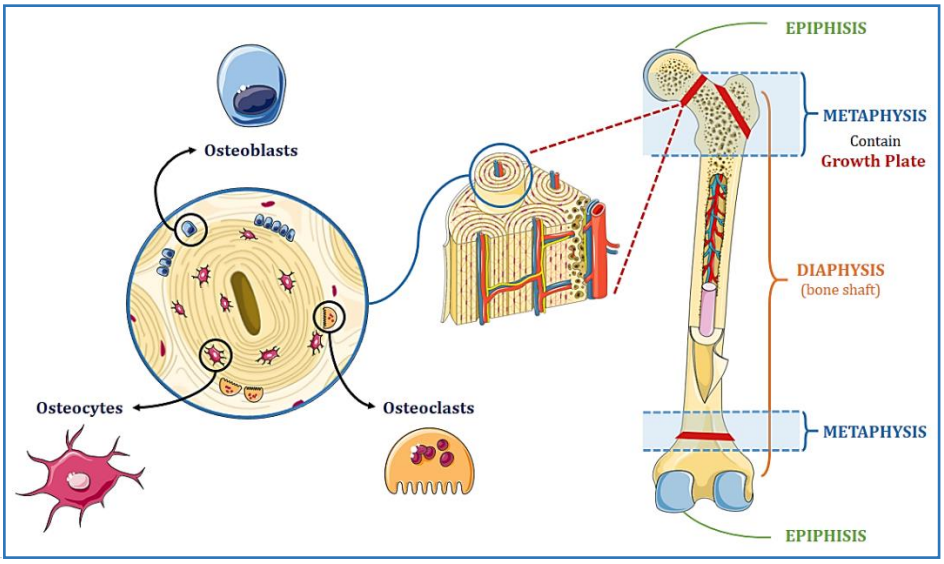

Figure 02: Localization of Osteosarcoma within the long Bones depicted using a medical art servier [9.12.17] (https://smart.servier.com/).

In order to comprehend osteosarcoma, it is crucial to recognize the significant role of osteoblasts in the process of bone formation and maintenance. Osteoblasts are specialized cells derived from mesenchymal cells that play a key role in synthesizing and depositing the extracellular matrix necessary for new bone formation [12.44.45]. However, when mutations occur in osteoblasts, they can give rise to malignant osteoblast-like cells (**figure 03**) [43.46.47.48.49]. which exhibit similar characteristics to osteoblasts but contribute to increased tumor aggressiveness, including the ability to sustain proliferative signaling, evade growth suppressors, resist cell death, enable replicative immortality, induce angiogenesis, and activate invasion and metastasis [13.47.49].

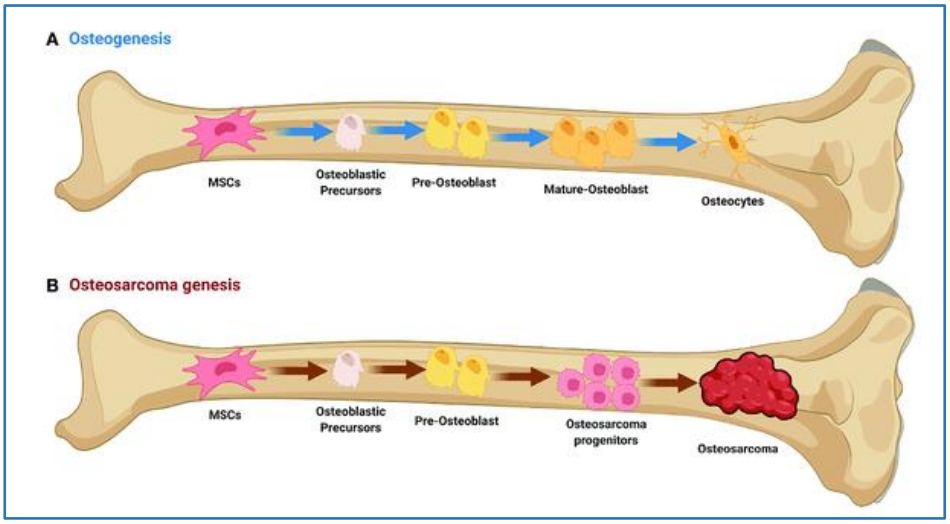

Figure 03: Osteogenesis and Osteosarcoma genesis. **(A)** Initiation of osteogenic differentiation from mesenchymal stem cells (MSCs). **(B)** Defects in osteogenesis lead to osteosarcoma genesis.[13.49].

3. Characteristics of the Osteosarcoma Cell Line SaoS-2

The Saos2, a human osteosarcoma cell line, derived from a primary osteosarcoma in an 11-year-old Caucasian girl by Fogh et al in **1973**, displays a highly metastatic nature [49.51.52]. Additionally, this cell line exhibits some of the well-characterized features of the osteoblastic phenotype, including the production of tissue-unspecific alkaline phosphatase and the ability to express specific receptors [44.52.53.54.55]. SAOS-2 cell line arises from rare mutations occurring in bone-forming cells but it should be noted that these cells do not naturally exist in the human body [14.56.57].

Morphologically, SAOS-2 cells exhibit an adherent growth pattern and display either a spindle-shaped or polygonal shape. They possess a diameter of approximately **10-20** micrometers and exhibit a high nuclear-to-cytoplasmic ratio. The cells contain a round to oval nucleus with a well-defined nucleolus [49.52.58.59].

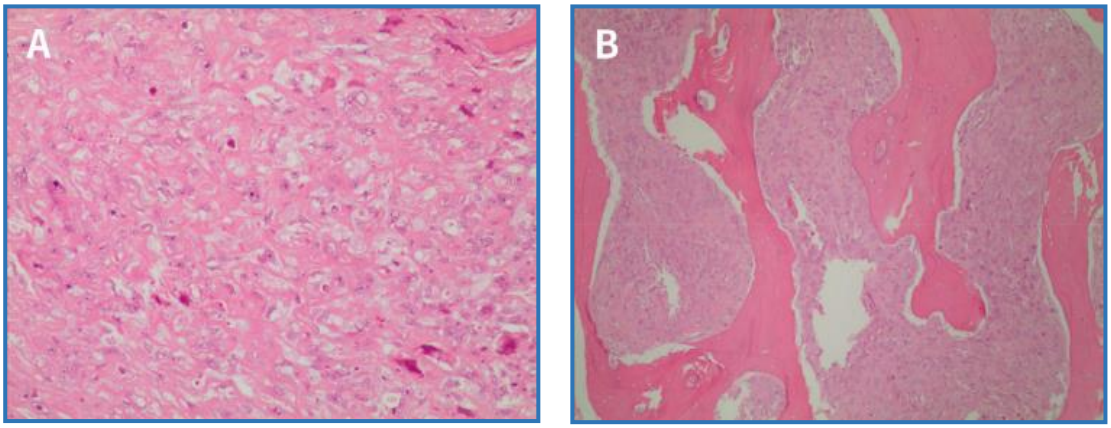

Figure 04: Presents the histological examination : (**A**) high Atypical Tumor Cells with Abundant Malignant Osteoid Production and Bone Invasion. (**B**) The tumor cells had abundant malignant osteoid production invading the host bone [60]

4. Classification of ostesarcoma

The classification system developed by the World Health Organization for bone tumors categorizes osteosarcoma into various subtypes [61.62]. based on several factors such as histologic features, biologic potential (grade), relationship to bone (intramedullary or surface), presence of multiple tumors (solitary or multifocal), and the initial condition of the underlying bone (primary or secondary) [63.64]. The subtypes include:

4.1. Conventional OS:

accounting for approximately **85%** of cases, is the most prevalent subtype. It is a high-grade solitary tumor that originates within the medullary cavity of a typically healthy bone, commonly found in long bones such as the femur, tibia, and humerus [35]. This subtype can be divided into three categories:

a) **Osteoblastic osteosarcoma:** This subtype consists of pleomorphic malignant cells closely associated with the surface of the neoplastic bone [35.65].

b) **Chondroblastic osteosarcoma:** It is characterized by a predominant chondroid matrix along with non-chondroid elements. The neoplastic chondrocytes exhibit severe cytologic atypia and are found within lacunar spaces [35.65].

c) **Fibroblastic osteosarcoma:** This subtype is typically composed of spindle-shaped, highly pleomorphic malignant cells arranged in a herringbone or storiform pattern, resembling fibrosarcoma or malignant fibrous histiocytoma. It exhibits a minimal osseous matrix [35.65].

4.2. Telangiectatic osteosarcoma:

This subtype is rare, accounting for less than **4%** of all osteosarcoma cases. It is more commonly observed in the second decade of life and primarily affects long tubular bones. However, it has also been known to arise in soft tissues outside of the bone [35].

4.3. Small-cell osteosarcoma:

This subtype is rare and constitutes approximately **1.5%** of osteosarcomas. It is characterized by the presence of small, round tumor cells and is often found in the bones of the hands and feet [35].

4.4. Low-grade osteosarcoma:

This is a slow-growing cancer with a low tendency to metastasize. It accounts for **1–2%** of all osteosarcoma cases. Compared to conventional osteosarcoma, low-grade osteosarcoma tends to occur at a slightly older age and exhibits a longer symptomatology [35].

4.5. Secondary OS:

This subtype constitutes a minority of cases and typically arises in sites of previous bone infarction, chronic osteomyelitis, or pre-existing primary benign bone tumors (such as osteochondroma, enchondroma, and giant cell tumor) are present [35].

5. Risk factors:

The precise cause of osteosarcoma remains largely unknown, and it can occur spontaneously. The exact causative factors are not always evident. Nevertheless, certain factors have been identified that could elevate the risk of developing this particular form of bone cancer:

- Having a history of radiation therapy (Radiation exposure) [66,67].
- Inherited genetic conditions. For example, genitic mutation [16].
- Certain bone disorders, such as Paget's disease, and exposure to certain chemicals, such as vinyl chloride [16,68].

6. Clinical manifestations of osteosarcoma

Commonly observed symptoms of osteosarcoma include prolonged, episodic pain, soft tissue mass, subsequent localized swelling, limited range of motion, weight loss, skin hypothermia, and spontaneous bone fractures lacking apparent etiology [36].

7. Diagnostic approach

In recent years, the diagnostic approach for malignant bone neoplasms has involved the utilization of various tools of medical imaging, including local plain radiography, X-rays, magnetic resonance imaging **(MRI)**, computed tomography **(CT)**, positron emission tomography **(PET)**, laboratory testing for serum tumor markers, or a combination of these techniques [17,18,69,70,71]. Additionally, several serum markers have been investigated for their diagnostic, prognostic, and recurrence monitoring potential [17,72]. Notably, lactate dehydrogenase (**LDH**) and alkaline phosphatase (**ALP**) have proven to be valuable biomarkers. Laboratory analysis has shown that **ALP** levels can be elevated by nearly **40%** in OS patients [73]. Furthermore, higher levels of **LDH** have been identified as a predictive factor for a poorer prognosis [74].

Osteosarcoma exhibits distinctive radiographic features that allow for its differentiation from other types of cancer. When the tumor reaches the outer cortical surface, the periosteum undergoes dissection from the bone. Consequently, the inner periosteum's cambium layer responds by generating new bone, exhibiting an open or discontinuous middle section known as **Codman angle**. Furthermore, other periosteal reactions can manifest as radiographic densities resembling **sunbursts** or **hair-on-end** pattern [17,35,75].

Figure 05: X-ray shows an osteosarcoma in the distal femur (thighbone). **(Left)** Note the formation of new bone in a typical **"sunburst"** periosteal reaction. **(Right)** When viewed from the side, a **Codman triangle** can also be seen rising from the bone [76].

8. Stages of osteosarcoma

After confirming the diagnosis of osteosarcoma, additional tests should be conducted to determine if cancer cells have spread to other areas of the body. This assessment is done using the Musculoskeletal Tumour Society staging system [77] (Reported in **Table 01**) is based on:

- Tumour grade (**I =** low grade; **II =** high grade)
- Tumour extension (**A=** intraosseous involvement only, **B=** intra/extraossseous extension)
- Presence of distant metastases (**III**)

Table 01: Surgical staging of bone sarcomas [17]

Stage	Grade	Site	Metastasis
IA	Low	Intracompartmental	No
IB	Low	Extracompartimental	No
IIA	High	Intracompartimental	No
IIB	High	Extracompartimental	No
III	Any	Any	Regional or distant

9. Treatment Approaches for Osteosarcoma

9.1. Surgical treatment

Prior to the 1970s, surgical excision was the primary treatment option for osteosarcoma in cases of local recurrence [20.21]. The goal of surgery is to completely ablate the tumor, along with any previously biopsied or contaminated tissue [21.27.78.79]. However, the location and extent of the tumor can make resection challenging. Even when feasible, tumor resection often results in damage to nerves and muscles, leading to significant functional impairment [21.27.78.79]. If

possible, the surgeon may employ a bone graft or artificial bone to preserve the limb (**figure 06**) [21.78.80.81]. In certain situations where the tumor is difficult to treat or has metastasized, amputation may be necessary, typically resulting in 5-year survival rates of 20% [69.82.83]. Nonetheless, the invasiveness of osteosarcoma can lead to issues such as recurrence or bone defects [27.79].

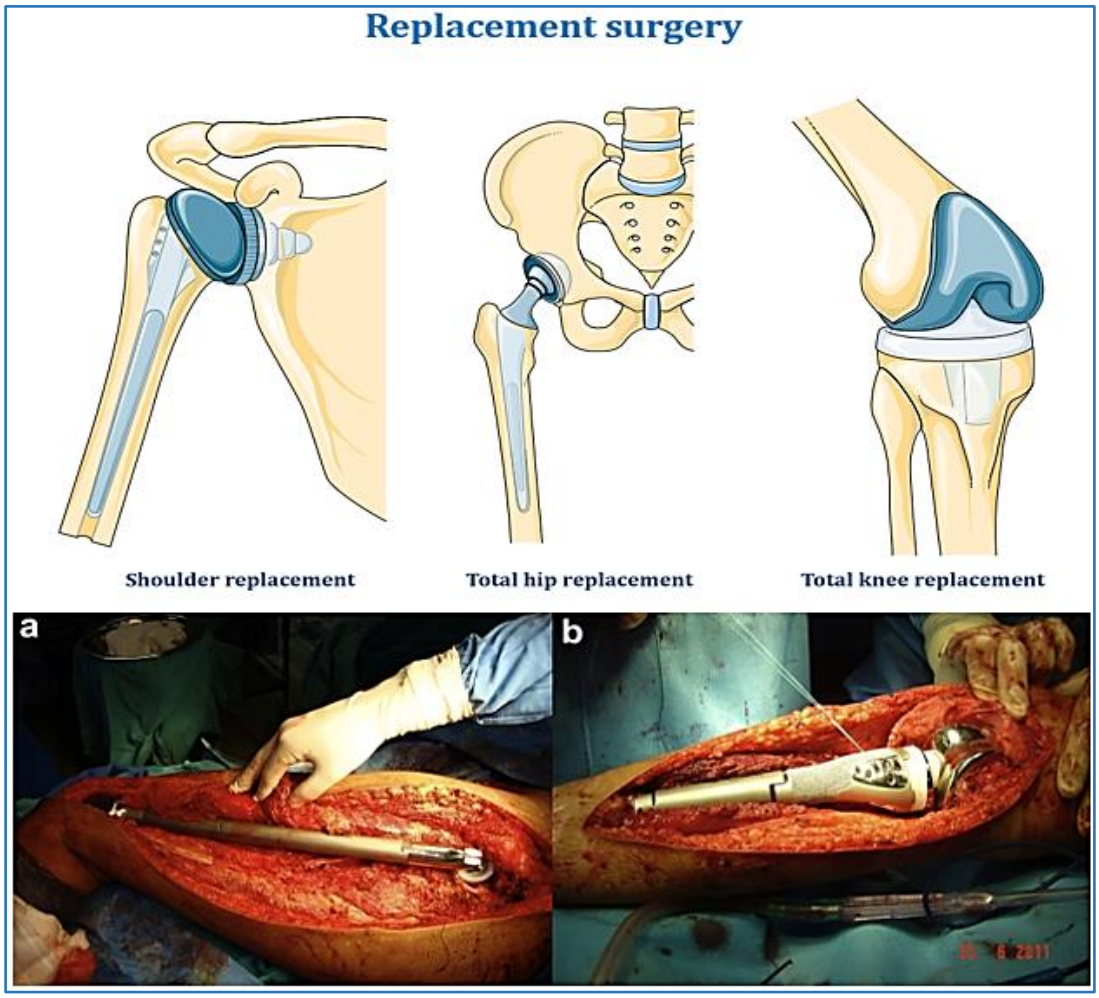

Figure 06: Replacement surgery of OS depicted using a medical art servier (https://smart.servier.com/) [84]. A total femur (**a**) and a proximal tibia (**b**) megaprosthesis in situ [81].

9.2. Chemotherapy

At present, chemotherapy is the primary treatment for this disease [22]. Chemotherapeutic drugs are utilized to target and kill cancer cells in osteosarcoma [23.78.85]. These drugs include adriamycin (**ADM**), cisplatin (**CDDP**), doxorubicin (**DOX**), high-dose methotrexate (**HD-MTX**), ifosfamide (**IFO**), epirubicin (**EPI**), and bleomycin, cyclophosphamide, and dactinomycin (**BCD**) [35.86]. Their use has been shown to improve the survival rate of patients with OS [87.88.89]. Chemotherapy regimens are administered intravenously, orally, or through a combination of both methods [82.90.91]. Aggressive adjuvant and neoadjuvant chemotherapy have

significantly enhanced survival rates in recent years, particularly for high-grade osteosarcoma (**from 20% to 70%**) [20.92.93.94].

The combination therapy of multi-agent chemotherapy and aggressive surgery has been shown to reduce the risk of recurrence and significantly improve the **5-year** survival rate of patients to some extent **(figure 07)** [19.95.96.97.98.99]. Typically, neoadjuvant chemotherapy is initiated **1–10** weeks prior to surgery. With proper coordination, the interruption of chemotherapy is temporary, and the resumption of therapy can typically begin within **2–3** weeks after surgery. Following surgical resection and a brief period for wound healing, maintenance chemotherapy is usually continued for a duration of **29** weeks [78.100]. After treatment, patients should adhere to a schedule of regular check-ups to monitor for any potential signs of recurrence or side effects resulting from the treatment.

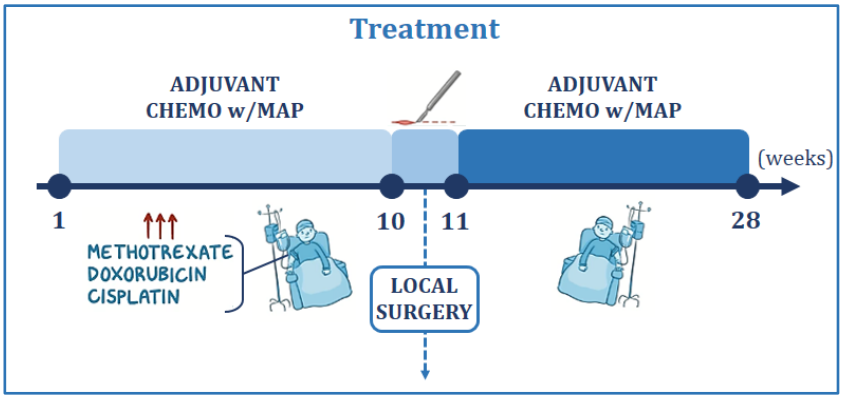

Figure 07: The combination therapy strategy of OS depicted using a medical art servier [19] (https://smart.servier.com/)

Evaluation of the treatment response through imaging before and after the completion of initial chemotherapy determines the final surgical approach [20.101.102]. Although radiological methods such as conventional X-ray, CT **(Figure 08)** [20.103].

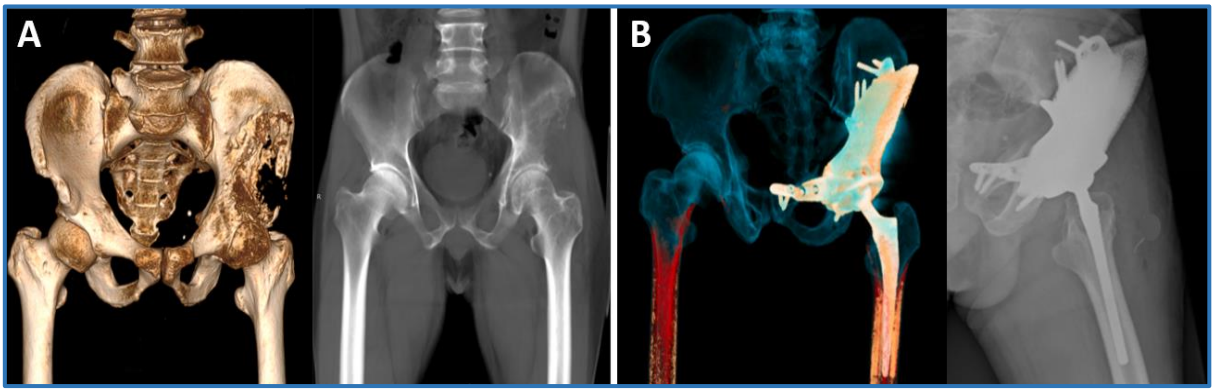

Figure 08: Treatment response through imaging. **A).** Pre - operation in CT 3D and X Ray. **B).** Postoperative CT 3D and X Ray [80].

Despite the current effectiveness of available treatments, there are still some problems [46]. Nevertheless, chemotherapy is accompanied by side effects such as chemotherapy-induced toxicities, a lack of specificity for the tumor cells, and a relatively painful procedure [24.104.105]. Furthermore, surgical removal of osteosarcomas may surpass the bone's self-repair capabilities, posing significant challenges for the restoration of bone tissue's structural and functional integrity [106.107.108]. Consequently, the development of new therapeutic approaches is crucial and practically significant to overcome these challenges while minimizing side effects [109.110.111]. In contrast, targeted therapies offer greater specificity towards tumor cells, resulting in wider therapeutic indices and, consequently, reduced toxicity. These anticancer drugs specifically focus on molecular abnormalities found in tumor cells within the signaling pathways associated with oncogenesis [32.85].

10. Studied proteins:

The objective of our research is to identify a novel targeted therapeutic approach for selectively inhibiting the growth of SAOS2 cancer cell line, associated with human osteosarcoma, while minimizing any adverse effects on non-cancerous cells. This objective will be achieved through a comprehensive investigation of a specific pathway and key protein within the cancer cells. By inhibiting them, we aim to impede the proliferation and accumulation of SaOS2 cells.

We have targeted five previously unstudied or minimally researched proteins crucial to the process under study. These proteins were selected for their association with a ligand at specific binding sites, which facilitated our analysis. The structural depictions are provided below:

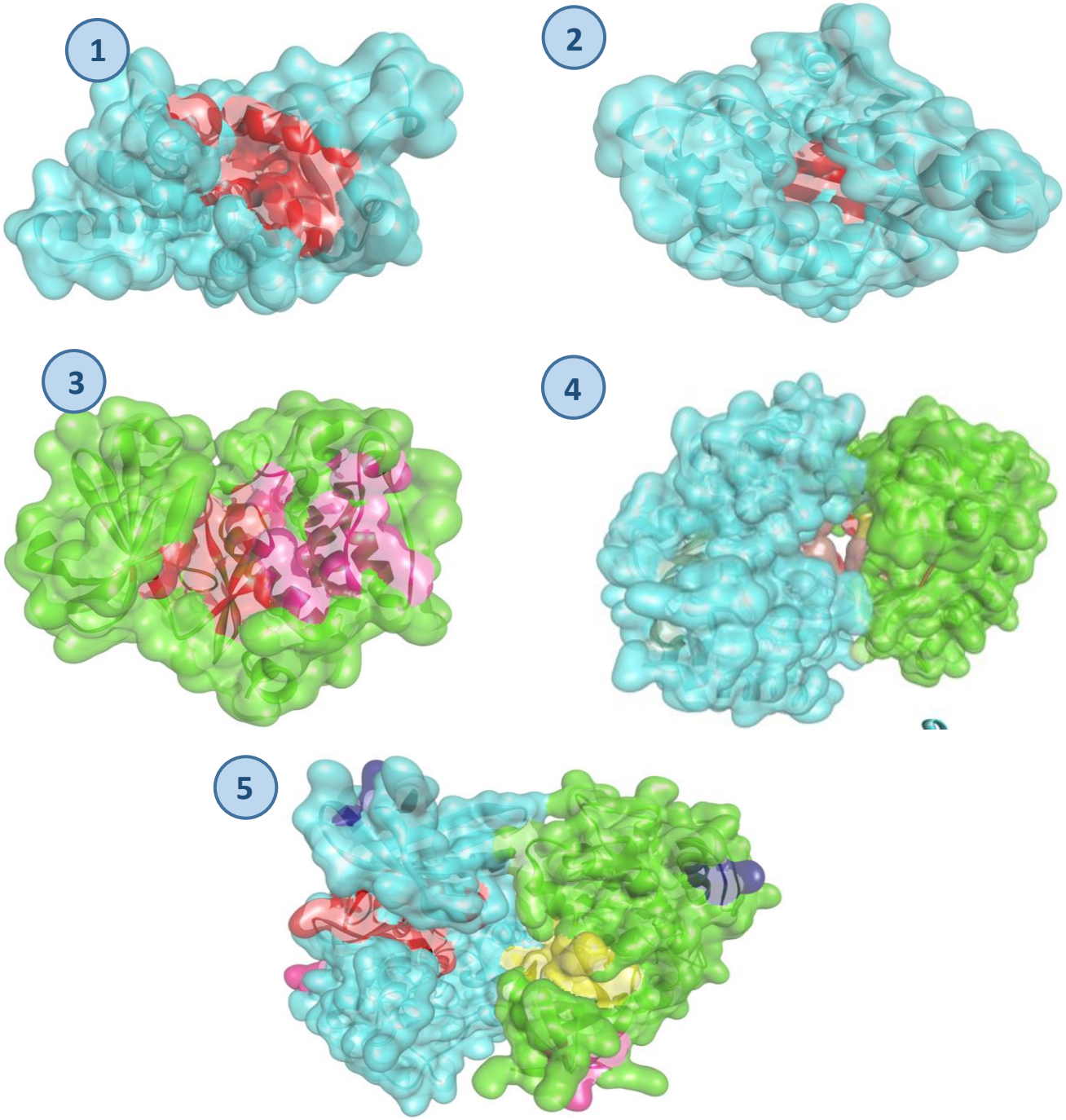

Figure 09: 3D structural representation of human osteosarcoma targets and its active sites in sphere format.

1) Estrogen Receptor (**1uom**); contains one chain (in blue) with one catalytic site (in red).
2) Heat Shock Protein 90 (**4BQG**); contains one chain (in blue) with one catalytic site (in red).
3) Serine/threonine-protein kinase pim-1 (**4I41**); contains one chain (in green) with two catalytic sites (in red and pink).
4) Histone deacetylase 8 (**4QA3**); contains two chains (blue and green) with eight binding sites, chain 1 contains two binding sites (in gray and red) and the second chain contains four binding sites (in red, pink, yellow and dark blue).
5) BMP-2-inducible protein kinase (**5i3r**); contains two chains (in blue and green) with four active sites, chain 1 contains two binding sites (in red and pink) and the second chain contains two binding sites (in pink and yellow).

After selecting our goal protein, we have obtained the following information using UNIPROT web server (**http://www.uniprot.org/**):

1. Enzymes section

PDB ID	Protein name	Enzyme class number	localization	cofactor binding site	Predected MUTAGENESIS
5I3R	BMP-2-inducible protein kinase	EC:2.7.11.1	Nucleus	/	/

Catalytic activity: **ATP + L-seryl-[protein] = ADP + H+ + O-phospho-L-seryl-[protein]**

ATP + L-threonyl-[protein] = ADP + H+ + O-phospho-L-threonyl-[protein]

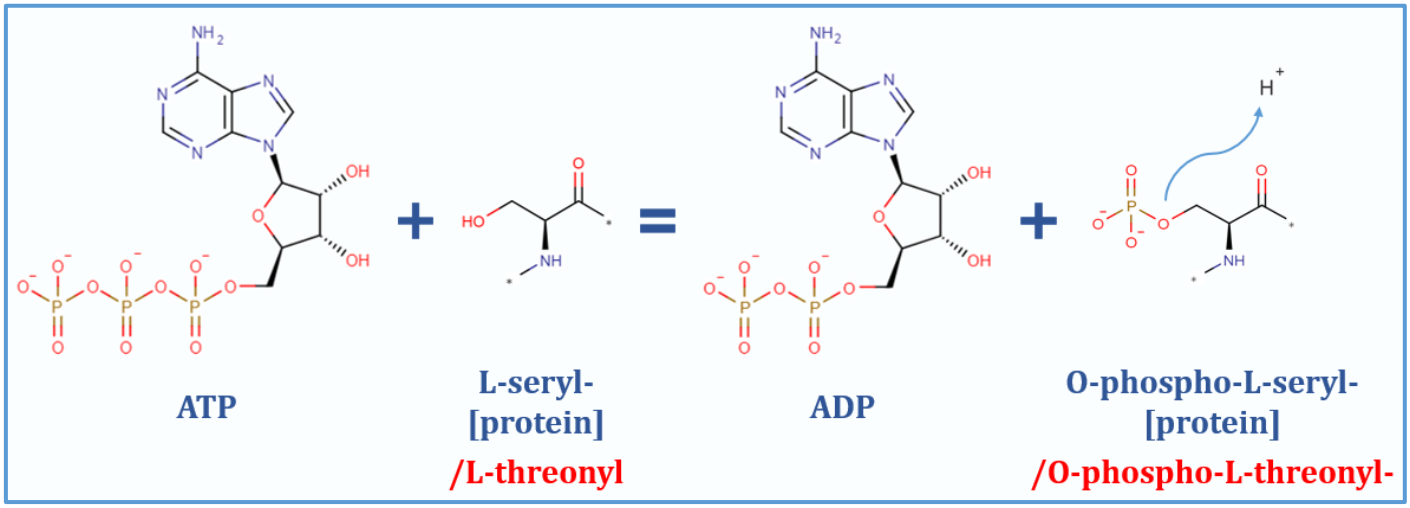

4BQG	Heat Shock Protein 90	EC:3.6.4.10	Nucleus Cytoplasm, Cell membrane, Mitochondrion	1 (Mg2+)	3 mutations in GLU39, ASP85, GLY89, LEU180

Catalytic activity: **ATP + H2O = ADP + H+ + phosphate**

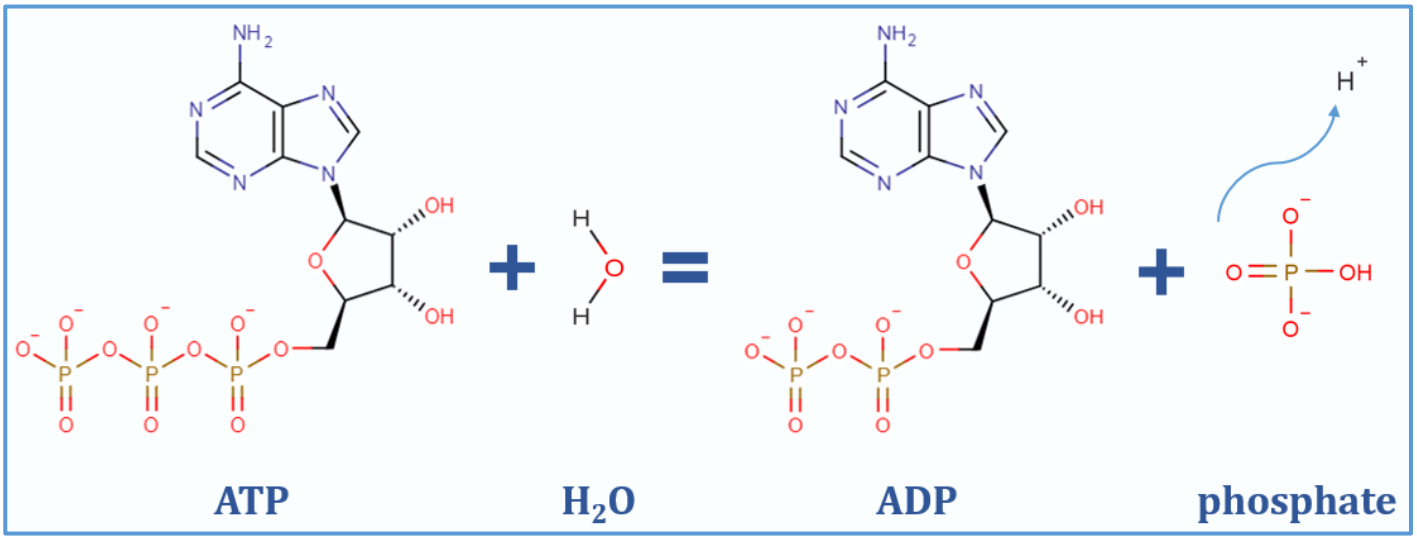

4I41	Serine/threonine-protein kinase pim-1	EC:2.7.11.1	Cytoplasm, Nucleus, Cell membrane	1 (Mg2+)	4 mutations in HIS55, PRO68, ASN69, LEU180

Catalytic activity: ATP + L-threonyl-[protein] = ADP + H+ + O-phospho-L-threonyl-[protein]

ATP + L-seryl-[protein] = ADP + H+ + O-phospho-L-seryl-[protein]

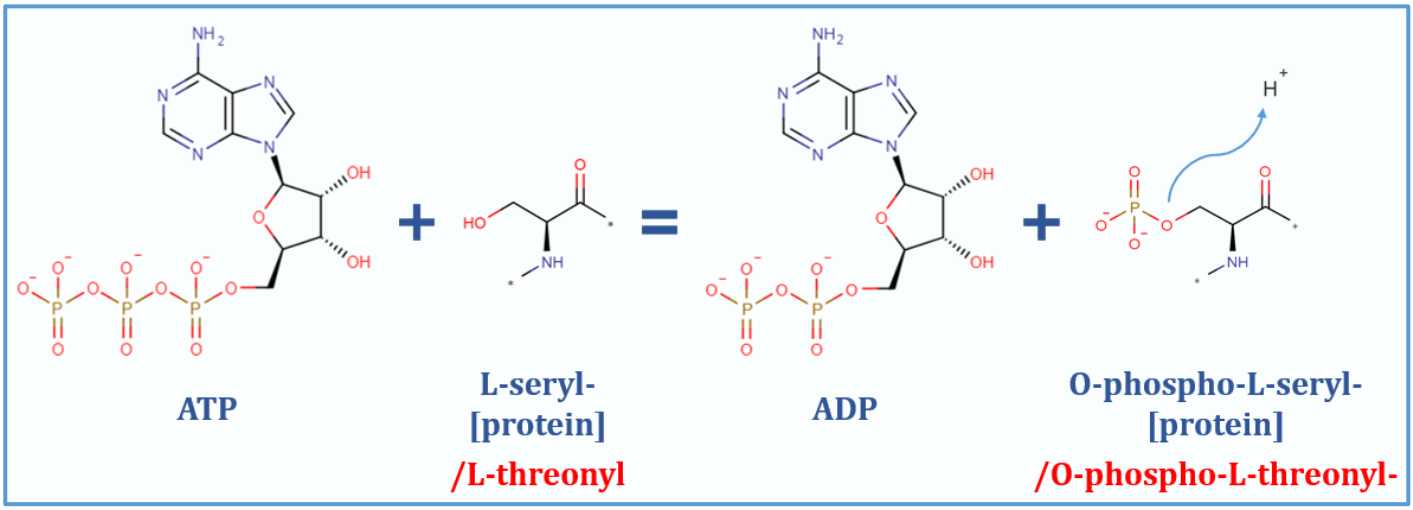

4QA3	Histone deacetylase 8	EC:3.5.1.98	Nucleus, Cytoplasm	1 (a divalent metal cation)	4 mutations in Ser39, Asp101, His143, Tyr306

Catalytic activity: H2O + N6-acetyl-L-lysyl-[protein] = acetate + L-lysyl-[protein]

H2O + N6-butenoyl-L-lysyl-[protein] = (2E)-2-butenoate + L-lysyl-[protein]

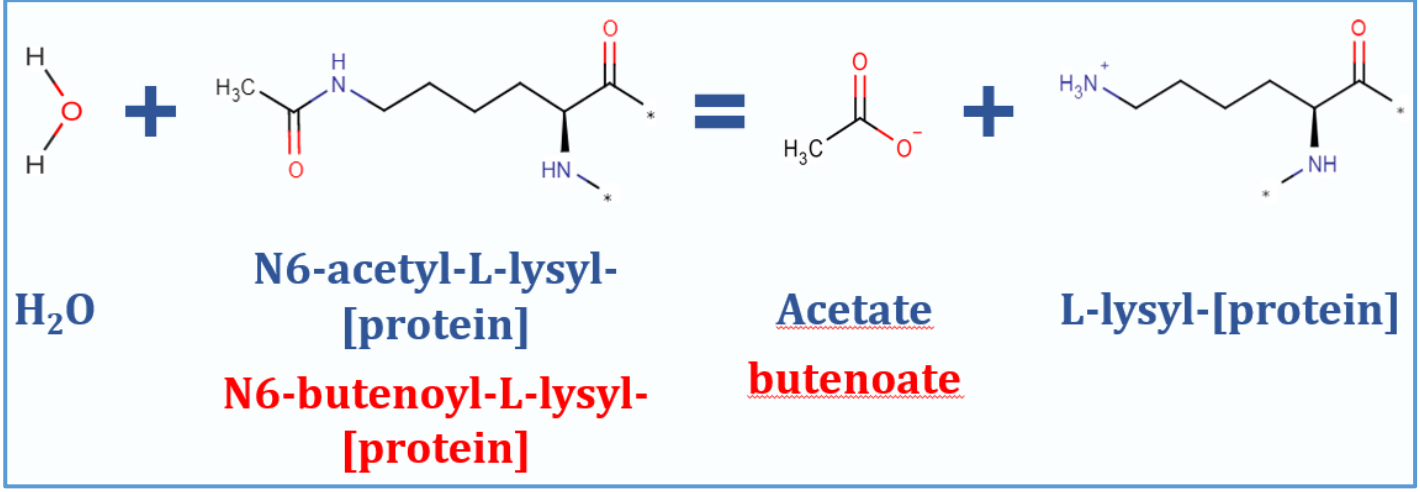

1. Reseptor section

PDB ID	Protein name	localization	Predected MUTAGENESIS
1UOM	Estrogen Receptor	Cytoplasm, Nucleus, Cell membrane	8 mutations in Val68, Val80, Glu84, Ile90, Cys151, Tyr241, Leu243, Leu244

Table 02: Table representing important information about the five studied human osteosarcoma targets, the table is devised by 2 sections: (1) enzymes section containind 4 enzymes (**PDB ID**: **5i3r, 4bqg, 4i41** and **4qa3,** respectively), (2) resepter section representing the Estrogen Receptor (**PDB ID: 1UOM)**

11. Studied marine species

The limited availability of research on the anticancer properties of marine alkaloids against human osteosarcoma cell lines Saos2 was the primary motivation for selecting marine sources. These sources offer substantial untapped potential, as they are largely unexplored, coupled with harboring molecules with promising pharmaceutical and therapeutic utility. Specifically, our research focused on the examination of marine organisms belonging to the phyla Porifera (**sponges**) and Ascidiaceae (**tunicates**).

11.1. Marine sponges

Marine sponges are primitive multicell animals with spineless creatures and soft bodies that are immobile and serve seawater as a filter for small food particles that have existed for millions of years. Marine sponges have been viewed as a medication treasury with huge therapeutic and pharmacological potential because of their broad variety of natural products [112]. The selected marine alkaloids are **Coscinamide A, B,** and **C** [113], **Leucettamine B** [114], and **Dispacamide** [115], belonging to the ***Coscinoderma matthewsi, Leucetta microraphis,*** and ***Agelas genus***, respectively[116].

a) *Coscinoderma matthewsi*

Taxonomy:

Kingdom: Animalia
Class: Demospongiae
Ordre: Dictyoceratida
Family: Spongiidae
Genus: *Coscinoderma*
Species: ***Coscinoderma matthewsi***

Figure 10: Pictures of ***Coscinoderma matthewsi*** and their systematics according to SpongeMaps Platform (**http://www.spongemaps.org**)

b) *Leucetta microraphis*

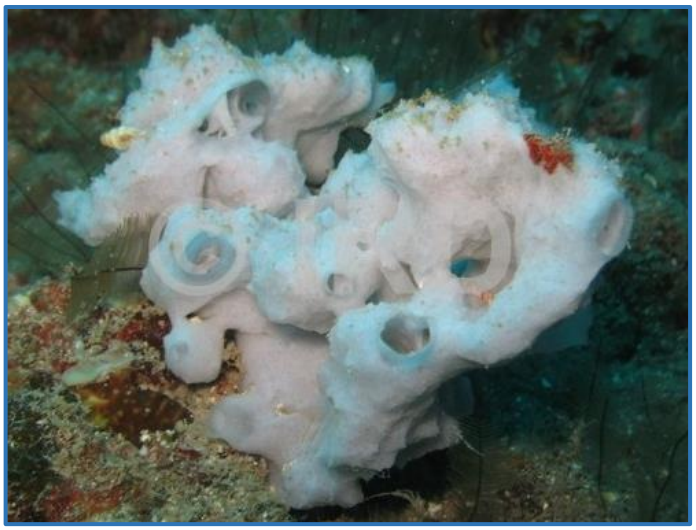

Taxonomy:

Kingdom: Animalia
Class: Calcarea
Ordre: Clathrinida
Family : Leucettidae
Genus : *Leucetta*
Species : ***Leucetta microraphis***

Figure 11: Pictures of ***Leucetta microraphis*** and their systematics according to SpongeMaps Platform (**http://www.spongemaps.org**)

c) *Agelas genus*

Taxonomy:

Kingdom: Animalia
Class: Demospongiae
Ordre: Agelasida
Family: Agelasidae
Genus: *Agelas*
Species: ***Agelas conifera***

Figure 12: Pictures of ***Agelas genus*** and their systematics according to SpongeMaps Platform (**http://www.spongemaps.org**)

11.2. Marine Ascidiacea

Marine Ascidiacea are the largest and most diverse class belonging to the species of tunicate [117]. There are approximately **3,000** described species. Alkaloids represent the highest percentage of the bioactive compounds of marine Ascidiacea **(around 70%)** [118]. Marine alkaloids that we worked on are **Eudistomins Y1** [119] and **Polyandrocarpamines A** [120]. belonging to the ***Cystodytes dellechiajei*** and ***Didemnum molle***, respectively [121].

a) *Cystodytes dellechiajei*

Taxonomy:

Kingdom: Animalia
Class: Ascidiacea
Ordre: Aplousobranchia
Family: Polycitoridae
Genus: *Cystodytes*
Species: ***Cystodytes dellechiajei***

Figure 13: Pictures of ***Cystodytes dellechiajei*** and their systematics according to World Register of Marine Species Platform **(https://www.marinespecies.org/).**

b) *Didemnum molle*

Taxonomy:

Kingdom: Animalia
Class: Ascidiacea
Ordre: Aplousobranchia
Family: Didemnidae
Genus: *Didemnum*
Species: ***Didemnum molle***

Figure 14: Pictures of ***Didemnum molle*** and their systematics according to World Register of Marine Species Platform **(https://www.marinespecies.org/).**

MATERIALS AND METHODS

1. Softwares, databases and web servers

1.1. Databases

1.1.1. RCSB Protein Data Bank

The Protein Data Bank (**PDB**) is a widely recognized and extensively utilized online repository, which is located at **(www.rcsb.org/pdb/).** That provides a comprehensive collection of experimentally determined 3D structures of biological macromolecules, such as proteins, nucleic acids, and complex assemblies. The PDB serves provid structural and functional attributes, as well as interactions, of biological molecules.

1.1.2. Pubchem

PubChem is a publicly accessible database of chemical molecules and related information maintained by the National Center for Biotechnology Information (**NCBI**). With over **220** million unique chemical substances, including small molecules, peptides, and natural products. The PubChem server offers users a range of tools and resources for accessing and analyzing chemical data, visualization tools and molecular similarity. This chemobank can be accessed for free through a web-based user interface: **(pubchem.ncbi.nlm.nih.gov/**).

1.2. Softwares

1.2.1. Autodock Vina

AutoDock Vina is a molecular docking software program utilized in drug discovery for *in silico* studies. It calculates the binding energy between a ligand and receptor to predict their binding mode, using an empirical scoring function and Monte Carlo algorithm. The software is widely used to identify potential drug candidates and study protein-ligand interactions, making it a valuable tool for *in silico* drug discovery and molecular modeling studies.

1.2.2. Autodock Tools

AutoDock Tools is a software package designed for molecular docking simulations in the context of *in silico* drug discovery. Its graphical user interface provides users with the ability to prepare and analyze ligand and receptor molecules, as well as visualize the results of docking results obtained from AutoDock Vina. ADT is user-friendly and allows for the preparation, visualization of the predicted binding mode, binding energy, and hydrogen bond interactions between the ligand and receptor.

1.2.3. Discovery Studio

Discovery Studio is a comprehensive software suite for molecular modeling and simulation, designed to support drug discovery and materials science research. It is a widely-used tool in the field of *in silico* drug design, enabling researchers to predict the behavior and properties of molecules and materials, and to visualize and analyze their structures and interactions, making it a powerful tool for accelerating the drug discovery process. In this study, The Discovery Studio version 2017 software was used to generate visual analysis of Enzyme-inhibitor interaction diagrams.

1.2.4. Chemdraw

ChemDraw is a widely recognized and extensively used software application for creating and editing chemical structures, offering a user-friendly interface and a comprehensive range of drawing and editing tools. It facilitates the creation of 2D structures of chemical compounds, with the added capability of customization options of assigning colors to specific elements such as oxygen and nitrogen. Furthermore, ChemDraw offers convenient options for exporting and saving drawings in a variety of commonly used formats, including **PDF, PNG**, and **SVG**.

2. Structure-activity Relationship (SAR)

The main goal of this study was to examine the effects of seven novel alkaloid compounds on human osteosarcoma targets through the utilization of *in silico* molecular docking. In order to predict the binding mode and strength of an interaction between two or more molecules, typically a small molecule (known as a ligand) and a larger macromolecule (known as a receptor). Molecular docking (**Md**) is one of the most powerful computational techniques. It enables estimation of the binding affinity of the complex as well as prediction of the 3D structure created by the ligand-receptor interaction [122]. We used Autodock Vina to perform molecular docking in this study and investigate the qualitative modeling of the discovered compounds and their impacts on the targets for human OS. Molecular docking was set as a specific docking type that allows the inhibitors full flexibility and part flexibility to the receptor. We aimed to identify the inhibition mechanism(s) and interactions involved, specifically focusing on hydrogen and hydrophobic bonds.

3. Preparation of molecular docking parameters

3.1. Targets preparation

We have chosen five targets (**4 enzymes and 1 receptor**); they are involved in human osteosarcom pathology and were admitted as pharmacological targets for the development of

new anti-tumor drugs. As a start, we have reached the crystal structures using the RCSB Protein Data Bank web server **(www.rcsb.org/pdb/).**

In molecular docking, the protein must be prepared following those essential steps:

- Firstly, by removing any possible ligands, co-crystallized solvents, heteroatoms, and unnecessary water molecules except those required in the active site.
- Secondly, polar hydrogens and partial charges, which define the correct ionization and tautomeric states, were added to the structure while using Autodock Tools version 1.5.6.
- Finally, as a fundamental procedure, we have meticulously selected the active site of the targets to optimize the ligands' accessibility to the catalytic site. Subsequently, the grid box center and the dimensions of the binding pocket were determined based on the grid coordinates (x, y, and z).

We must mention that all parameters are defaulted, except that the number of output conformations was set to one. The number of docking runs was set at 10. Whish refers that the obtained solutions number was equal to 10. The extra step is preparing the docking folder and the necessary files and commands. Finally, the generated docking results were directly loaded into the Discovery Studio visualizer (**DSV**) program. The best poses were chosen according to their minimum binding energy values in kcal/mol; the smaller the number, the bigger the potential affinity of our ligands towards the selected targets. **Table 03** displays all parametters, **PDB ID** and grix box cordination.

3.2. Ligand preparation

The 3D structures of the seven alkaloids, Coscinamide A **(mol1),** Leucettamine B **(mol2),** Polyandrocarpamine A **(mol3),** Coscinamide B **(mol4),** Coscinamide **(mol5),** Dispacamide **(mol6),** and Eudistomin Y1 **(mol7),** were retrieved in the **SDF** file format from the PubChem database **(pubchem.ncbi.nlm.nih.gov)**. Discovery Studio Visualizer was used to convert them into **PDB** file format. Next, the ligands were opened in **ADT** to be prepared by considering torsional flexibility and finally converted into pdbqt file format. This conversion was necessary to facilitate loading the file into Autodock Vina. While the **2D** structures of these molecules were generated using ChemDraw 16.0, The studied compounds information can be found in **Table 04**, and a structural representation is provided in **Figure 15**

Table 03: Osteosarcoma targets parametters, PDB ID and grix box cordination

PDB ID	Protein name	Gene expression	resolution (Å)	molecular weight (KDa)	Chain number	Amino Acid number	grid box parameter	NPP 20/23
1uom	Estrogen Receptor	ESR1	2.28	29.4	1 (A)	232	-1.263*23.248*52.219 16*12*18	2
5I3R	BMP-2-inducible protein kinase	BMP2K	2.40	69.04	2 (A/B)	302 (2)	13.38*18.51 *47.59 12*18*10	3
4BQG	Heat Shock Protein 90	HSP90AA1	1.90	26.08	1 (A)	209	-17.298*-19.85 *-1.402 10*16*14	5
4I41	Serine/threonine-protein kinase pim-1	PIM1	2.70	33.43	1 (A)	273	-15.779*2.642 *-37.607 16*14*16	3
4QA3	Histone deacetylase 8	HDAC8	2.88	87.6	2 (A/B)	365 (2)	2.446*23.585 *13.483 10*10*14	1

NPP 20/23: Number of published papers between 2020 and 2023

Table 04: Information about the seven chosen alkaloids

Source of alkaloid	IUPAC	Compound's Name	PubChem CID	Class	Molecular weight (Da)
Marine Sponge ***Coscinoderma matthewsi***	*N*-[(*E*)-2-(6-bromo-1*H*-indol-3-yl) ethenyl]-2-(1*H*-indol-3-yl)-2-oxoacetamide	Coscinamide A **(mol1)**	5352103	Indole	408.2
Marine Sponge ***Leucetta microraphis.***	(5*Z*)-2-amino-5-(1,3-benzodioxol-5-ylmethylidene)-3-methylimidazol-4-one	Leucettamine B **(mol2)**	10037501	Imidazole	245.23
Marine Ascidian ***Cystodytes dellechiajei***	2-amino-4-(4-hydroxy-3-methoxybenzylidene)-1H-imidazol-5(4H)-one	Polyandrocarpamine A **(mol3)**	103724273	2-Amino-imidazolin	233.22
Marine Sponge ***Coscinoderma matthewsi***	2-(1*H*-indol-3-yl)-*N*-[(*E*)-2-(1*H*-indol-3-yl) ethenyl]-2-oxoacetamide	Coscinamide B **(mol4)**	5352104	Indole	329.4
Marine Sponge ***Coscinoderma matthewsi***	*N*-[(*E*)-2-(5-bromo-1*H*-indol-3-yl) ethenyl]-2-(7-hydroxy-1*H*-indol-3-yl)-2-oxoacetamide	Coscinamide C **(mol5)**	5352105	Indole	424.2
Marine Sponges ***Agelas. conifera***	*N*-[(3*Z*)-3-(2-amino-5-oxo-1*H*-imidazol-4-ylidene) propyl]-4,5-dibromo-1*H*-pyrrole-2-carboxamide	Dispacamide **(mol6)**	135481784	2-Amino-imidazolin	405.05
Marine Ascidian ***Didemnum molle***	(4-hydroxyphenyl) -(9*H*-pyrido[3,4-b] indol-1-yl) methanone	Eudistomin Y1 **(mol7)**	24800709	β-Carboline	288.3

IUPAC: international Union of Pure and Applied Chemestrey. /CID: Compound ID.

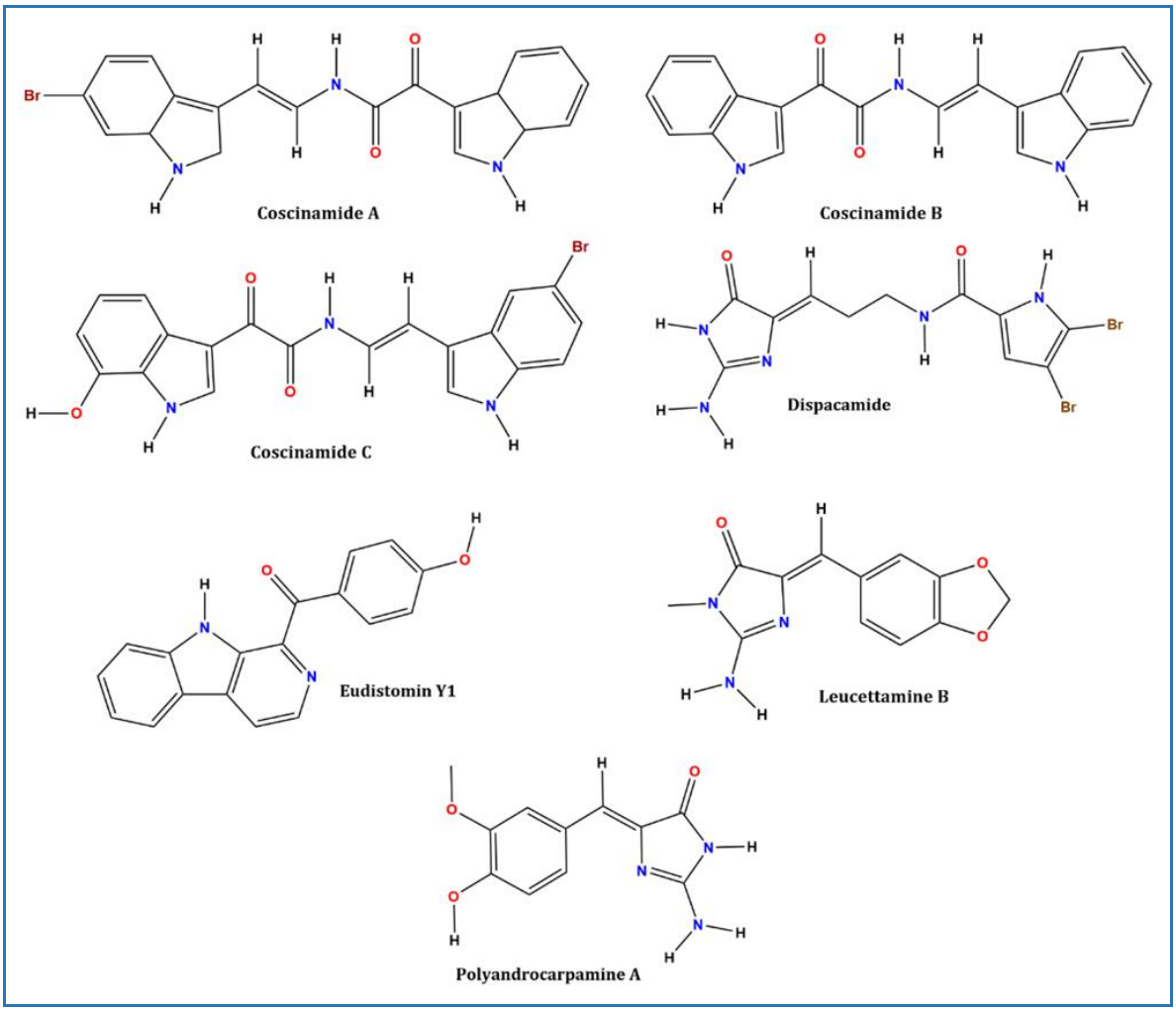

Figure 15: 2D structure of the seven marine alkaloids

4. ADMET settings

To evaluate the drug-likeness prediction of our alkaloids, we have used ADMET tools in order to examine their effects on the human body. ADME/Tox refers to the process of studying the absorption, distribution, metabolism, excretion, and toxicity of drugs. Whish offer an evaluation of the pharmacological and toxicological capasity, and it has become an appropriate methodology for employing *in silico* drug development and discovery processes. It also plays an important role in drug candidate success, especially in pre-clinical stages. The used tools: SwissADME (**www.swissadme.ch/**), and AdmetSAR (**lmmd.ecust.edu.cn/admetsar2**) web tools are available with free access. The canonical SMILES of the seven alkaloids obtained from PubChem Database were inserted into the servers online, and the ADMET profile was chosen based on the most commonly used parameters [123,124].

The lipinski rule of five enables the determination of the potential oral administration of a chemical compound with medicinal properties in humans [125].

According to this rule, a compound is considered suitable for oral administration if it meets at least three (3) of the following four (4) criteria:

- It has a maximum molecular weight of **500 g/mol.**
- Its partition coefficient (**logP**) or lipophilicity is ≤ **5.**
- The number of hydrogen bond donors is limited to ≤**5.**
- The number of hydrogen bond acceptors is limited to ≤ **10.**

Absorption is the process of moving a drug from an extravascular site of administration into the systemic circulation to reach its site of action [126]. This process is indeed very complex and depends on many parameters, including a drug's physicochemical properties, and it involves three important parameters such as:

- **The caco-2 cell permeability (nm/sec):** is a human colorectal carcinoma epithelial cell line used to predict human intestinal drug absorption and efflux [127].
- **Human Intestinal Absorption (HIA%):** an important indicator of the intestinal absorption of orally administered drugs. It's usually quantified as a portion of the drug that reaches the portal vein (**HIA= D-blood/D-oral**). Here, D-blood represents the amount of a substance that has reached the portal vein, while D-oral corresponds to the total amount of the orally administered substance [127].
- **Lipophilicity of the compound:** This parameter is associated with the permeability of a drug through biological membranes. Compounds with low lipophilicity may exhibit decreased permeability, while highly hydrophilic compounds are typically unable to passively diffuse through these membranes [126].

Distribution refers to the reversible movement of a drug from one location to another within the human body, commonly involving diffusion through the bloodstream into various tissues [126]. This process is influenced by three important parameters:

- **Blood-brain barrier penetration (C.brain/C.blood):** is a specialized barrier formed by endothelial cells that tightly regulates the passage of small molecules and water into and out of the brain while preventing larger molecules from entering the central nervous system (**CNS**) [128]. This parameter is represented by the ratio of the drug concentration in the brain (C-brain) to the drug concentration in the blood (C-blood) [129]:

logBB= log (Cblood/Cbrain)

- **skin permeability (logKp, cm/hour):** This parameter relates to the study of drug penetration through the skin barrier [127].
- **Plasma protein binding (%):** It represents the percentage of a drug that binds to plasma proteins, which can influence both pharmacokinetics and pharmacodynamics. This parameter is used to estimate drug-drug interactions [127].

The metabolism of drugs involves a complex process of biotransformation, where drugs are structurally modified by various enzymes, contributing significantly to drug development and safety [130].

- **Cytochrome P450 enzymes (CYP450):** These enzymes are primarily located in the smooth endoplasmic reticulum and mitochondria of hepatocytes and intestines [131]. The are responsible for metabolizing approximately 80% of xenobiotics through oxidation [132]. Inhibition of CYP450 enzymes by the studied ligands can result in toxicity or a decrease in the therapeutic effectiveness of drugs [133].

Excretion refers to the process of eliminating compounds from the body to prevent accumulation and potential toxicity. It is crucial to ensure that both administered compounds and their metabolites are effectively excreted through renal (urine), fecal, and sweat routes [134].

- **Total clearance (CLtot.) (mL/min/kg):** This parameter quantifies the rate at which a drug is irreversibly eliminated from the body [135].
- **Half-life time (T1/2)**: It represents the time required for the concentration of a drug (typically in blood or plasma) to decrease to half of its initial value [136].

Toxicity is a critical factor in drug development, as the early determination and identification of toxicity can significantly save time and reduce development costs [126]. The toxicity profile summarizes:

- **The Ames test:** is a test that determines the ability of a chemical or drug to induce mutations in DNA, providing valuable insights into its genotoxic potential [127].
- **HERG (human ether-related gene channel)** is an important potassium channel involved in regulating heart function. Inhibition of this channel by a compound can have adverse effects on cardiac activity [137].
- **Carcinogenicity test:** refers to the ability of a chemical to cause cancer in animals or humans. This test evaluates the potential of a compound to induce carcinogenic effects, typically through in vivo testing on rats and mice [127].

- **Human Hepatotoxicity:** This aspect focuses on the evaluation of the compound's potential toxicity to the liver, a vital organ involved in drug metabolism and detoxification [138].
- **LD50 (LD50 of acute toxicity):** represents the lethal dose at which 50% of a population of test subjects (usually animals) succumb to the acute toxicity of a compound. It provides an indication of the compound's potency and potential harm at high doses [126].

5. Cytotoxic activity CLC-Pred:

We used the CLC-Pred (Cell Line Cytotoxicity Predictor) web service to perform *in silico* predictions of the cytotoxic effects of our chemical compounds on both non-transformed and cancer cell lines based on their structural formulas. It is a comprehensive platform for researchers who are interested in studying and developing drugs using cell lines. The website provides detailed information such as the origin of each cell line, growth characteristics, and other relevant information such as genotypic and phenotypic features on a wide range of cell lines, including cancer cell lines. The CLC-Pred also presents the results as Pa and Pi values, with the most effective chemicals having a higher probability of Pa values than Pi taken into consideration as potentiating substances with cytotoxic action [139].

6. Protein-protein interactions analysis

STRING (**Search Tool for Recurring Instances of Neighboring Genes**) is a distinguished database and an esteemed web resource (**http://string-db.org/**) dedicated to facilitating the integration of multiple data sets by sketching a map of potential protein-protein interactions (PPIs) within various organisms [140.141]. This comprehensive undertaking includes both physical and functional interactions [142]. It weights and integrates information from various sources, such as experimental repositories, computational predictions, function annotation, network analyses, and automated text mining [142.143]. PPI analysis helps uncover the mechanisms of an interaction to understand the basics of cell functions, including stable complexes, metabolic pathways, and regulatory interactions [141.144].

In the present study, our objective is to elucidate *in silico* PPI prediction methods, with a particular focus on investigating the interrelationships among various oncogenic targets. This knowledge has the potential to significantly contribute to the development of more efficacious therapeutic approaches and shed light on the disease's mechanisms of action and inhibition. Notably, our interactive study focuses on the esteemed organism Homo sapiens as the organism of interest.

RESULTS AND DISCUSSION

1. Structure-activity relationship (SAR)

The aim of our in-silico investigation is to evaluate novel drugs by examining the modes of interaction between selected ligands and the catalytic sites of the five specified targets.

The findings presented in **Table 05** illustrate the binding energies of the seven compounds with osteosarcoma target, along with various interactions such as inhibition constant **(Ki),** hydrogen bonds, and distances between amino acids within the enzyme active site after docking evaluation. However, It is important to note that the binding energy serves as the primary parameter. It provides insight into the strength and affinity of the ligand-receptor interaction. Higher binding energy indicates weaker interaction and vice versa. Our focus is to identify the ligand with the lowest binding energy. Molecular docking investigations have clearly demonstrated that all the compounds exhibit favorable steric and chemical complementarity with the substrat-binding site, as indicated by minimum energy values, **RR** percentage, the number of hydrogen bonds, and visual analysis of the resulting poses enhances our understanding of the interaction patterns. The resulting poses were analyzed visually to understand the interaction pattern. All results can be found in **Table 05** and **Figure 16**.

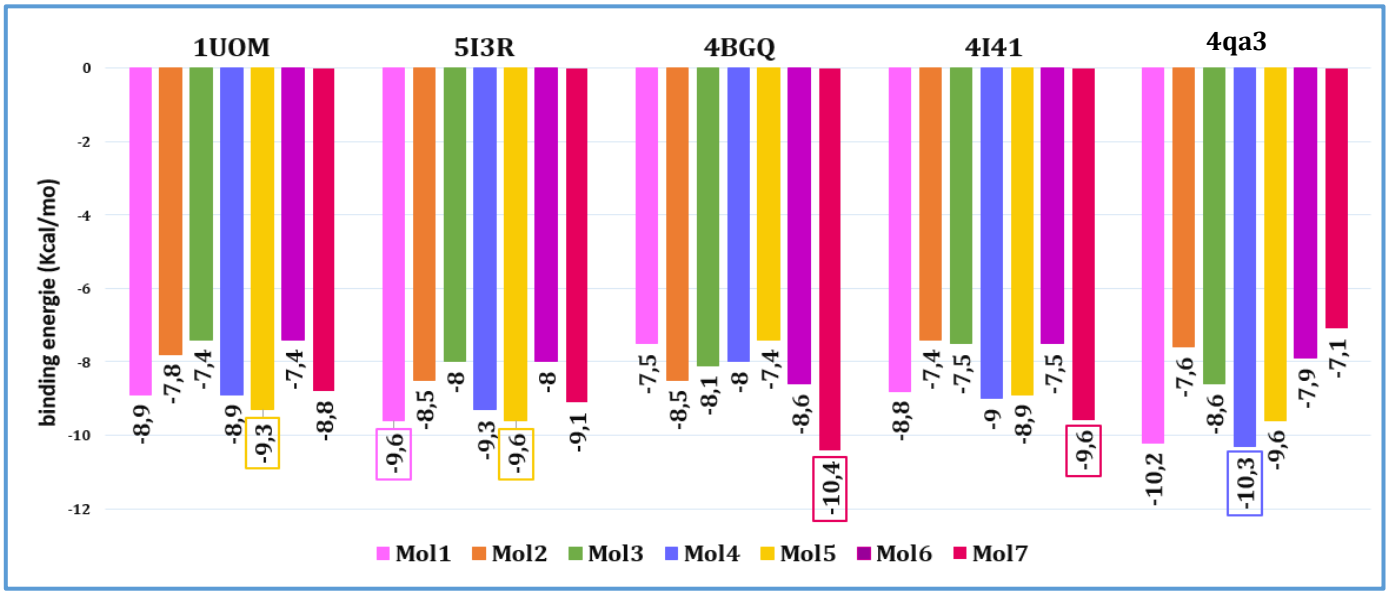

Figure 16 : Grouped histogram representation of binding energy values of the complex target-inhibitors

Table 05: Molecular docking results of the seven compounds against human osteosarcoma targets

Ligand	ΔG Affinity (kcal/mol)	Ki (µM) *	RR%	Closest residues	Hydrogen bonds / Length (Å)	Hydrophobic interactions
(PDB ID: 1uom)						
Pti	-11.5	$3.63*10^{-3}$	92	Ala350. Asp351. Trp383. Leu387. Met388. Leu391. Arg394. Phe404. Ile424. His524. Leu525. Leu536.	Leu387 (2.62); Arg394 (2.10)	Π-alkyl, alkyl, carbon, Π-Π T shaped
Mol1	-8.9	0.29	100	Met388. Leu378. Leu391. Phe404. Ala350. Asp351. Leu364. Leu525	/	Π-alkyl, Π-anion, Π-sulfur, Π-Π T shaped
Mol2	-7.8	1.88	100	Leu346. Ala350. Glu353. Leu387. Met388. Leu391. Phe404. Ile424.	Leu346 (2.40)	Π-alkyl, alkyl, carbon, Π-Π T shaped
Mol3	-7.4	3.71	100	Leu346. Leu349. Ala350. Glu353. Leu387. Arg394.	Glu353 (2.58; 2.78); Leu387 (2.32)	Π-alkyl, carbon
Mol4	-8.9	0.29	100	Leu346. Ala350. Asp351. Leu387. Met388. Leu391. Phe404. Leu525.	/	Π-alkyl, Π-anion, Π-sulfur, Π-Π T shaped
Mol5	-9.3	0.14	100	Leu346. Ala350. Asp351. Leu387. Met388. Leu391. Arg394. Phe404. Leu525.	Leu387 (2.34); Arg394 (2.33)	Π-alkyl, Π-anion, Π-sulfur, Π-Π T shaped
Mol6	-7.4	3.71	90	Leu346. Trp347. Leu349. Ala350. Asp351. Glu353. Leu387. Arg394. Leu525.	Leu387 (2.85); Glu353 (2.63; 3.04)	Π-alkyl, Π-anion, carbon
Mol7	-8.8	0.34	100	Ala350. Leu384. Leu387. Leu391. Phe404. Met421. His524. Leu525.	Phe404 (2.41)	Π-alkyl, Π-Π T shaped
(PDB ID: 5i3r)						
Idk	-10.8	$1.18*10^{-2}$	90	Leu57. Ala58. Val65. Ala77. Glu131. Cys133. Gln137. Lys182. Asn185. Leu187. Cys197.	Glu131 (2.63); Cys133 (2.05; 2.11) Gln137 (2.45; 2.59); Asn185 (2.00)	Π-alkyl, alkyl, carbon, Π-sulfur
Mol1	-9.6	$9.02* 10^{-2}$	100	Leu57. Ala58. Val65. Ala77. Lys79. Met130. Leu187. Cys197. Asp198.	Met130 (2.99)	Π-alkyl, Π-sulfur, Charge-charge
Mol2	-8.5	0.57	100	Leu57. Ala58. Val65. Ala77. Met130. Cys133. Gln137. Leu187. Cys197. Asp198.	Gln137 (2.69); Asp198 (1.98) Cys197 (2.97)	Π-alkyl, carbon, Π-sulfur
Mol3	-8.0	1.34	100	Leu57. Ala58. Val65. Ala77. Met130. Gly136. Gln137. Leu187. Cys197. Asp198.	Gln137 (2.57); Cys197 (2.72) Asp198 (2.25)	Π-alkyl, Π-sulfur, Π-sigma, carbon
Mol4	-9.3	0.14	100	Leu57. Ala58. Val65. Ala77. Lys79. Met130. Leu187. Cys197. Asp198.	Met130 (3.06)	Π-alkyl, Π-sulfur, Π-sigma, carbon
Mol5	-9.6	$9.02* 10^{-2}$	100	Leu57. Ala58. Gly60. Val65. Ala77. Met130. Glu131. Cys133. Leu187. Cys197. Asp198.	Glu131 (2.79); Cys133 (2.24)	Π-alkyl, Π-sulfur, Π-sigma, Charge-charge
Mol6	-8.0	1.34	100	Leu57. Ala58. Tyr132. Cys133. Leu187. Asp198.	Cys133 (1.91; 2.32); Asp198 (2.16)	Π-alkyl, Π-sigma

Mol7	-9.1	0.21	100	Leu57. Ala58. Gly60. Ser63. Val65. Ala77. Met130. Gln137. Leu187. Cys197.	Gly60 (2.66); Ser63 (2.53)	Π-alkyl, Π-sulfur, Carbon, Π-sigma
(PDB ID: 4bqg)						
50Q	-8.8	0.34	100	Asp93. Leu103. Leu107. Phe138. Tyr139. Val150. Trp162.	Asp93 (2.03)	Π-alkyl, alkyl, Π-sigma, Π-Π Stacked
Mol1	-7.5	3.13	80	Asn51. Ser52. Ala55. Asp93. Met98. Leu107. Phe138. Tyr139. Thr184.	Asn51 (2.15); Tyr139 (2.35) Thr184 (2.66)	Π-alkyl, Π-sulfur, Charge-charge
Mol2	-8.5	0.57	90	Asn51. Ala55. Met98. Leu107. Phe138. Trp162.	/	Alkyl, Π-sulfur, Π-sigma, carbon, Π-Π Stacked, Π-Π T shaped,
Mol3	-8.1	1.13	100	Asn51. Ser52. Ala55. Asp93. Met98. Leu107. Phe138. Tyr139. Val150. Trp162.	Asp93 (1.99; 2.95)	Π-alkyl, Π-sulfur, carbon, Π-Π Stacked
Mol4	-8.0	1.34	80	Asn51. Ser52. Ala55. Asp93. Met98. Leu107. Phe138. Val150. Trp162.	Asn51 (2.72); Ser52 (2.84)	Π-alkyl, Π-sulfur; carbon, Π-donor, Π-Π Stacked, Π-Π T shaped, amine-Π Stacked
Mol5	-7.4	3.71	100	Asn51. Ser52. Ala55. Asp93. Met98. Leu107. Phe138. Tyr139. Val150. Trp162. Thr184.	Asn51 (2.12); Asp93 (2.99) Thr184 (2.96)	Π-alkyl, Π-sulfur, Π-sigma, Charge-charge
Mol6	-8.6	0.48	90	Asn51. Ser52. Ala55. Asp93. Met98. Leu107. Phe138.	Asn51 (2.55); Asp93 (2.02; 2.78)	Π-alkyl, Π-sigma, carbon
Mol7	-10.4	$2.33* 10^{-2}$	100	Asn51. Ser52. Ala55. Asp93. Met98. Leu107. Phe138. Val150. Trp162.	Asp93 (2.07)	Π-alkyl, Π-sigma, Π-Π T shaped, Π-Π Stacked
(PDB ID: 4i41)						
Mix	-8.5	0.57	90	Phe49. Val52. Ala65. Ile104. Leu120. Glu171. Asn172. Leu174. Ile185. Asp186.	Asn172 (2.28); Asp186 (2.07)	Π-alkyl, carbon, Π-sigma, Π-Π Stacked
Mol1	-8.8	0.34	100	Gly45. Phe49. Val52. Ala65. Asp128. Phe130. Glu171. Ile185. Asp186.	/	Π-alkyl, carbon, Π-sigma, Π-anion, Π-Π Stacked, Π-Π T shaped,
Mol2	-7.4	3.71	100	Gly45. Phe49. Val52. Asp128. Glu171. Ile185	Asp128 (2.40)	Π-anion, carbon, Π-sigma, Π-Π Stacked
Mol3	-7.5	3.13	100	Phe49. Val52. . Lys67. Asp128. Glu171. Ile185.	Asp128 (2.13); Glu171 (2.03; 3.07)	Π-alkyl, Π-sigma, Π-Π Stacked
Mol4	-9.0	0.24	100	Val52. Alla65. Lys67. Asp128. Glu171. Leu174. Ile185.	Ile185 (2.52)	Π-anion, carbon, Π-sigma, Π-Π Stacked
Mol5	-8.9	0.29	100	Phe49. Val52. Ala65. Lys67. Ile104. Leu120. Asp128. Phe130. Asp131. Glu171. Ile185. Asp186.	Asp131 (1.97)	Π-alkyl, Π-sigma, Π-anion, Π-cation, Π-donor, Π-Π T shaped
Mol6	-7.5	3.13	100	Leu44. Phe49. Val52. Ala65. Lys67. Leu174. Ile185. Asp186.	Asp186 (2.05)	Π-alkyl, Π-sigma, Π-Π Stacked
Mol7	-9.6	$9.02*10^{-2}$	100	Leu44. Phe49. Val52. Ala65. Ile104. Leu120. Glu171. Leu174. Ile185.	Glu171 (2.45; 3.07)	Π-alkyl, Π-sigma, Π-Π T shaped

(PDB ID: 4qa3)						
tsn	**-7.1**	**6.16**	**100**	**Tyr100. Asp101. His142. Phe152. Asp178. His180. Phe208. Asp267.**	**Asp178 (2.15); Asp267 (2.17)**	**Π-alkyl, carbon, Π-sigma, Π-donor, Charge-charge, metal-acceptor, Π-Π T shaped**
Mol1	**-10.2**	**$3.27*10^{-2}$**	**90**	**Gly140. Trp141. Asp178. His180. Phe208. Asp267. Met274. Gly303. Gly304.**	**Gly140 (2.16)**	**Π-alkyl, Π-cation, Π-anion, Π-sulfur, Charge-charge, Π-Π Stacked**
Mol2	**-7.6**	**2.64**	**90**	**His143. His148. Gly151. Phe152. His180.**	**Gly151 (2.66)**	**Π-alkyl, Π-sigma, carbon, Π-Π Stacked, Π-Π T shaped,**
Mol3	**-8.6**	**0.48**	**90**	**Arg37. Trp141. His143. Phe152. His180. Gly303. Gly304. Trp306.**	**Arg37 (2.75); Gly303 (1.98)**	**Π-Π T shaped, Π-Π Stacked**
Mol4	**-10.3**	**$2.76*10^{-2}$**	**100**	**Gly140. Trp141. Asp178. His180. phe208. Asp267. Gly303. Gly304.**	**Gly140 (2.14)**	**Π-cation, Π-anion, Π-Π Stacked, amine-Π Stacked**
Mol5	**-9.6**	**$9.02*10^{-2}$**	**80**	**Trp141. Phe152. Cys153. His180. Gly303. Gly304. Phe208.**	**/**	**Π-cation, Π-sulfur, Π-Π Stacked**
Mol6	**-7.9**	**1.59**	**100**	**Gly140. Trp141. His142. His143. Phe152. Phe208. Gln263. Gly303. Gly304. Tyr306.**	**Gly140 (2.69); His142 (2.40) Gln263 (2.88; 3.10); Gly303 (2.61)**	**Acceptor-acceptor, Π-Π Stacked**
Mol7	**-7.1**	**6.16**	**80**	**His143. Tyr306.**	**/**	**Acceptor-Acceptor, Π-Π T shaped**

Colored aminoacids: represent the the catalytic and binding amino acids.
50Q: 5-(3,4-dichloro-phenoxy)-benzene-1,3- diol.
IDK: N-[6-(3-{[(cyclopropylmethyl)sulfonyl] amino} phenyl)-1H-indazol-3-yl] cyclopropanecarboxamide.
KI: Inhibitory constant. **$Ki = \exp^{(\Delta G \times 1000 / 1.986 \times 298)}$ Molar**
MIX: 1,4-dihydroxy-5,8-bis({2-[(2-hydroxyethyl) amino] ethyl} amino)-9,10-anthracenedione.
PTI: 2-phenyl-1-[4-(2-piperidin-1-yl-ethoxy)-phenyl]-1,2,3,4-tetrahydro-isoquinolin-6-OL.
RR%: repetition rate.
TSN: Trichostatin A.

Prior to conducting an analysis of our docking results, it is imperative that we accurately identify our selected human osteosarcoma targets in order to determine the particular mechanism of action of each ligand and to validate the outcomes obtained through our experimentation.

A. Estrogen Receptor (PDB ID 1UOM)

Estrogen reseptor (ER) is a nuclear hormone receptor. Plays a key role in the regulation of gene expression and affects cellular proliferation and differentiation in target tissues [145]. Also mediates membrane-initiated estrogen signaling involving various kinase cascades [146]. The active site of ERS is composed of a number of key AA residues that are critical for ligand binding and receptor activation and function. These residues include glutamine, aspartate, histidine, and arginine, which form hydrogen bonds and other interactions with their ligands [145]. As described in **Appendix 02.**

Upon targeting this receptor, the results indicate that all molecules were securely positioned within the substrate-binding site, both deeply and horizontally.

- **Coscinamide C (Mol5)**

Coscinamide C demonstrated the highest ranking with an energy of -9.3 kcal/mol, indicating a strong affinity and a RR of 100% (**Table 05**). The indole ring within **Mol5** exhibited the highest reactivity, being directed towards the binding site and interacting with 50% of the amino acids. Notably, it formed two hydrogen bonds with Leu387 and Arg394 and contributed to 83% of hydrophobic interactions (HIs), including interactions with Leu346, Ala350, Leu387, Leu391, Phe404, and Leu525. Out of the 14 favorable interactions observed, 12 were attributed to the indole ring, highlighting its significance in the preferred orientation within the active site. The position and characteristics of the indole ring played a critical role in the inhibitory mechanism, leading to enzyme stabilization. ·

- **Coscinamide A (Mol1)**

Ranked second, **Mol1** displayed an energy of -8.9 kcal/mol, indicating a strong affinity and a RR of 100% (**Table 05**). Similar to **Mol5**, the indole ring within **Mol1** exhibited the highest reactivity. It was oriented towards the binding site and interacted with 50% of the amino acids (AA) involved, forming 100% HIs. Out of the 12 favorable interactions observed, 11 were attributed to the indole ring, emphasizing its crucial role in the preferred orientation within the active site. The position and characteristics of the indole ring also played a critical role in the inhibitory mechanism. Furthermore, the nonpolar nature of the molecule facilitated additional HIs, resulting in enzyme stabilization.

- **Coscinamide B (Mol4)**

Coscinamide B exhibits the same docking position and results as **Mol1**. The indole ring, expected to have the most reactive function, interacts with 43% of the AA forming it, resulting in 12 interactions. It is also oriented towards the binding site, enabling 100% HIs without any hydrogen bonds. The hydrophobic interactions (HIs) primarily involve Leu346, Ala350, Leu387, Leu391, Phe404, and Leu525. The indole ring clearly plays a significant role in achieving optimal orientation within the active site. The nonpolar nature of the molecule further contributes to a high percentage of HIs, leading to enhanced stability.

- **Eudistomin Y1 (Mol7)**

Eudistomin Y1 achieved the third rank with an energy of -8.8 kcal/mol, indicating a high affinity and a RR of 100% (**Table 05**). The β-carboline ring within **Mol7** exhibited the highest reactivity. It interacted with 50% of the AA forming the binding site. Furthermore, it formed a hydrogen bond with Phe404, and 92% of the interactions were of a hydrophobic nature, involving Ala350, Leu384, Leu387, Leu391, Phe404, Met421, Ile424, His524, and Leu525. Notably, seven of these interactions were formed with the β-carboline ring, highlighting its importance in the inhibition mechanism of 1uom. Additionally, the nonpolar nature of the molecule contributed to the stability of the complex.

- **Leucettamine B (Mol2)**

Leucettamine B attained the fourth position with an energy of -7.8 kcal/mol, indicating a high affinity and a RR of 100% (**Table 05**). The most reactive component within **Mol2** was the imidazole ring, which interacted with 36% of the amino acids forming it, resulting in 7 interactions. Notably, it formed three hydrogen bonds with Leu346, Glu353, and Met388. Additionally, it maintained 70% HIs with Ala350, Leu387, Leu391, Phe404, and Ile424. While imidazole alkaloids might not exhibit the highest stability with regard to 1uom, they demonstrated a strong affinity for our enzyme.

- **Polyandrocarpamine A (Mol3)**

Polyandrocarpamine A achieved the fifth position with an energy of -7.4 kcal/mol, indicating a high affinity and a RR equal to 100% (**Table 05**). The 2-aminoimidazoline ring was oriented towards the binding site and interacted with 29% of the amino acids forming it, resulting in a total of seven interactions. Notably, four of these interactions involved hydrogen bonds formed with Leu346, Glu353, and Leu387. The remaining interactions involved HIs with LEU346, LEU349, ALA350, and LEU387, accounting for 50% of the interactions. Although the stability of 1uom was comparatively lower than that of other inhibitors, the presence of

nonpolar amino acids played a significant role in maintaining stability. This suggests that nonpolar inhibitors can trigger more HIs, which have an influence on the overall stability of the complex.

- **Dispacamide (Mol6)**

Dispacamide, similar to polyandrocarpamine A, exhibited identical docking results. The 2-aminoimidazole ring within dispacamide displayed the highest reactivity, being directed towards the catalytic site and interacting with 36% of the amino acids forming it. It formed five hydrogen bonds with Leu346, Thr347, Glu353, and Leu387, along with six HIs, accounting for 50%, involving Ala350, Leu349, Leu387, and Leu525. These interactions resulted in a total of 11 favorable interactions. Our findings suggest that marine alkaloids, including Dispacamide, demonstrated remarkable stability with 1uom due to the presence of nonpolar amino acids, particularly leucine and alanine, which played a crucial role in all ligands' docking, supported by HIs.

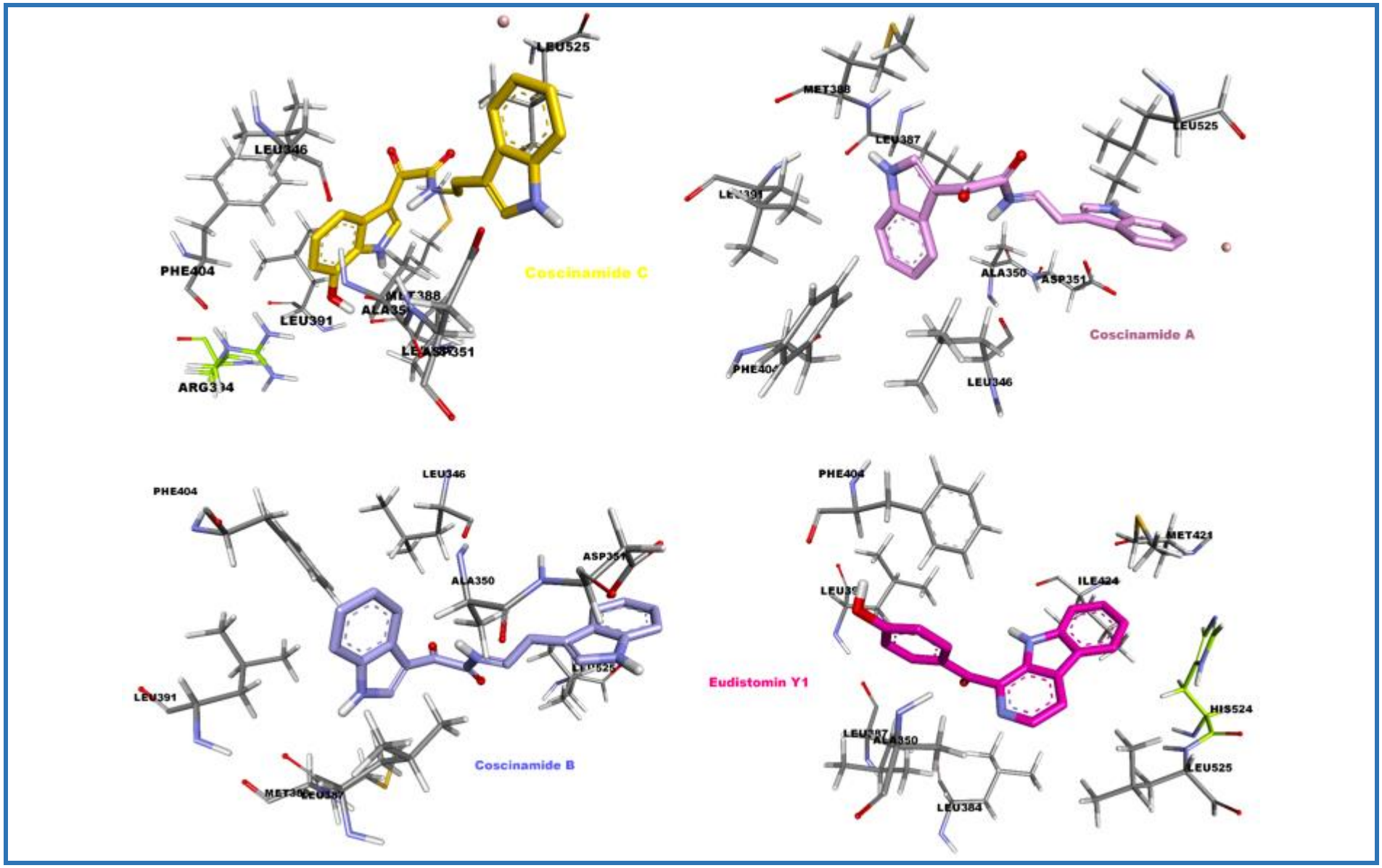

Figure 17 A: 3D structural interactions between the active site of Estrogen Receptor and the seven ligands. **1)** Coscinamide C **(Mol5)** 3D structure post docking is presented in sticks and colored in **yellow**. **2)** Coscinamide A **(Mol1)** 3D structure post docking is presented in sticks and colored in **light violet**. **3)** Coscinamide B **(Mol4)** 3D structure post docking is presented in sticks and colored in **light blue. 4)** Eudistomin Y1 **(Mol7)** 3D structure post docking is presented in sticks and colored in **dark pink.**

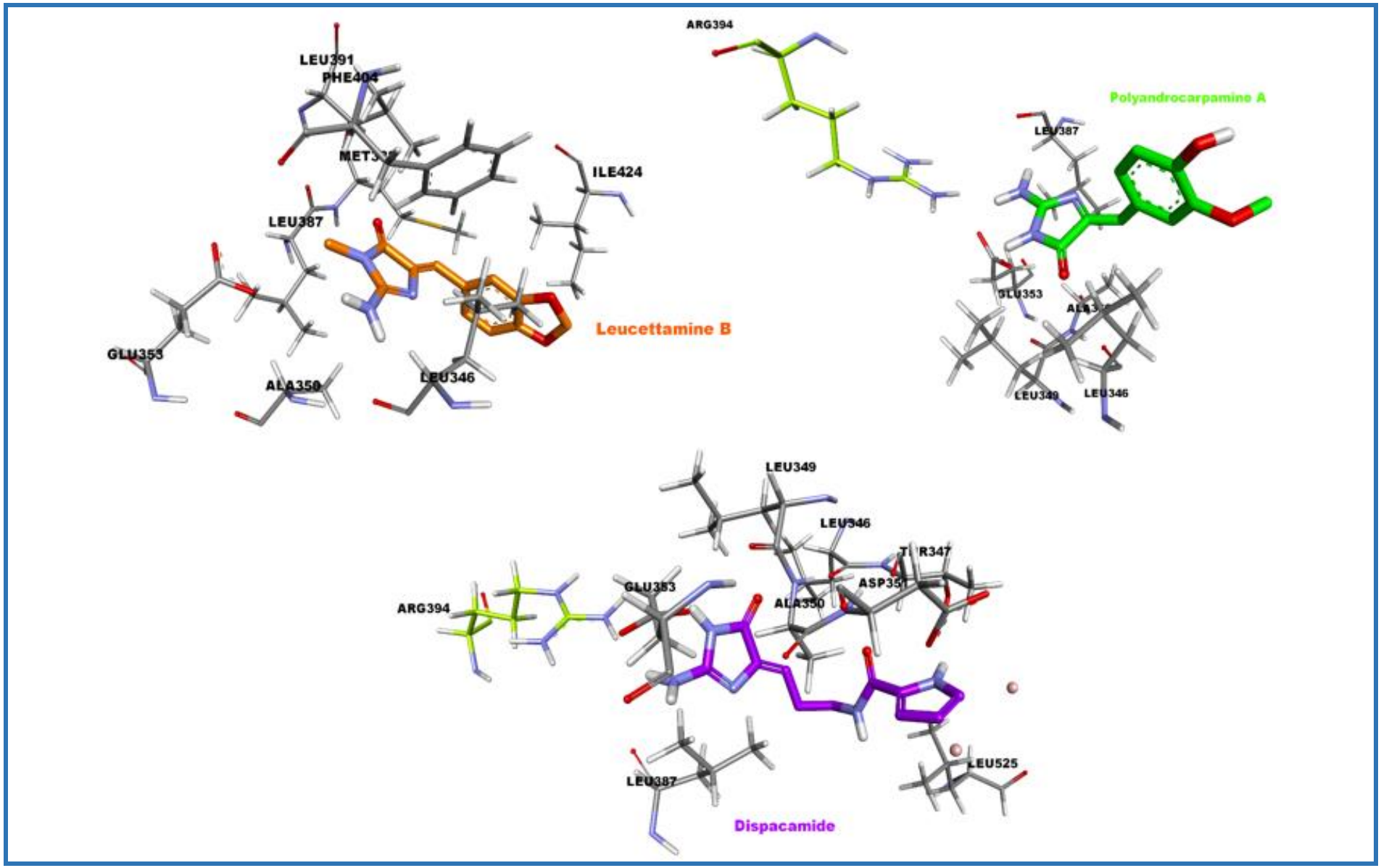

Figure 17 B: **5)** Dispacamide **(Mol6)** 3D structure post docking is presented in sticks and colored in **dark violet**. **6)** Leucettamine B **(Mol2)** 3D structure post docking is presented in sticks and colored in **orange**. **7)** Polyandrocarpamine A **(Mol3)** 3D structure post docking is presented in sticks and colored in **green**.

B. BMP-2-inducible protein kinase (PDB ID 5i3r)

BMP2K, or BMP-2-inducible protein kinase, is an enzyme in humans that is also found in mice and has kinase activity. BMP2 has so many roles in cardiogenesis, embryogenesis, neuronal growth, intramembranous and endochondral ossification, and is expressed in osteocytes and osteoblast cells. Binding to BMP type I and type II serine/threonine kinase receptors leads to the activation of several downstream signaling pathways along with upregulation of the BMP-2 gene. Once BMP-2 binds to the BMP receptor, phosphorylation of BMPRIa by BMPRII leads to adipogenesis, chondrogenesis, and osteogenesis, whereas phosphorylation of BMPRIb leads to apoptosis and cell death [147]. Composed of 2 sites, 1 is the catalytic site and the other is ATP site (**Appendix 02**).

- **Coscinamide A (Mol1)**

Coscinamide A achieved the top ranking, boasting an energy value of -9.6 kcal/mol and demonstrating a high affinity with a remarkable RR% of 100% (**Table 05**). The most reactive function was the indole ring; it was oriented to the binding site and interacted with 40% of the AAs, forming 83% of HIs with Leu57, Ala58, Val65, Ala77, Leu187, and Cys197. Among the 14 favorable interactions, 10 were formed with the indole ring, which is responsible for the most preferred orientation in the active site. The polarity of Mol1 resulted in more HIs and, therefore, more complex stability.

- **Coscinamide C (Mol5)**

Coscinamide C has similar docking outcomes as **Mol1** and shares similar characteristics. The most reactive functional group within Mol5 is directed towards the binding site. It binds with 40% of its AAs, forming two hydrogen bonds with Glu131 and Cys133 and 77% HIs, involving Leu57, Ala58, Val65, Ala77, Leu187, and Cys197. The indole ring forms 12 of the 15 favorable interactions, which determines its preferred orientation in the active site. while the molecule's polarity contributes to a high percentage of HIs, further stabilizing the enzyme.

- **Coscinamide B (Mol4)**

With an energy value of -9.3 kcal/mol, coscinamide B secured the second position in the ranking, signifying its high affinity with a remarkable RR% of 100% (**Table 05**). The most reactive function was also the indole ring, which interacted with 53% of the amino acids forming it, with 12 interactions; it was also oriented to the binding site, achieving 83% HIs with two hydrogen bonds with Lys79 and Met130. The high percentage of HIs was a result of the polarity of the molecule, and the position of the indole ring inside the active site ensured the best orientation.

- **Eudistomin Y1 (Mol7)**

Eudustomin Y1 was ranked third with an energy of -9.1 kcal/mol, and it also had a high affinity with a RR% of 100% (**Table 05**). We located the most reactive function in Mol7, which was the β-Carboline ring; it was directed to the binding site, interacted with 40% of the amino acids forming it, and formed four hydrogen bonds with Gly60, Ser63, Gln137, and Cys197. Also, 67% of the interactions were hydrophobic, with Leu57, Ala58, Val65, Ala77, Leu187, and Cys197. Among 15 favorable interactions, 10 were formed with the β-carboline ring, which makes it responsible for the best orientation and position inside the active site and also the inhibition mechanism.

- **Leucettamine B (Mol2)**

Leucettamine B was ranked fourth with an energy of -8.5 kcal/mol and a RR% of 100% (**Table 05**). The imidazole ring of Mol4 was the most reactive with 8 interactions, interacting with 53% of the amino acids forming it. It forms five hydrogen bonds with Cys133, Gln137, Cys197, and Asp198, and 58% HIs with Leu57, Ala58, Val65, Ala77, Leu187, and Cys197. Imidazole alkaloids might not be the preferred type even with high stability to 5i3r, but they can be considered moderate inhibitors.

- **Polyandrocarpamine A (Mol3)**

Polyandrocarpamine A attained the fifth position in the ranking, exhibiting an energy value of -8.0 kcal/mol and showcasing a high RR% of 100% (**Table 05**). The 2-aminoimidazoline ring serves as the most reactive functional group, being oriented towards the binding site and interacting with 47% of the amino acids forming the site. This interaction led to the formation of a total of thirteen interactions, including four hydrogen bonds with Gly136, Gln137, Cys197, and Asp198. The remaining interactions comprised 55% HIs involving Leu57, Ala58, Val65, and Ala77. The decreased HIs is explained by the polarity of the molecule; a polar molecule will produce less HIs and, as a result, decrease the stability of the complex.

- **Dispacamide (Mol6)**

Dispacamide shares the same docking results as Mol3. The most reactive function of Mol6 was the 2-aminoimidazole ring, which was directed to the catalytic site and interacted with 40% of the amino acids forming it, formed four hydrogen bonds with Tyr132, Cys133, and Asp198, and had 38% HIs with Leu57, Ala58, and Leu187. Mol2, Mol3, and Mol6 all belong to the imidazole class of alkaloids, which we think explains the low affinity.

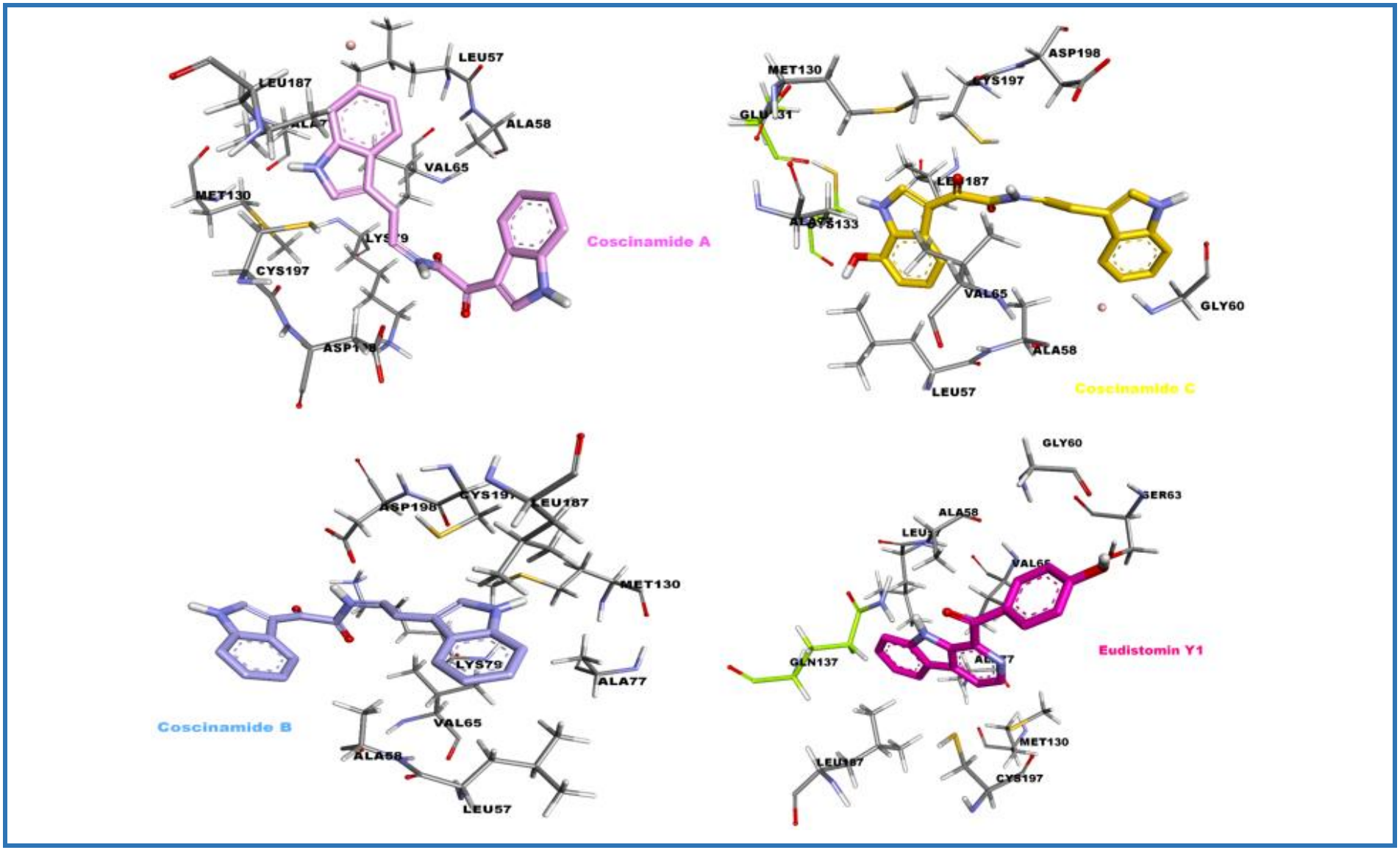

Figure 18 A: 3D structural interaction between the active site of BMP-2-inducible protein kinase (**PDB ID 5i3r**) and the seven ligands. **1)** Coscinamide A **(Mol1)** 3D structure post docking is presented in sticks and colored in **light violet.** **2)** Coscinamide C **(Mol5)** 3D structure post docking is presented in sticks and colored in **yellow**. **3)** Coscinamide B **(Mol4)** 3D structure post docking is presented in sticks and colored in **light blue**. **4)** Eudistomin Y1 **(Mol7)** 3D structure post docking is presented in sticks and colored in **dark pink.**

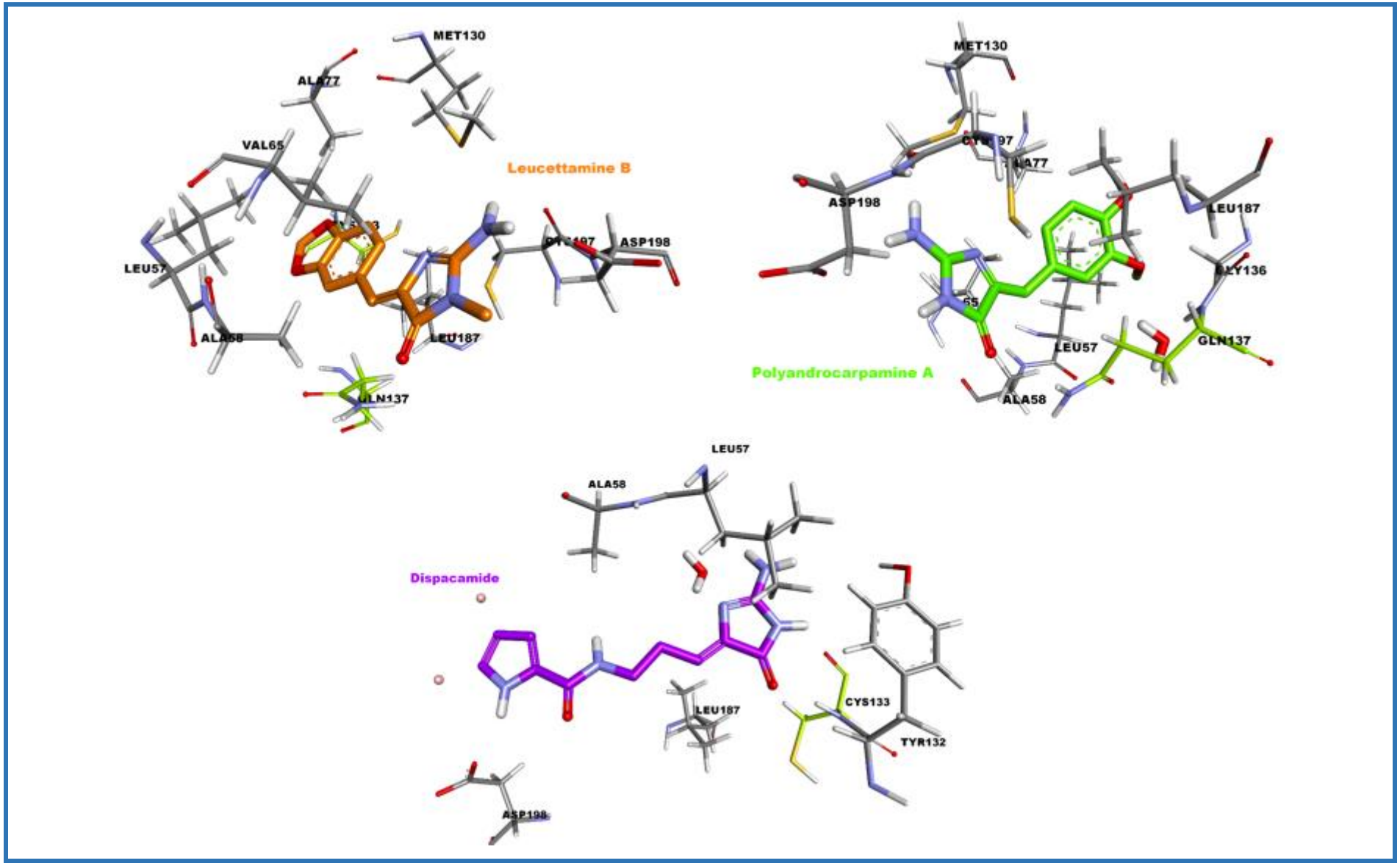

Figure 18 B: **5)** Leucettamine B **(Mol2)** 3D structure post docking is presented in sticks and colored in **orange**. **6)** Polyandrocarpamine A **(Mol3)** 3D structure post docking is presented in sticks and colored in **green**. **7)** Dispacamide **(Mol6)** 3D structure post docking is presented in sticks and colored in **dark violet.**

C. Heat Shock Protein 90 (PDB ID 4BQG)

Hsp90 is an ATP-dependent molecular chaperone that is vital for the conformational maturation, structural maintenance, stability, and function of several oncogenic proteins involved in tumor generation and progression, including p53 mutants [148.149]. Hsp90 performs its function by binding an ATP to its adenine-binding pocket, which is located in the N-terminal domain of the protein, as illustrated in **Appendix 02** [149.150.151]. Therefore, natural inhibitors targeting this pocket can effectively suppress tumors by disrupting multiple oncogenic pathways at once due to Hsp90 dysfunction [149.150].

For HSP90, the molecules were docked in the ATP binding site and were fixed deeply and horizontally into it, except Mol1, Mol4, and Mol5, which were fixed deeply but vertically, resulting in blocking it completely.

- **Eudistomin Y1 (Mol7)**

Eudistomin Y1 was ranked first with an energy of -10.4 kcal/mol and had a high affinity with a RR% of 100% (**Table 05**). The most reactive function was the β-carboline ring; it was directed to the binding site, interacted with 50% of the amino acids forming it, and formed one hydrogen bond with Asp93. 92% of the interactions were of the hydrophobic type (10 in terms of numbers), with Asn51, Ala55, Met98, Leu107, Phe138, Val150, and Trp162 being formed with the β-carboline ring, suggesting its importance in the inhibition mechanism. The polarity of Mol7 triggered more HIs (92%) which led to high stability of the inhibition complex.

- **Dispacamide (Mol6)**

Dispacamide was ranked second with an energy of -8.6 kcal/mol and also had a high affinity with a RR% of 90% (**Table 05**). The most reactive function was the 2-aminoimidazole ring, which was directed to the catalytic site and interacted with 50% of the amino acids forming it and formed seven favorable interactions: three hydrogen bonds with Asn51 and Asp93 and 57% HIs with Ala55, Met98, Leu107, and Phe138. The presence of nonpolar amino acids such as leucine and alanine helped the marine alkaloids exhibit high stability.

- **Leucettamine B (Mol2)**

Leucettamine B secured the third rank with an energy value of -8.5 kcal/mol and a notable RR% of 90% (**Table 05**). Among the functional groups present, the imidazole ring of Mol2 demonstrated the highest reactivity, engaging in a total of seven interactions. This imidazole ring formed interactions with 41% of the amino acids constituting the site. Notably, it established one hydrogen bond with Asn51 and displayed 83% HIs with Ala55, Leu107, Phe138, and Trp162.

- **Polyandrocarpamine A (Mol3)**

Polyandrocarpamine A was ranked fourth with an energy of -8.1 kcal/mol and an RR% of 100% (**Table 05**). The main function of Mol3 is the 2-aminoimidazoline ring, which was pointed to the binding site and interacted with only 25% of the amino acids forming it. It formed a total of nine interactions, three of which were hydrogen bonds with Asp93 and Tyr139. The rest of the interactions were 38% hydrophobic, with Leu107, Phe138, and Val150. Mol3 is a polar inhibitor; the polarity led to fewer HIs (38%), resulting in decreased stability compared to other inhibitors.

- **Coscinamide B (Mol4)**

Coscinamide B was ranked fifth with an energy of -8.0 kcal/mol and a RR% of 80% (**Table 05**). The main function of Mol4 was the indole ring; it was oriented to the binding site with 59% HIs, which is 10 interactions with Asn51, Ser52, Ala55, Leu107, Phe138, Val150, and Trp162. Among the 18 favorable interactions, 14 were formed with the indole ring, which also interacted with 50% of the amino acids forming it, which shows that it is responsible for the most preferred orientation in the active site.

- **Coscinamide A (Mol1)**

Coscinamide A was ranked sixth with an energy of -7.5 kcal/mol and a RR% of 80% (**Table 05**). The most reactive function in Mol1 is the same as that in Mol4 because they belong to the same group. The ring was oriented to the binding site and interacted with 50% of the amino acids, forming 63% HIs, including 9 interactions with Asn51, Ser52, Ala55, Met98, Leu107, and Phe138. Among the 17 favorable interactions, 12 were formed with the indole ring, which is responsible for the most preferred orientation in the active site. The polarity of coscinamide A helped to centralize it next to the hydrophobic amino acids.

- **Coscinamide C (Mol5)**

Coscinamide C was ranked seventh and last among the other inhibitors with an energy of -7.4 kcal/mol and a RR% of 100% (**Table 05**). Even though it was ranked last, there is no major difference with Mol1. The most reactive function in Mol5 is the same as in other family members. The ring was directed to the binding site and interacted with 50% of the amino acids forming it, forming six hydrogen bonds with Asn51, Asp93, Trp162, and Thr184 and 61% HIs, which means eleven interactions with Asn51, Ser52, Ala55, Met98, Leu107, Phe138, Val150, and Trp162. Among the 19 favorable interactions, 14 were formed with the indole ring, which made it responsible for the most preferred orientation in the active site. The polarity of Mol5 helped the molecule centralize next to the hydrophobic AAs.

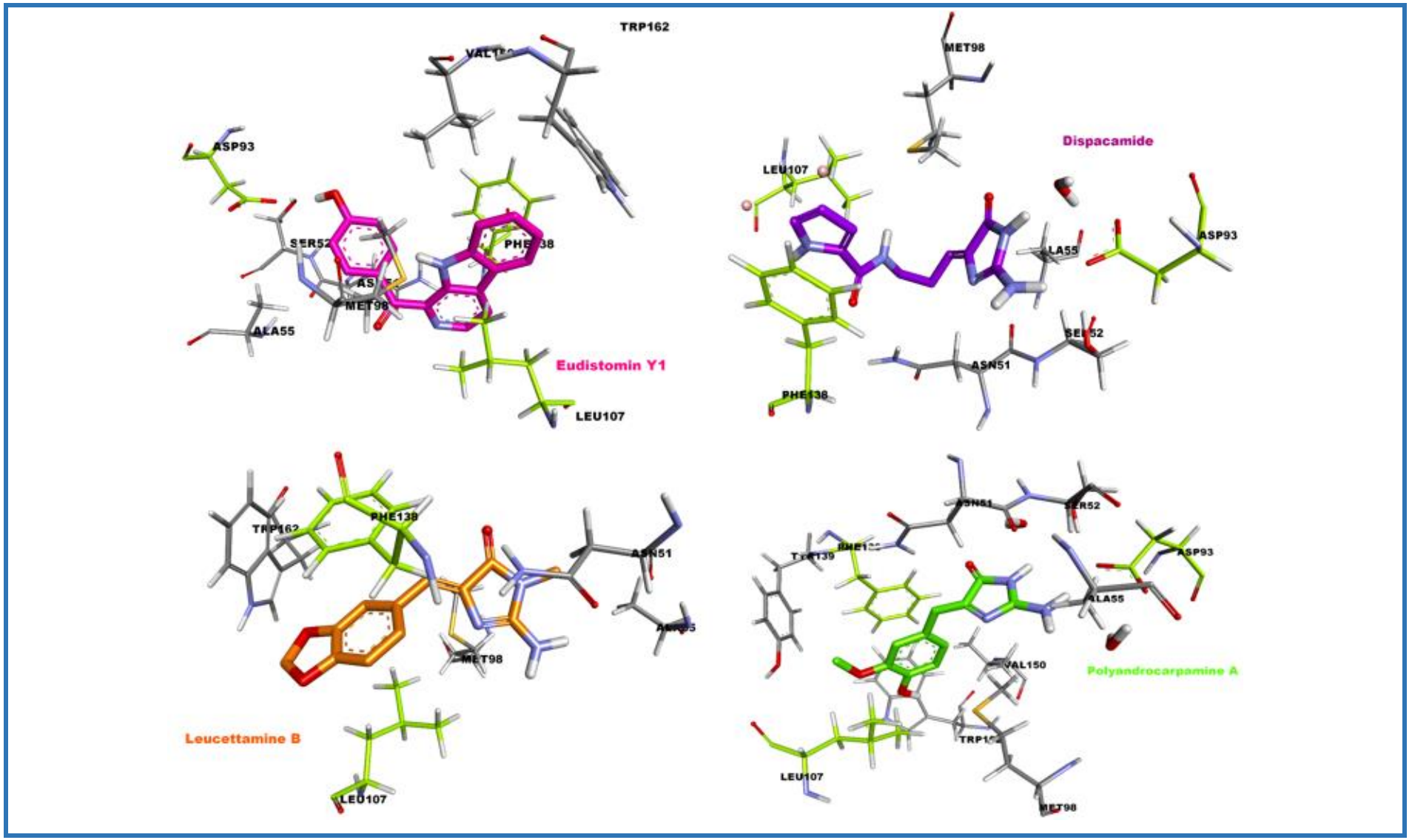

Figure 19 A: 3D structural interaction between the active site of Heat Shock Protein 90 (**PDB ID 4BQG**) and the seven ligands. **1)** Eudistomin Y1 **(Mol7)** 3D structure post docking is presented in sticks and colored in **dark pink.** **2)** Dispacamide **(Mol6)** 3D structure post docking is presented in sticks and colored in **dark violet.** **3)** Leucettamine B **(Mol2)** 3D structure post docking is presented in sticks and colored in **orange**. **4)** Polyandrocarpamine A **(Mol3)** 3D structure post docking is presented in sticks and colored in **green**.

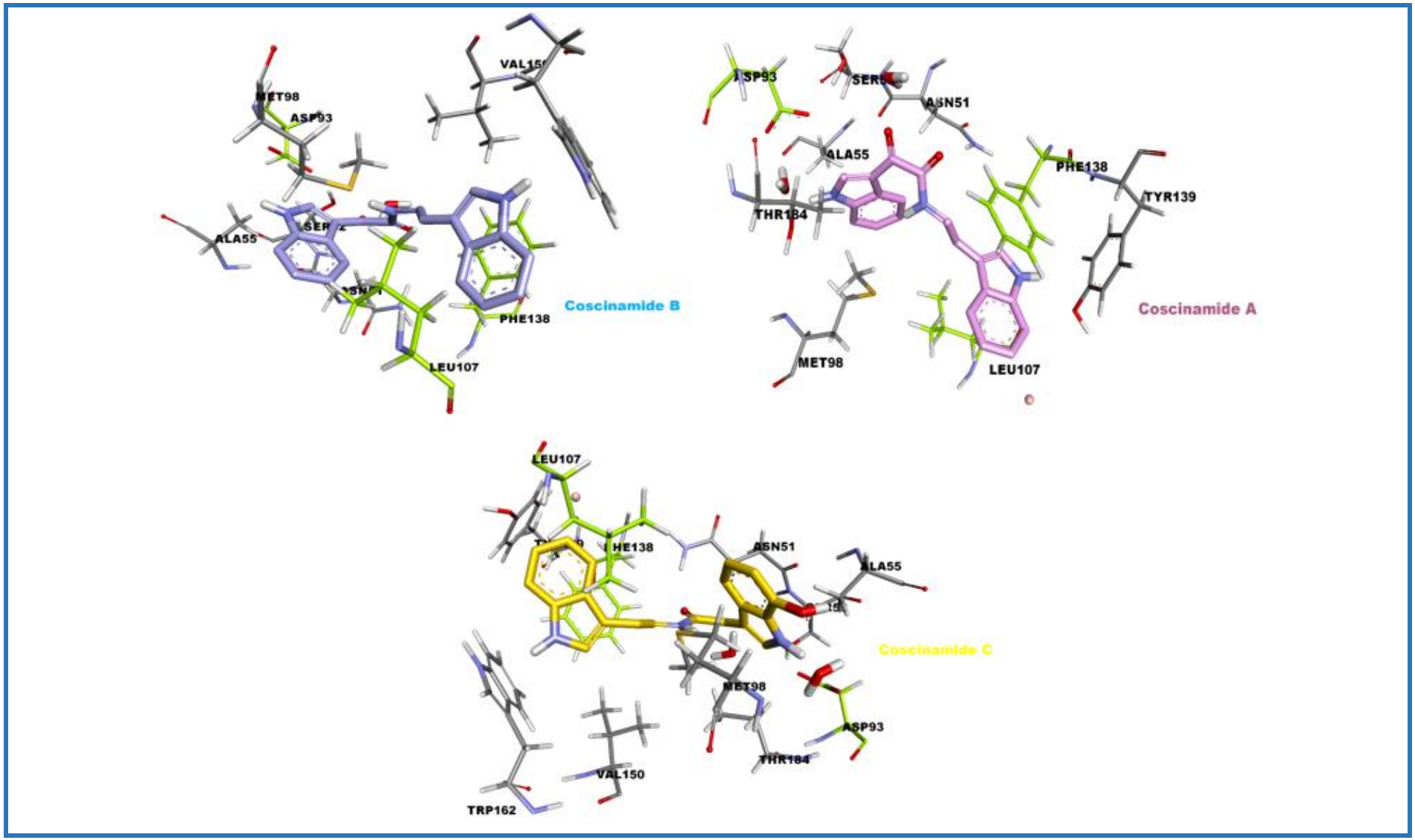

Figure 19 B:.**5)** Coscinamide B **(Mol4)** 3D structure post docking is presented in sticks and colored in **light blue. 6)** Coscinamide A **(Mol1)** 3D structure post docking is presented in sticks and colored in **light violet. 7)** Coscinamide C **(Mol5)** 3D structure post docking is presented in sticks and colored in **yellow**.

D. Serine/threonine-protein kinase pim-1 (PDB ID 4i41)

Pim1 is a serine/threonine kinase that participates in various biological functions, such as cell transformation, proliferation, and the ability to prolong cell survival. Additionally, Pim1 has two active sites, including an ATP-binding site and a substrate-binding pocket; these sites are illustrated in **Appendix 02** [152.153.154]. Pim1 differs from other protein kinases due to a unique conformation of Pro123 in the hinge region (residues 121–126), which hinders the establishment of a regular hydrogen bond between the adenine group of ATP and the specific pocket [152.154]. Therefore, any malfunctions in this interaction lead to Pim1 dysfunction [154].

- **Eudistomin Y1 (Mol7)**

Eudistomin Y1 demonstrated superior performance in the study, exhibiting an energy of -9.6 kcal/mol and a remarkable affinity with a RR% of 100% (**Table 05**). The β-carboline ring displayed the highest reactivity towards the binding site and establishing interactions with 64% of the AAs. With 16 favorable interactions, including two hydrogen bonds with Glu171. Furthermore, the majority of interactions (88%) were of a hydrophobic nature, encompassing 14 interactions with Leu44, Phe49, Val52, Ala65, Ile104, Leu120, Leu174, and Ile185. These interactions played a pivotal role in ensuring the overall stability of Eudistomin Y1.

- **Coscinamide B (Mol4)**

Coscinamide B achieved the second rank in terms of energy, exhibiting a value of -9.0 kcal/mol with a RR% of 100% (**Table 05**). The indole group, which serves as its primary reactive function, was directed towards the binding site and established interactions with 55% of the AAs constituting the site. Additionally, it engaged in 89% OF HIs with Val52, Ala65, Lys67, Leu174, and Ile185. Among the 13 favorable interactions observed, 10 were specifically formed with the indole ring. The combination of a high percentage of HIs and a substantial number of favorable interactions involving the primary ring suggests its preferred orientation.

- **Coscinamide C (Mol5)**

Coscinamide C attained the third position in terms of energy, boasting a value of -8.9 kcal/mol with a RR% of 100% (**Table 05**). Similarly, to other members of its family, Mol5 features an indole ring as its functional group. It was directed towards the binding site and established interactions with 55% of the AAs. Notably, it formed two hydrogen bonds with Asp131 and Ile185. It exhibited 77% HIs, forming ten interactions with Val52, Ala65, Lys67, Ile104, Leu120, Phe130, Leu174, and Ile185. Overall, 17 favorable interactions were observed, with 12 of them involving the indole ring. The significant number of interactions, combined

with the molecule's polarity, indicates the crucial role in maintaining the stability of the complex.

- **Coscinamide A (Mol1)**

Coscinamide A secured the fourth position with an energy value of -8.8 kcal/mol and a remarkable RR% of 100% (**Table 05**). Similar to its counterparts, Mol1 belongs to the same family, thus featuring the indole ring as its most reactive functional group. The indole ring was directed towards the binding site interacting with 55% of the AAs constituting the site. Notably, 80% of HIs, with Val52, Ala65, Phe49, Phe130, and Ile185, and two hydrogen bonds with Gly45 and Asp186. Among the 14 interactions, nine were specifically formed with the indole ring. The position and characteristics of the last, along with the molecule's polarity, played a critical role in the mechanism of enzyme inhibition and stabilization.

- **Polyandrocarpamine A (Mol3)**

Polyandrocarpamine A was ranked fifth with an energy of -7.5 kcal/mol, it had a moderate affinity with a RR% of 100% (**Table 05**). 2-Aminoimidazoline ring which is the main function group was pointed to the binding site and interacted with 36% of the AAs forming in total eight interactions, three of them were hydrogen bonds with Asp128 and Glu171. The rest of the interactions were hydrophobic type (63%) with Phe49, Val52, Lys67 and Ile185. The polarity of Mol3 (Polar) played a major role in decreasing the stability by lowering the number of HIs.

- **Dispacamide (Mol6)**

Dispacamide was also ranked fifth and it shares the same docking results with Mol3. The most reactive function of Mol6 was the 2-Aminoimidazole ring, which was directed to the catalytic site and interacted with 55% of the AAs forming it resulting two hydrogen bonds with Lys67 and Asp186 and seven HIs (70%) with Leu44, Phe49, Val52, Ala65, Leu174 and Ile185. The polarity played a role in increasing the stability by increasing the number of HIs (70%).

- **Leucettamine B (Mol2)**

Leucettamine B obtained the last ranking, exhibiting an energy value of -7.4 kcal/mol and a RR% of 100% (**Table 05**). The imidazole ring was the most reactive, interacting with 36% of the AAs forming it, forming two hydrogen bonds with Gly45 and Asp128 and 60% HIs with Phe49, Val52, and Ile185. Imidazole alkaloids might not be the preferred type to ensure inhibition, but the polarity of the molecule and the position of the imidazole ring in this case showed some potential. Notably, Mol3, Mol6, and Mol2 all belong to the imidazole class of alkaloids, which we speculate may explain their observed low affinity.

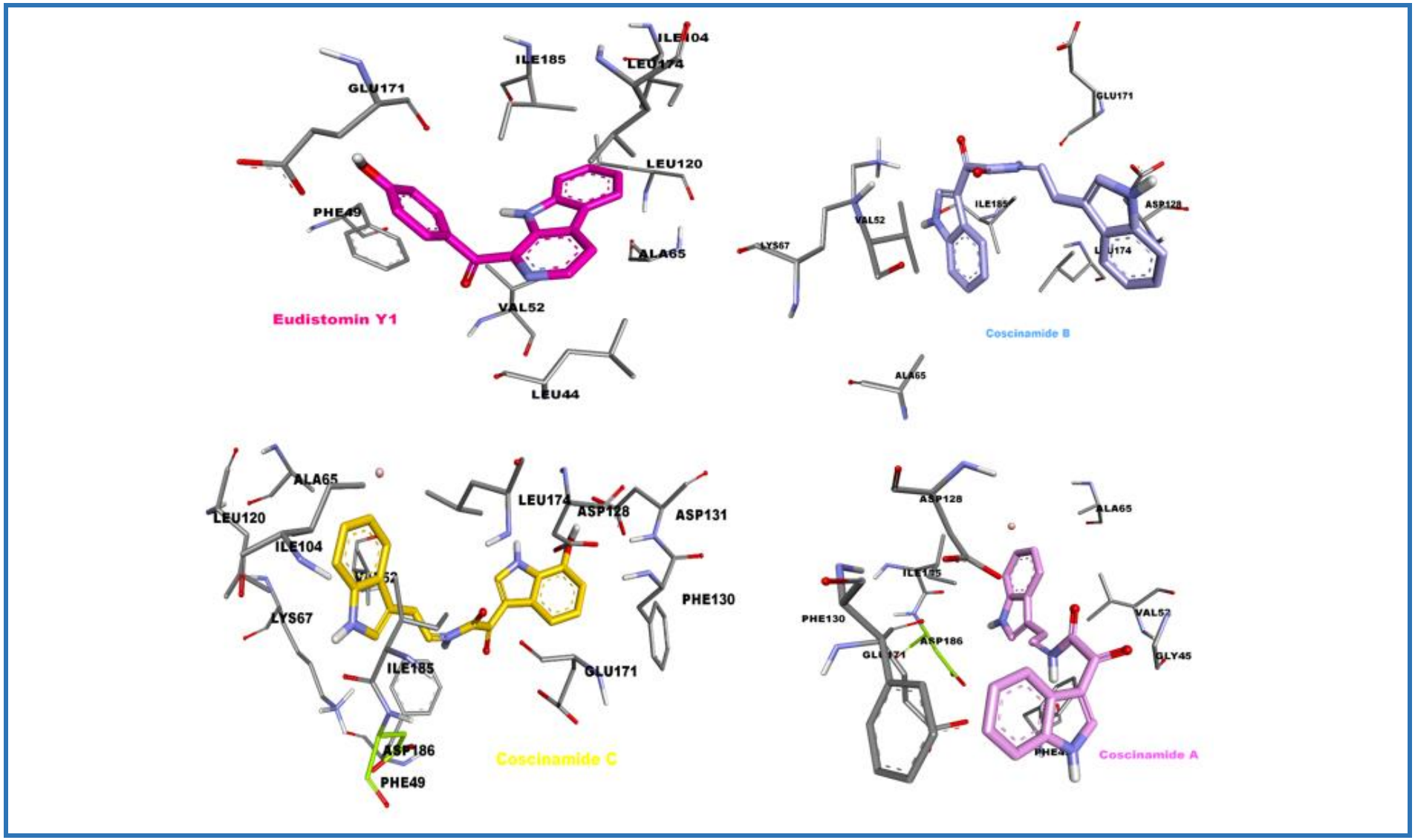

Figure 20 A: 3D structural interaction between the active site of Serine/threonine-protein kinase pim-1 **(PDB ID 4I41)** and the seven ligands. **1)** Eudistomin Y1 **(Mol7)** 3D structure post docking is presented in sticks and colored in **dark pink. 2)** Coscinamide B **(Mol4)** 3D structure post docking is presented in sticks and colored in **light blue**. **3)** Coscinamide C **(Mol5)** 3D structure post docking is presented in sticks and colored in **yellow**. **4)** Coscinamide A **(Mol1)** 3D structure post docking is presented in sticks and colored in **light violet.**

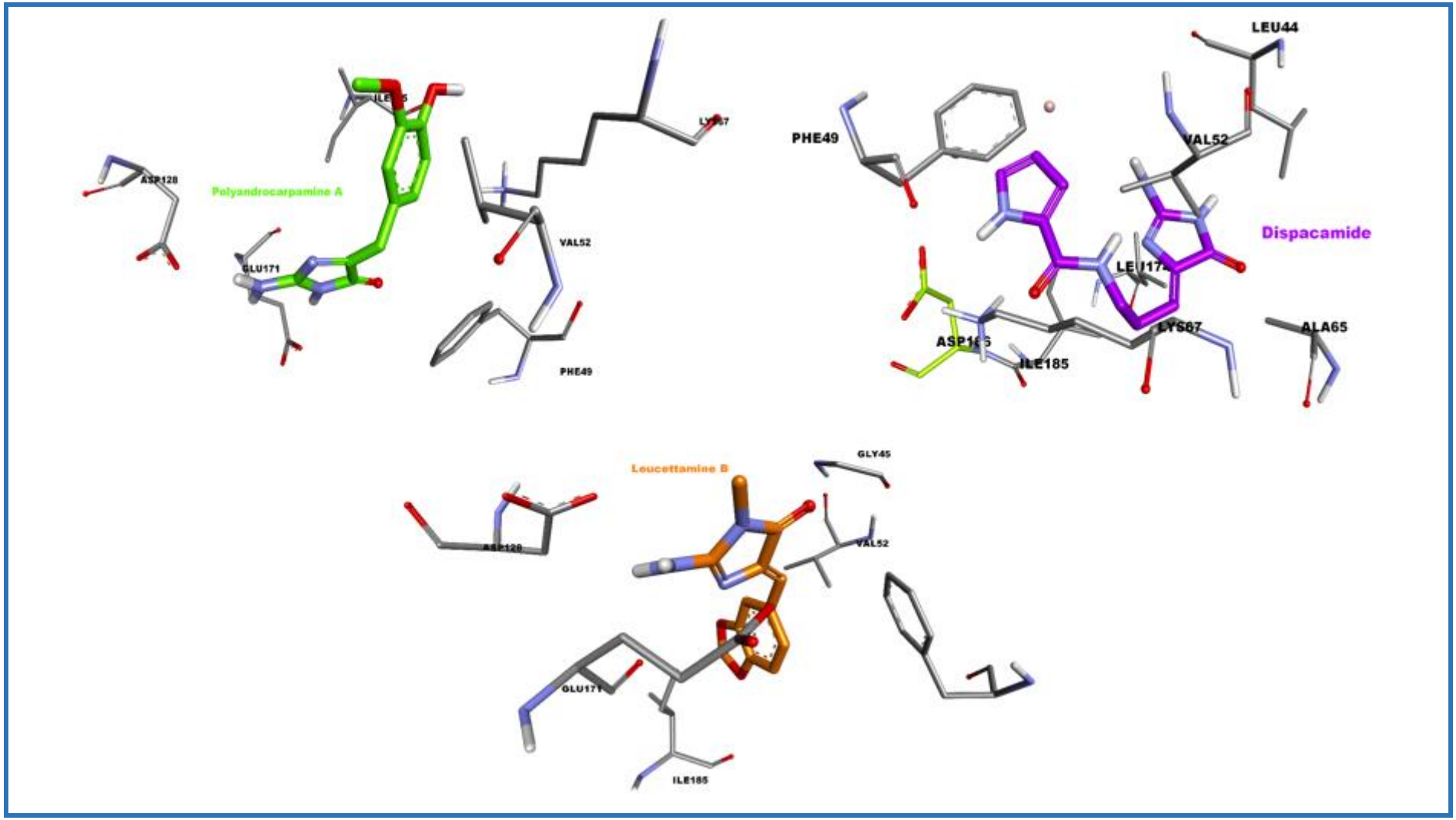

Figure 20 B: 5) Polyandrocarpamine A **(Mol3)** 3D structure post docking is presented in sticks and colored in **green**. **6)** Dispacamide **(Mol6)** 3D structure post docking is presented in sticks and colored in **dark violet**. **7)** Leucettamine B **(Mol2)** 3D structure post docking is presented in sticks and colored in **orange**.

E. Histone deacetylase 8 (PDB ID 4qa3)

Metal-dependent Histone deacetylase 8 (HDAC8) is a hydrolase that catalyzes the deacetylation of lysine residues on the N-terminal part of the core histones (H2A, H2B, H3, and H4) and non-histone protein substrates [155.156.157]. Plays an important role in the regulation of chromatin remodeling, gene transcriptional regulation, cell cycle progression, and proliferation [157.158]. Additionally, HDAC8 has more than six binding sites; the most important are the substrate binding and catalyc pocket (**Appendix 02**).

- **Coscinamide B (Mol4)**

Coscinamide B achieved the top rank with an energy of -10.3 kcal/mol, demonstrating a high affinity with a RR=100% (**Table 05**). The indole ring within the structure of **Mol4** exhibited the highest reactivity. It was directed towards the binding site and interacted with 60% of the amino acids forming it. Furthermore, it engaged in 80% HIs with Trp141, Phe208, Gly303, and Gly304. Out of the 14 favorable interactions observed, 9 were attributed to the indole ring, highlighting its crucial role in the preferred orientation within the active site. Additionally, the polarity of Coscinamide B contributed to an increased number of HIs, resulting in greater stability of the complex.

- **Coscinamide A (Mol1)**

Coscinamide A attained the second position with an energy of -10.2 kcal/mol, demonstrating a high affinity with a 90% RR percentage (**Table 05**). Being a member of the same group as **Mol4, Mol1** exhibited the indole ring as the most reactive functional group, it was directed towards the binding site and interacted with 70% of the AAs forming it, engaging in 80% HIs (8 interactions) with Trp141, Phe208, and Gly303. Out of the 15 favorable interactions observed, 10 were formed with the indole ring, establishing its crucial role in the preferred orientation within the active site. The high percentage of HIs was facilitated by the non-polar nature of the molecule, contributing to the overall stability of the complex.

- **Coscinamide C (Mol5)**

Coscinamide C obtained the third position with an energy of -9.6 kcal/mol, indicating a high affinity with an RR of 80%. Similarly, Mol5 exhibited the indole ring as the reactive functional group. wish interacted with 50% of the amino acids forming the binding site, engaging in HIs without forming any hydrogen bonds. Among the 11 favorable interactions, 10 involved the indole ring, highlighting its significance in achieving the preferred orientation within the active site, and the polarity of the molecule played a role in stabilizing the enzyme.

- **Polyandrocarpamine A (Mol3)**

Polyandrocarpamine A ranked fourth with an energy of -8.6 kcal/mol, demonstrating high affinity with a 90% RR percentage. The primary ring in **Mol3** is the 2-aminoimidazoline ring, which was oriented towards the binding site and interacted with 50% of the AAs. It formed a total of ten interactions, including four hydrogen bonds with Arg37, His180, Gly303, and Gly304. The remaining 60% of HIs, involving Trp141, His143, Phe152, His180, and Tyr306. The decrease in the percentage of HIs can be attributed to the polarity of the molecule, which consequently impacted the stability of the complex.

- **Dispacamide (Mol6)**

Dispacamide achieved the fifth rank with an energy of -7.9 kcal/mol and a 100% RR percentage. The 2-aminoimidazole ring exhibited the highest reactivity in **Mol6**, being directed towards the catalytic site and interacting with 50% of the AAs involved in its formation. It formed six hydrogen bonds with Gly140, His142, His143, Gln263, and Gly303, along with five HIs comprising 42% of the total percentage, involving Trp141, Phe152, Phe208, Gly303, and Gly304. The decreased percentage of HIs can be attributed to the presence of a low number of non-polar amino acids, such as leucine, alanine, and valine, resulting in lower stability.

- **Leucettamine B (Mol2)**

Leucettamine B attained the sixth position with an energy of -7.6 kcal/mol and a 90% RR percentage (**Table 05**). The imidazole ring in **Mol2** exhibited the highest reactivity, engaging with 35% of the amino acids involved in its formation through seven interactions. It formed two hydrogen bonds with His142 and Gly151, along with 71% HIs involving His142, His143, Phe152, and His180. Although imidazole alkaloids may not be the preferred type, the significant proportion of HIs contributed to the overall stability of the compound.

- **Eudistomin Y1 (Mol7)**

Eudistomin Y1 was ranked seventh and last among the inhibitors, with an energy of -7.1 kcal/mol and an RR percentage of 80%, according to the **Table 05**. The β-carboline ring in **Mol7** displayed the highest reactivity, interacting with 40% of the amino acids involved in its formation. However, no hydrogen bonds were formed, indicating that all interactions were exclusively of the hydrophobic type. Notably, none of these interactions were formed with the β-carboline ring itself, suggesting that it did not play a significant role in the orientation within the active site. These findings indicate that β-Carboline alkaloids may not possess sufficient affinity towards this specific target.

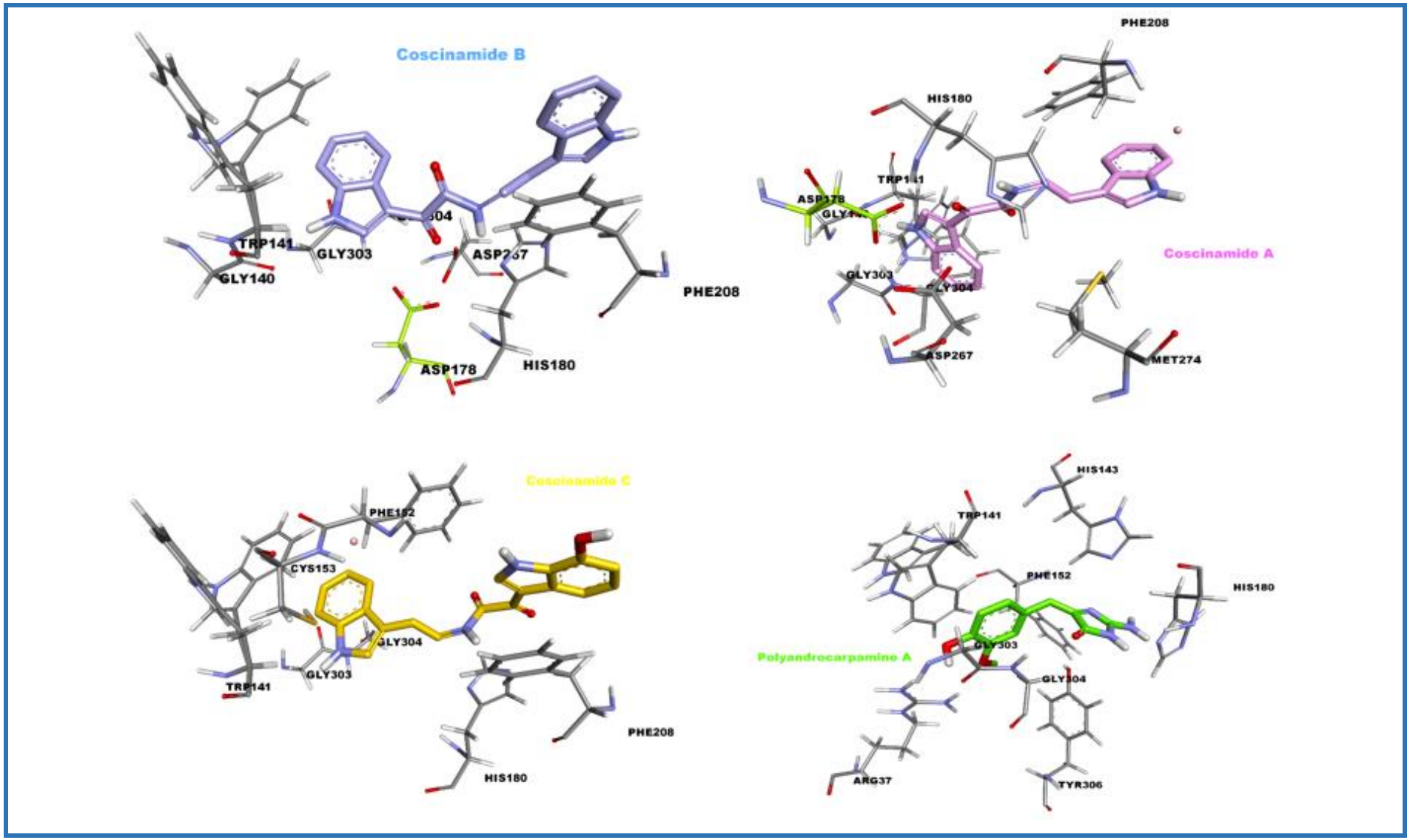

Figure 21 A: 3D structural interaction between the active site of the Histone deacetylase 8 **(PDB ID: 4QA3)** and the seven ligands. **1)** Coscinamide B **(Mol4)** 3D structure post docking is presented in sticks and colored in **light blue**. **2)** Coscinamide A **(Mol1)** 3D structure post docking is presented in sticks and colored in **light violet.** **3)** Coscinamide C **(Mol5)** 3D structure post docking is presented in sticks and colored in **yellow**. **4)** Polyandrocarpamine A **(Mol3)** 3D structure post docking is presented in sticks and colored in **green**.

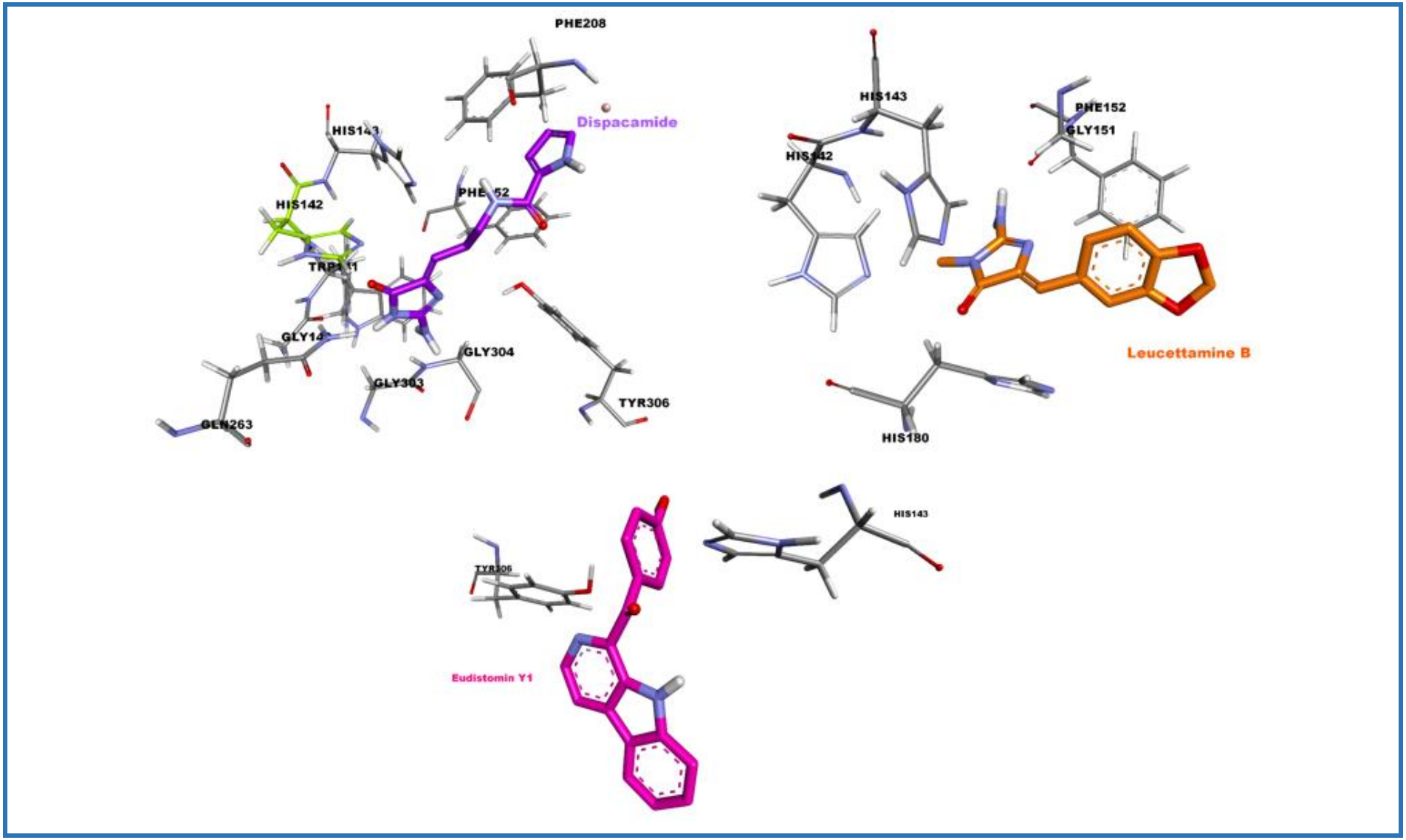

Figure 21 B: **5)** Dispacamide **(Mol6)** 3D structure post docking is presented in sticks and colored in **dark violet**. **6)** Leucettamine B **(Mol2)** 3D structure post docking is presented in sticks and colored in **orange**. **7)** Eudistomin Y1 **(Mol7)** 3D structure post docking is presented in sticks and colored in **dark pink.**

In order to gain a better understanding of the molecular docking result and the energies bounds, it is imperative to compare the best ligand outcomes, such as the binding energy and closest residues, with those of original ligand in each target, this approach enables a study of the specific binding mechanism, thereby providing insight into whether our ligand exhibits competitive capacity and high affinity to the target. The resulting analysis is presented below:

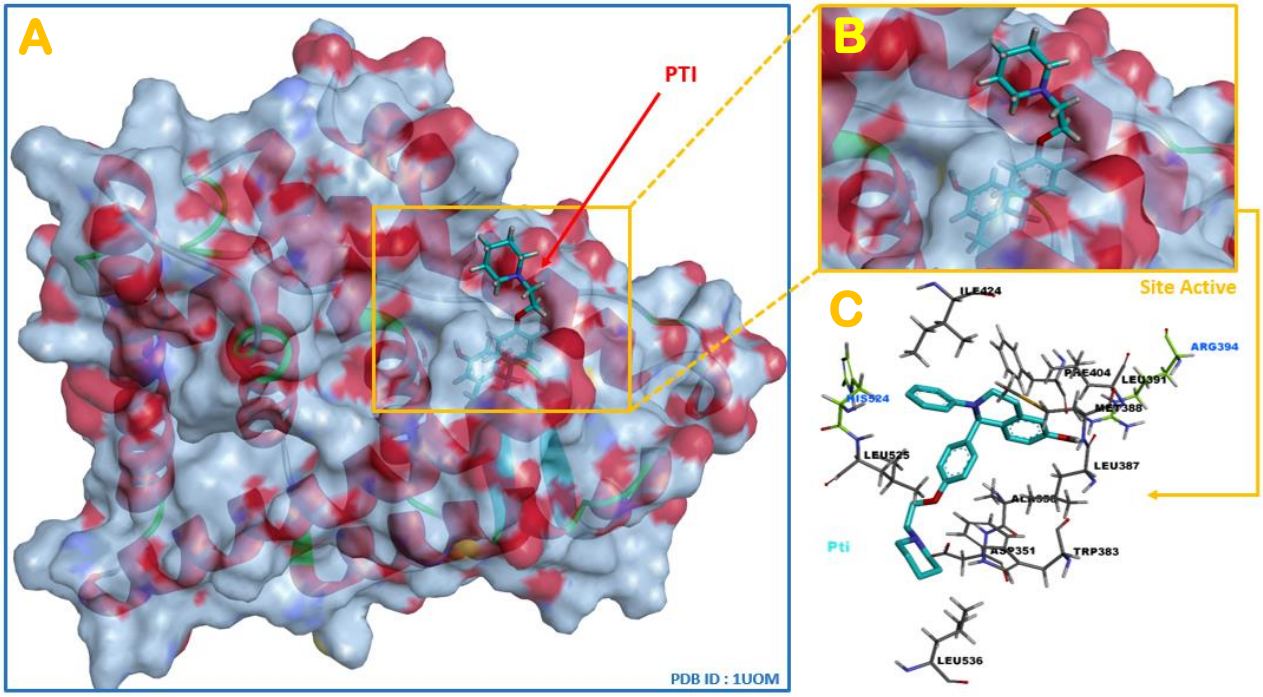

Figure 22: the interaction between the Estrogen receptor **(PDB ID: 1UOM)** and his original ligand **A:** the complex protein-ligand shown in spherical forma**; B: zoom in** to the binding site of the protein reveals the particular arrangement of the ligand; **C:** 3D interaction between **the natural ligand pti** (in blue) And the residues close to the active site of 1UOM (catalytic amino acids shown in green).

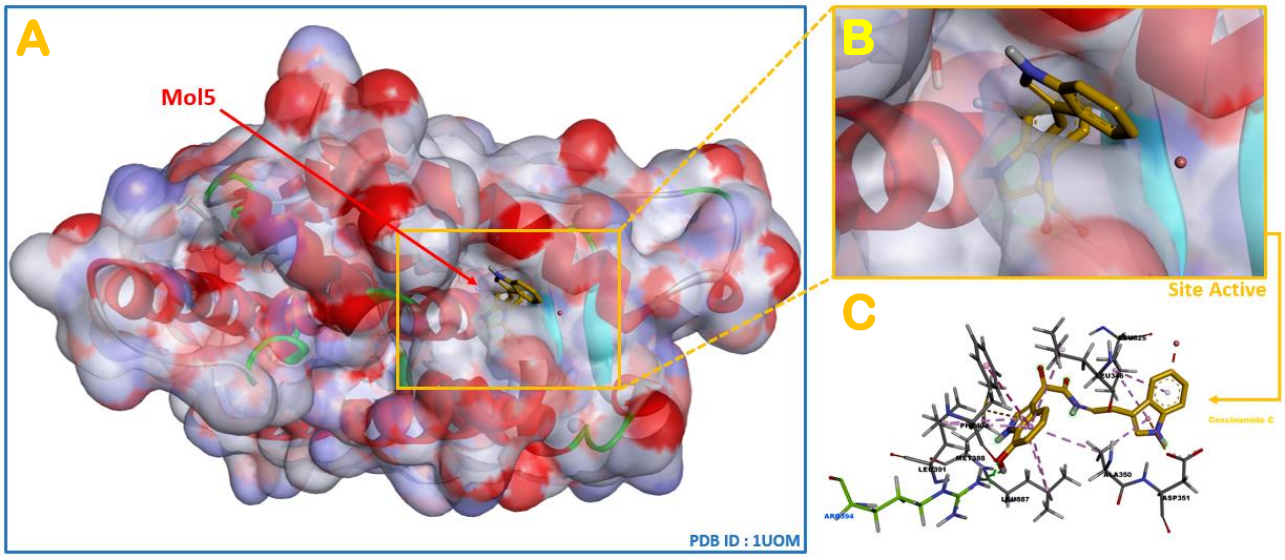

Figure 23: The interaction between the Estrogen receptor **(PDB ID: 1UOM)** and his best potential ligand **Mol5 A:** the complex protein-ligand shown in spherical forma**; B: zoom in** to the binding site of the protein reveals the particular arrangement of the ligand; **C:** 3D interaction between **Mol5** (in yellow) And the residues close to the active site of 1UOM (catalytic amino acids shown in green).

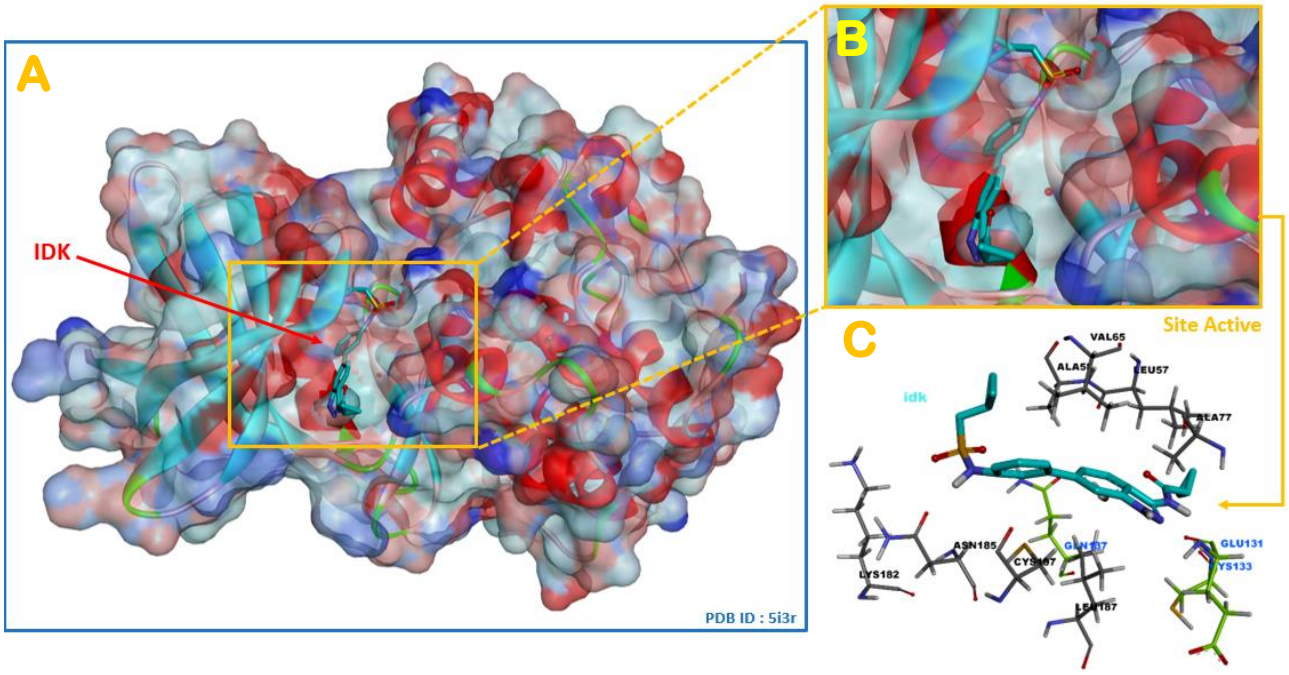

Figure 24: the interaction between the BMP-2-inducible protein kinase (PDB ID: 5i3r) and his original ligand **A:** the complex protein-ligand shown in spherical forma**; B: zoom in** to the binding site of the protein reveals the particular arrangement of the ligand; **C:** 3D interaction between **the natural ligand IDK** (in blue) And the residues close to the active site of 5i3r (catalytic amino acids shown in green).

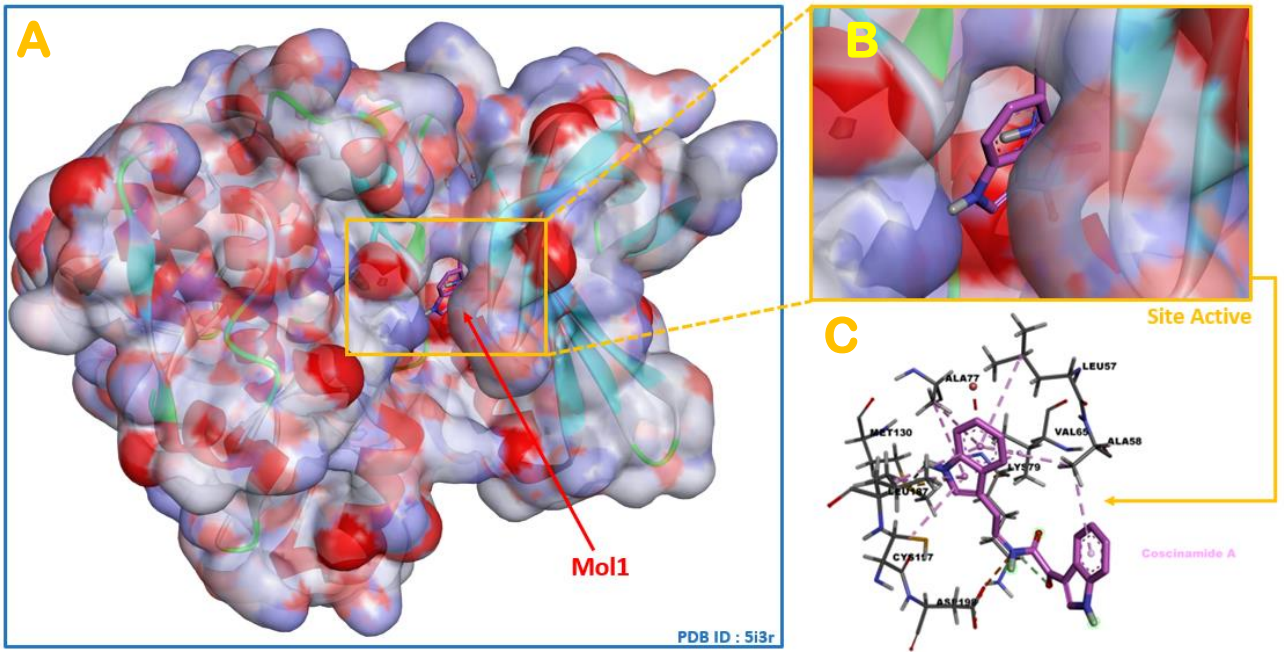

Figure 25: the interaction between the BMP-2-inducible protein kinase (PDB ID: 5i3r**)** and his best potential ligand **Mol1 A:** the complex protein-ligand shown in spherical forma**; B: zoom in** to the binding site of the protein reveals the particular arrangement of the ligand; **C:** 3D interaction between **Mol1** (in light pink) And the residues close to the active site of5i3r (catalytic amino acids shown in **grey).**

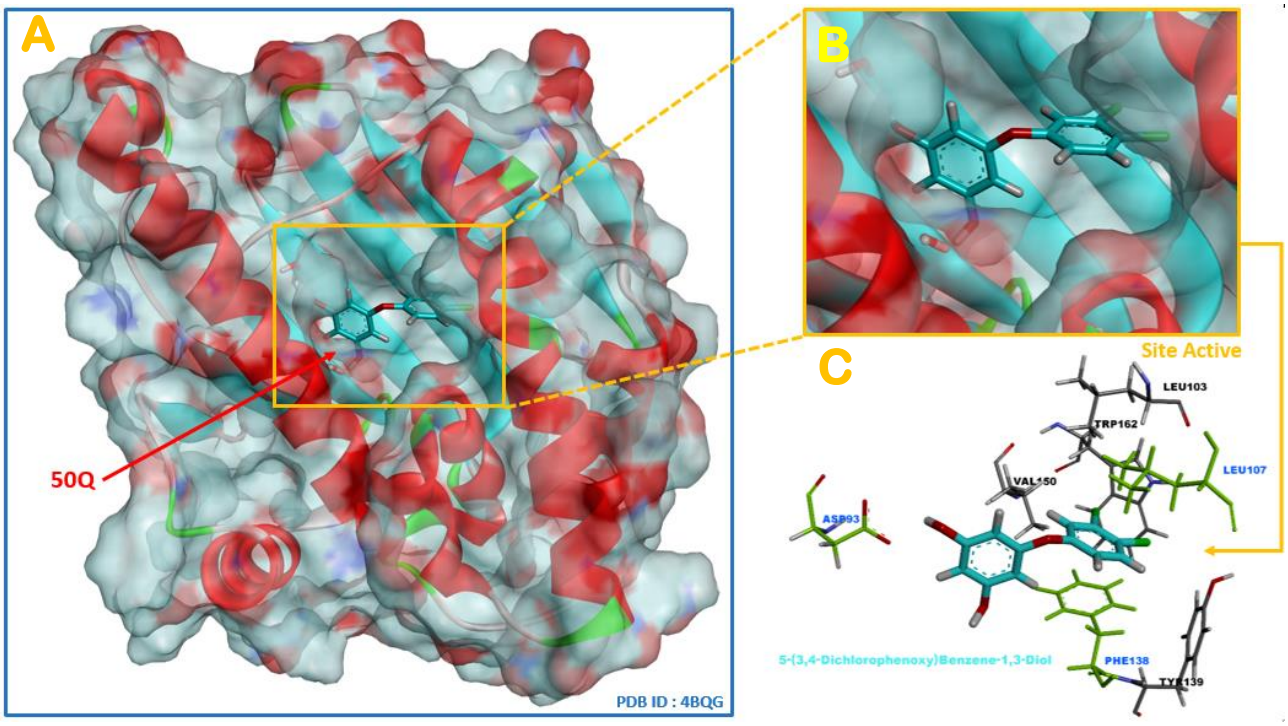

Figure 26: the interaction between the Heat Shock Protein 90 (PDB ID: 4bqg) and his original ligand **A:** the complex protein-ligand shown in spherical forma**; B: zoom in** to the binding site of the protein reveals the particular arrangement of the ligand; **C:** 3D interaction between **the natural ligand 50Q** (in blue) And the residues close to the active site of 4BQG (catalytic amino acids shown in green)

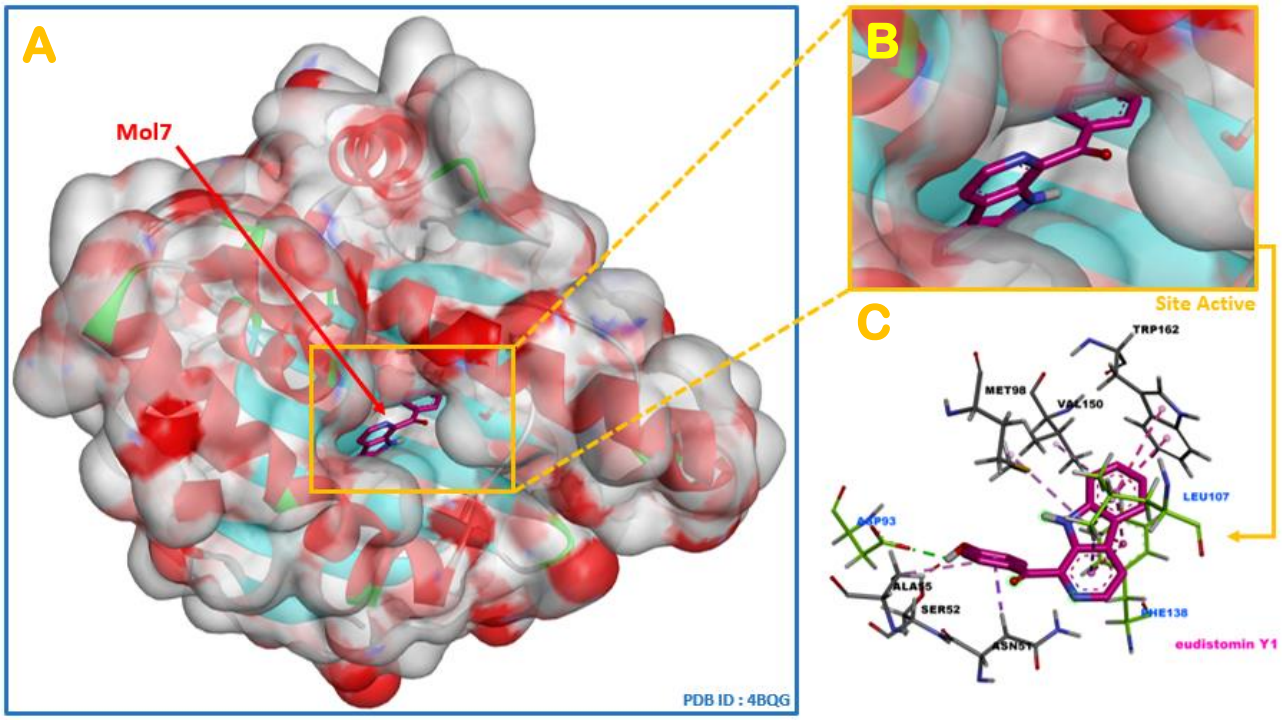

Figure 27: the interaction between the BMP-2-inducible protein kinase (PDB ID: 5i3r**)** and his best potential ligand **Mol7 A:** the complex protein-ligand shown in spherical shape**; B: zoom in** to the binding site of the protein reveals the particular arrangement of the ligand; **C:** 3D interaction between **Mol7** (in dark pink) And the residues close to the active site of 5i3r (catalytic amino acids shown in green)

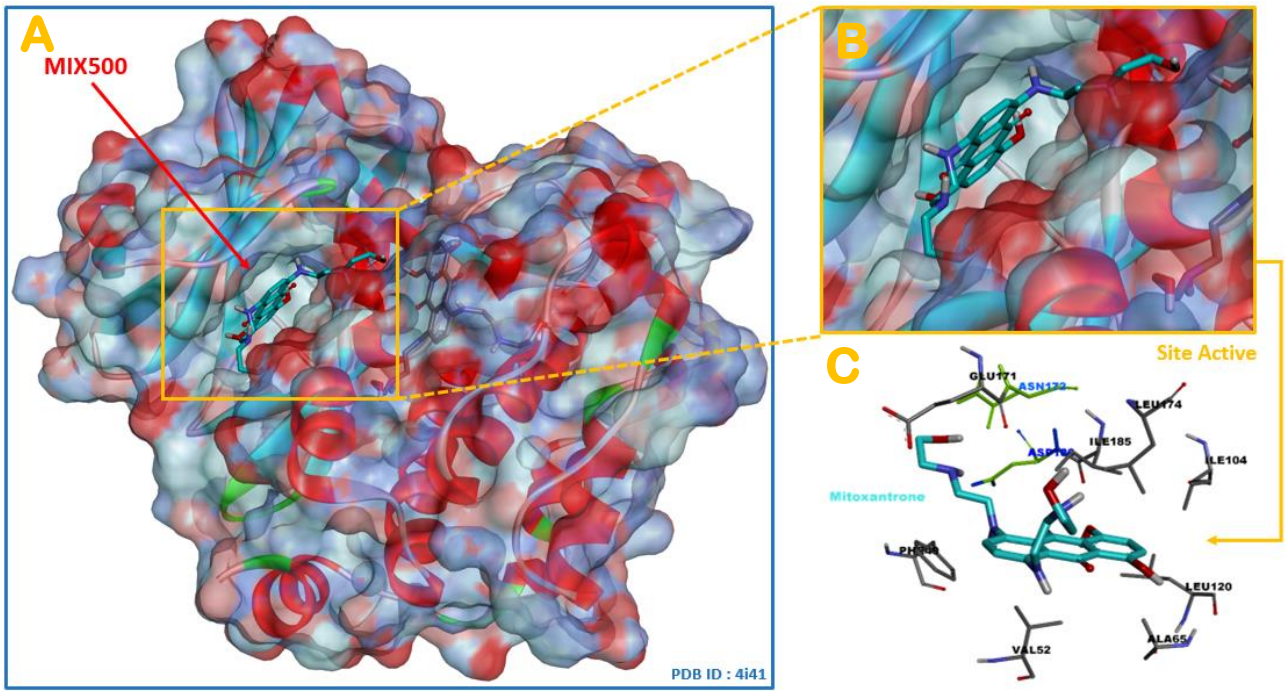

Figure 28: the interaction between the Serine/threonine-protein kinase pim-1 (PDB ID: 4i41) and his original ligand **A:** the complex protein-ligand shown in spherical forma**; B: zoom in** to the binding site of the protein reveals the particular arrangement of the ligand; **C:** 3D interaction between **the natural ligand MIX500** (in blue) And the residues close to the active site of 4i41 (catalytic amino acids shown in green)

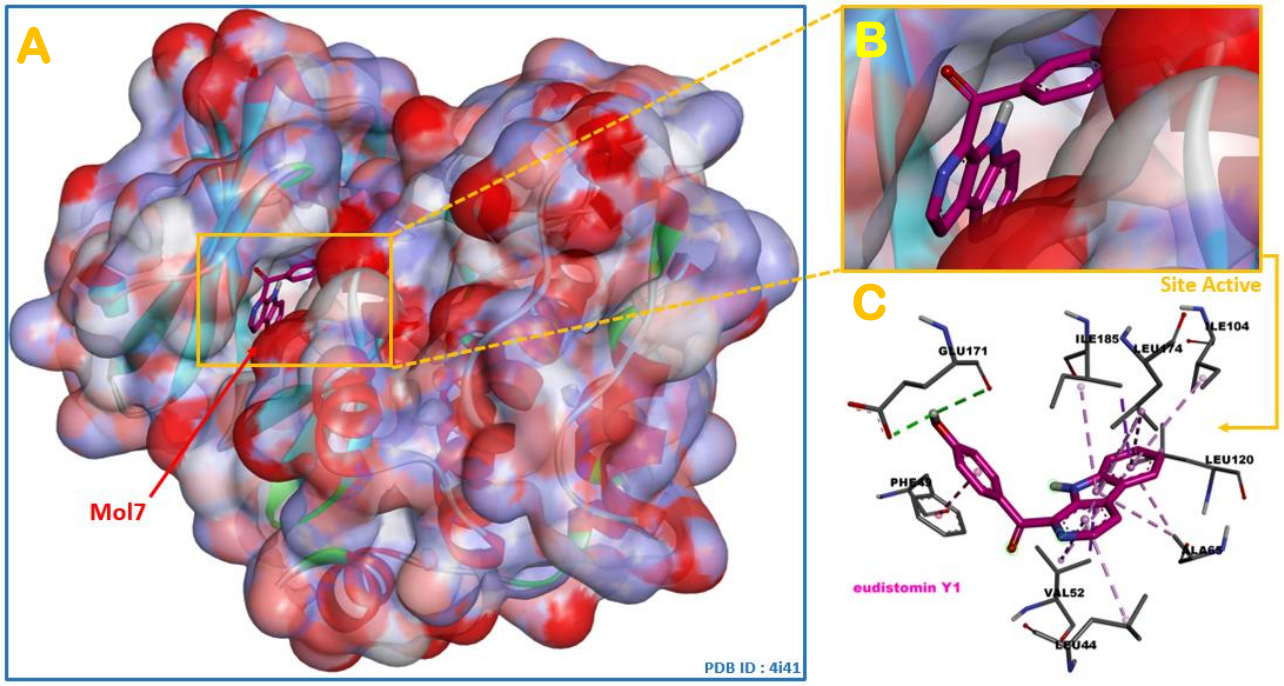

Figure 29: the interaction between the Serine/threonine-protein kinase pim-1 (PDB ID: 4i41**)** and his best potential ligand **Mol7 A:** the complex protein-ligand shown in spherical forma**; B: zoom in** to the binding site of the protein reveals the particular arrangement of the ligand; **C:** 3D interaction between **Mol7** (in dark pink) And the residues close to the active site of 4i41 (catalytic amino acids shown in grey)

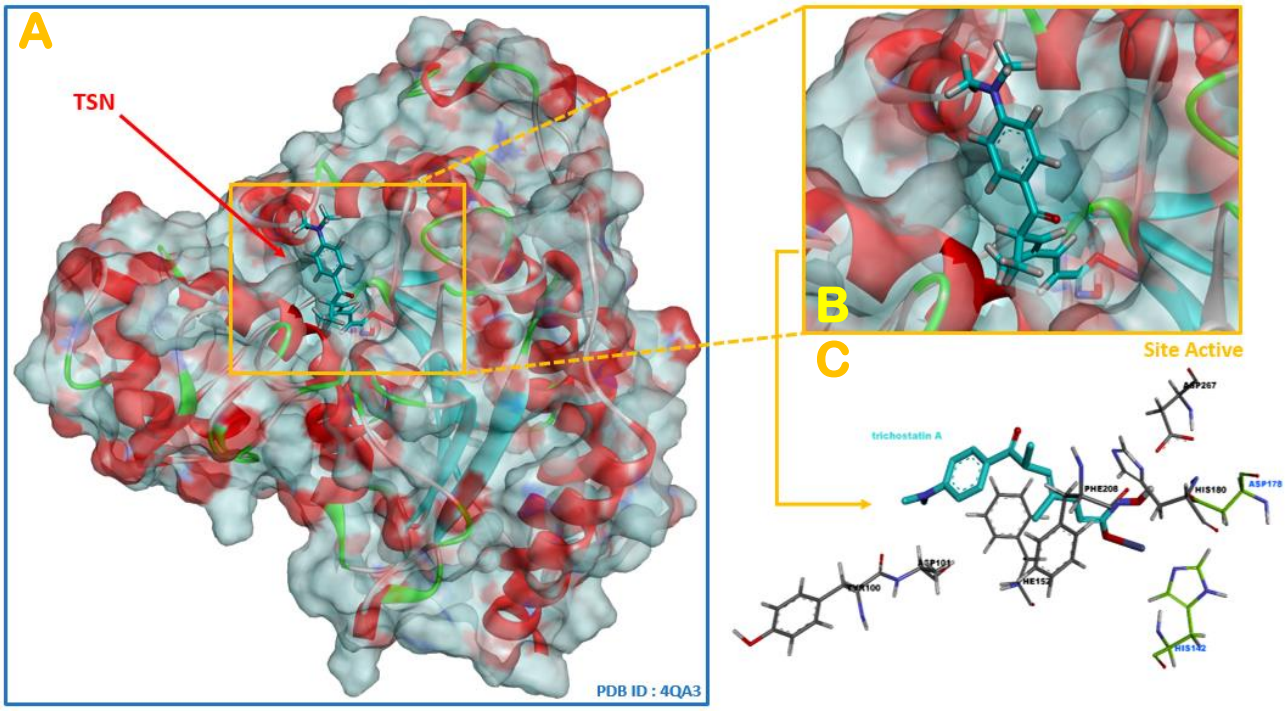

Figure 30: the interaction between the Histone deacetylase 8 (PDB ID: 4QA3) and his original ligand **A:** the complex protein-ligand shown in spherical forma**; B: zoom in** to the binding site of the protein reveals the particular arrangement of the ligand; **C:** 3D interaction between **the natural ligand TSN** (in blue) And the residues close to the active site of 4QA3 (catalytic amino acids shown in green)

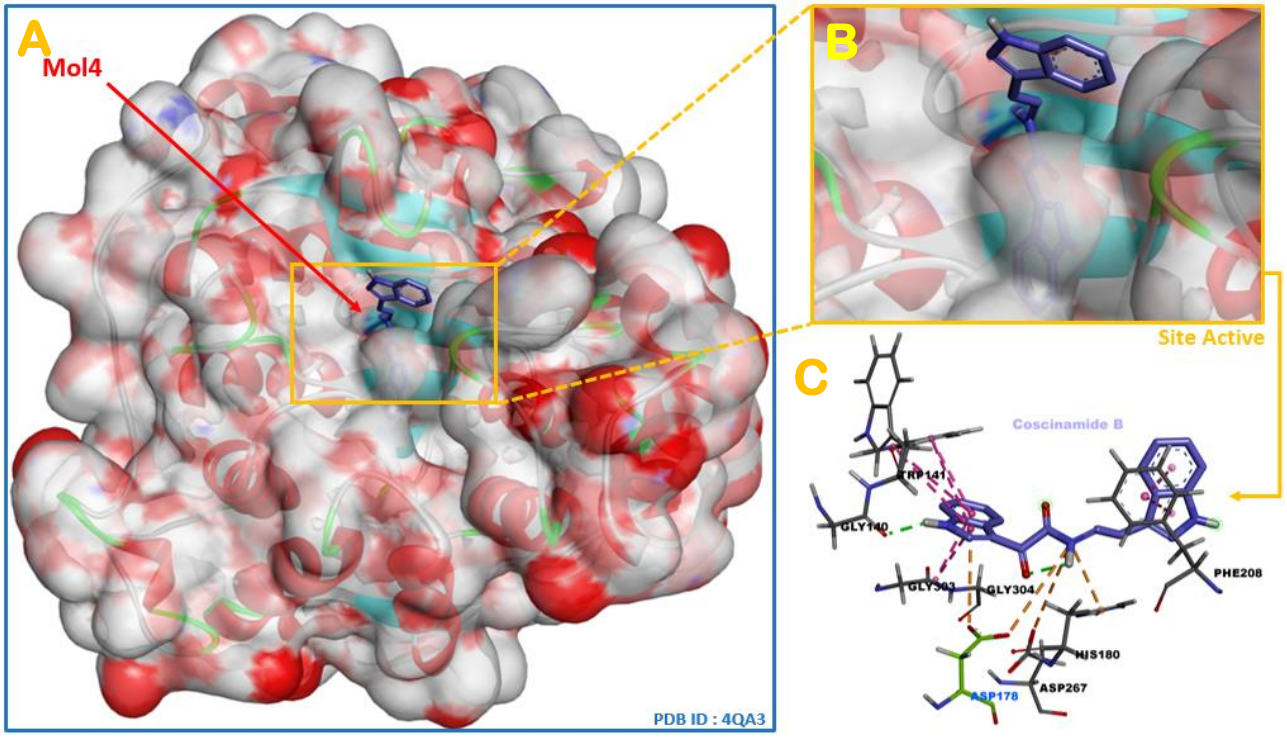

Figure 31: The interaction between the Histone deacetylase 8 (PDB ID: 4QA3) and his best potential ligand **Mol4, A:** the complex protein-ligand shown in spherical forma**; B: zoom in** to the binding site of the protein reveals the particular arrangement of the ligand; **C:** 3D interaction between **Mol4** (in blue) And the residues close to the active site of 4QA3 (catalytic amino acids shown in green)

2. Pharmacokinetics profil

The ADMET parameters have been calculated and verified for compliance with their standard ranges. According to Lipinski's rule, orally active compounds are expected to meet a minimum of three criteria: MW <500 g mol-1, logP <5, H-bond acceptors <10, and H-bond donors <10. It is noteworthy that all seven compounds in this study adhere to Lipinski's rule, suggesting a higher probability of oral bioavailability. Next, all investigated molecules exhibit favorable characteristics. They demonstrate high HIA% and skin permeability, suggesting efficient absorption and distribution within the body, and their small molecular structures suggest a potential capacity to traverse the BBB for central nervous system targeting. For the metabolism properties, the inhibition of CYP450 enzymes can impede the elimination of xenobiotics and their metabolites, potentially leading to the toxic accumulation in the body. Consequently, any findings suggesting this inhibition would be regarded as unfavorable. Regarding toxicity, all molecules exhibited remarkable results in terms of mutagenesis, skin sensitization, carcinogenicity, and LD 50 within the expected range. However, molecules mol2, 3, and 5 exhibited a potential hepatotoxicity. The findings unexpectedly indicated a medium risk of hERG inhibition, suggesting potential to induce cardiac arrhythmias. In conclusion, our analysis predicts a low total clearance (CLtot. < 5 mL/min/kg) and a relatively short half-life time (T1/2 <3h) for all investigated compounds. all results are summarized in **Tables 06** and **Figure 32.**

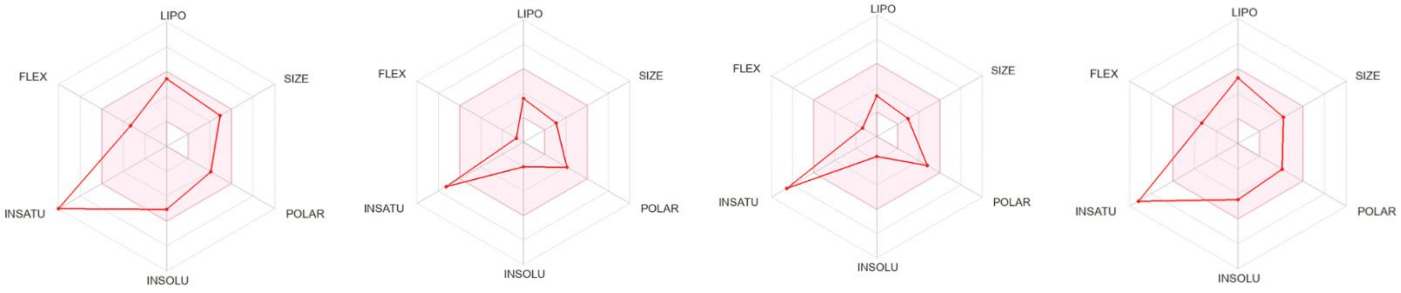

Coscinamide A (mol 1) **Leucettamine B (mol 2)** **Polyandrocarpamine A (mol 3)** **Coscinamide B (mol 4)**

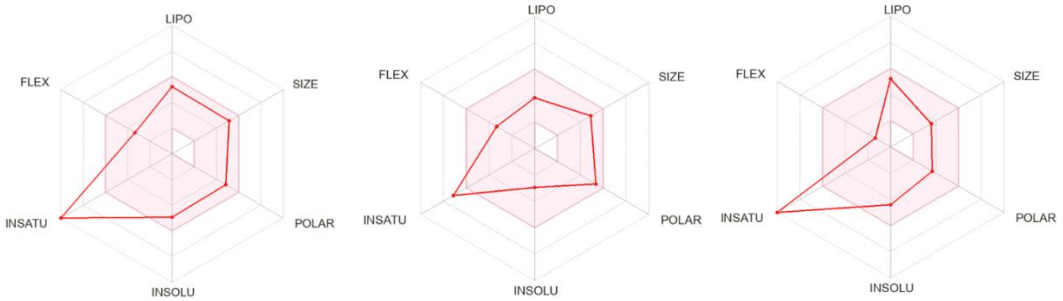

Coscinamide C (mol 5) **Dispacamide (mol 6)** **Eudistomin Y1 (mol 7)**

Figure 32: The Bioavailability Radar plots related to physicochemical properties of the studied complexes, The **pink** area represents the optimal range for each properties (Criteria: **Lipophilicity:** 0.7 <**XLOGP3**< +5.0, **size**: 150 <**MW**< 500 g/mol; **polarity**: 20<**TPSA**<130 Å^2; **solubility**: 0 <**log S**< 6; **saturation**: **fraction of carbons in the sp3 hybridization>0**.25; **flexibility**: 0.25<**rotatable bonds**<9). In this example, all compound are predicted orally bioavailable,

Table 06: ADMET results of the Physicochemical Properties of the seven marine alkaloids

	Coscinamide A	leucettamine B	Polyandrocarpamine A	Coscinamide B	Coscinamide C	Dispacamide	Eudistomin Y1
Physicochemical Properties							
Molecular Formula	$C_{20}H_{14}BrN_3O_2$	$C_{12}H_{11}N_3O_3$	$C_{11}H_{11}N_3O_3$	$C_{20}H_{15}N_3O_2$	$C_{20}H_{14}BrN_3O_3$	$C_{11}H_{11}Br_2N_5O_2$	$C_{18}H_{12}N_2O_2$
Molecular weight (g/mol)	408.25	245.23	233.22	329.35	424.25	405.05	288.30
rotatable bonds	5	1	2	5	5	5	2
H-bond acceptors	2	4	4	2	3	3	3
H-bond donors	3	1	3	3	4	4	2
Molar Refractivity	105.47	71.63	69.18	97.77	107.49	87.27	85.50
Log P (Crippen method)	3.418	0.543	0.186	2.655	3.123	0.506	3.171
LogS (µg/mL)	6.236	954.087	786.645	16.621	14.744	823.206	6.559
TPSA (Å²)	77.75	77.15	96.94	77.75	97.98	112.37	65.98
absorption							
Buffer solubility (mg/L)	2.06833	150.548	532.497	12.421	4.95604	18.4594	170.111
Caco-2 cell permeability (nm/sec)	21.16	21.023	20.9582	17.677	18.4032	13.3278	21.1943
Human intestinal absorption (HIA)	92.819661	94.504080	81.730232	91.188505	91.332927	83.770910	92.212163
distribution							
BBB penetration (C.brain/C.blood)	2.30484	0.31163	0.369255	1.18526	0.98183	0.108709	3.39979
Plasma protein binding (%)	95.651861	39.405034	38.326792	97.233574	96.296147	35.295478	88.397722
Skin Permeability (logKp, cm/hour)	-4.14658	-4.36508	-4.75678	-4.21666	-4.31518	-4.86697	-4.05522
Metabolism							
CYP1A2 inhibitor	Yes	Yes	No	Yes	Yes	Yes	Yes
CYP2C19 inhibitor	Yes	No	No	Yes	Yes	Yes	Yes
CYP2C9 inhibitor	Yes	No	No	Yes	Yes	No	No
CYP2D6 inhibitor	Yes	No	No	Yes	Yes	No	Yes
CYP3A4 inhibition	No	No	Yes	No	No	Yes	Yes
CYP3A4 substrate	Weakly	No	No	Weakly	No	No	No
Elimination							
$T_{1/2}$ (Hour)	1.773 h	0.669 h	0.546 h	1.904 h	1.516 h	1.067 h	1.72 h
CL (mL/min/kg)	0.87	1.635	1.464	1.506	0.851	0.975	1.955

Toxicity							
Ames test (mutagenesis)	No	No	No	No	No	No	No
Human Hepatotoxicity	No	Yes	Yes	No	Yes	No	No
skin sensitisation	No	No	No	No	No	No	No
Carcinogens	No, 0.8962	No, 0.9166	No, 0.9275	No, 0.9176	No, 0.9168	No, 0.9356	No, 0.9560
LD50 (mg/kg)	839.328	848.375	844.848	740.746	1126.227	577.442	774.201
Fish aquatic toxicity	Yes	Yes	No	No	Yes	No	No
hERG inhibition	medium_risk	low_risk	low_risk	medium_risk	medium_risk	medium_risk	medium_risk

Green: good /Yellow: medium /Red: off the range

$Å^2$: square Angstroms

BBB: blood-brain barrier

CL: total clearance

hERG inhibition: Human ether-a-go-go related gene channel inhibition

IC50: Inhibitory concentration 50

LogS: Solubility

Log P: lipophilicity

$T_{1/2}$: half-life time

TPSA: Topological Polar Surface Area

3. Cytotoxic activity CLC-Pred

Subsequent to the operation of the server, we performed an analysis of the CLC-Pred for various molecules, leading to noteworthy findings. Upon prediction, it demonstrated promising cytotoxic capacity against different types of pathologic cell lines in cancer. Remarkably, our ligands exhibited several results, respectively 3, 12, 22, 5, 2, 10, and 10, toward various cancer cell lines, with no predicted results towards non-tumoral cells. All results presented in (**Table 07)** confirm their safety and suggest that they could potentially serve as promising new treatments for various types of cancer, not limited to human osteosarcoma.

Table 07: The predicted biological cytotoxicity for all the chosen molecules on different types of tumor cell-line.

	Pa	Pi	Cell-line	Cell-line full name	tissue	Tumor type
	0.380	0.022	NCI-H295R	Adrenal cortex carcinoma	Adrenal cortex	Carcinoma
Mol1	0.392	0.087	MCF7	Breast carcinoma	Breast	Carcinoma
	0.348	0.057	PA-1	Ovarian carcinoma	Ovarium	Carcinoma
	0.454	0.031	SK-OV-3	Ovarian carcinoma	Ovarium	Carcinoma
Mol2	0.425	0.100	Hs 683	Oligodendroglioma	Brain	Glioma
	0.389	0.036	SNB-75	Glioblastoma	Nervous system	Glioblastoma
	0.432	0.036	MOLT-4	Acute T-lymphoblastic leukemia	Blood	Leukemia
Mol3	0.418	0.029	IGROV-1	Ovarian adenocarcinoma	Ovarium	Adenocarcinoma
	0.405	0.035	HCC 2998	Colon adenocarcinoma	Colon	Adenocarcinoma
	0.407	0.004	MES-SA/DxS	Uterine corpus sarcoma	Uterus	Sarcoma
Mol4	0.390	0.088	MCF7	Breast carcinoma	Breast	Carcinoma
	0.390	0.125	Hs 683	Oligodendroglioma	Brain	Glioma
	0.456	0.064	MCF7	Breast carcinoma	Breast	Carcinoma
Mol5	0.345	0.034	NCI-H295R	Adrenal cortex carcinoma	Adrenal cortex	Carcinoma
	0.758	0.002	PA-1	Ovarian carcinoma	Ovarium	Carcinoma
Mol6	0.474	0.015	SF-539	Glioblastoma	Brain	Glioblastoma
	0.435	0.031	DU-145	Prostate carcinoma	Prostate	Carcinoma
	0.830	0.003	Hs 683	Oligodendroglioma	Brain	Glioma
Mol7	0.398	0.018	NCI-H295R	Adrenal cortex carcinoma	Adrenal cortex	Carcinoma
	0.375	0.038	HOP-18	Non-small cell lung carcinoma	Lung	Carcinoma

4. Protein-protein interaction results

To validate the predicted interaction sets, we presented the results in **Figure 33**. Our analysis revealed more than 10 proteins associated with multiple pathways that directly interact with osteosarcoma targets or participate in pathways relevant to this form of cancer. Additionally, we provided precise details regarding their localization within the cancer cell.

Furthermore, our prediction results demonstrate that the majority of our selected targets exhibit potential involvement in diverse cancer types, including Prostate Cancer, Breast Cancer, microRNAs Cancer, proteoglycans in Cancer, and bone marrow cancer cells. These findings highlight the association between these proteins and their pathogenic capacity. Additionally, we have investigated the relationships among our five targets and observed strong interactions between most of them. In summary, these results not only corroborate our previous findings but also reinforcing the significance of our study.

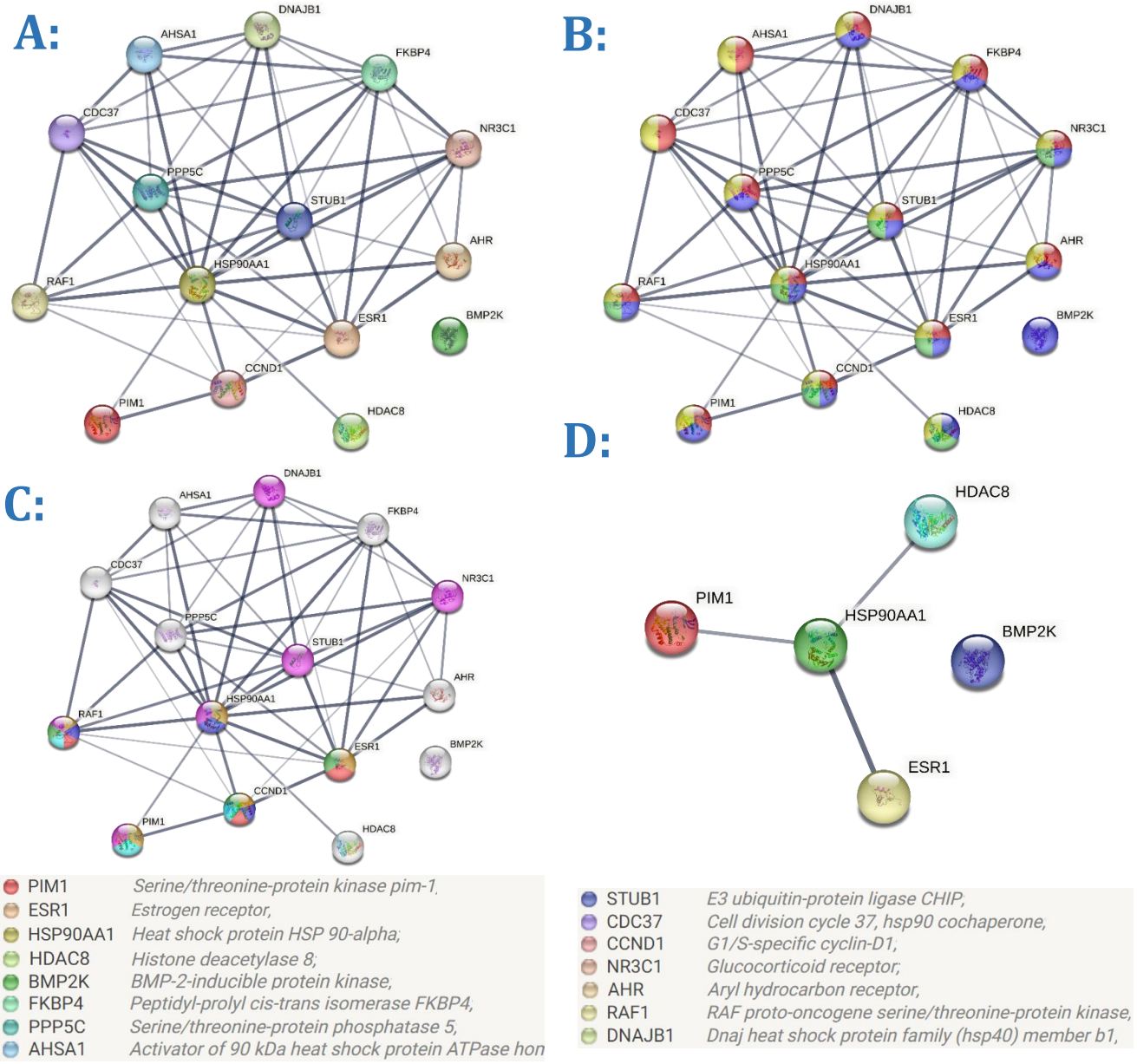

Figure 33: *in silico* Protein-protein interaction analyses of 1UOM, 5I3R, 4I41, 4BQG, and 4QA3 on the STRING website.

A) confidence view of the five targets network showing functional association with 10 proteins; a node represents different proteins; an edge represents the predicted PPI functional associations. line thickness indicates the strength of data support.

B) confidence view shows the localization of each protein in the cell (**Cytosol** or **nucleus** or **nucleoplasm** or **cytoplasme**)

C) Evidence view shows the relationship between these proteins in other cancer types (**Pathways in cancer** /**Prostate Cancer** /**Breast Cancer**/**microRNAs Cancer**/**proteoglycans in Cancer**/**bone morrow cancer cell**).

D) confidence view of the five studied targets network.

CONCLUSION

In summary, osteosarcoma is an aggressive form of bone cancer characterized by unknown molecular pathways governing its etiology and pathophysiology. Our research focuses on elucidating these pathways by employing *in silico* targeting of osteosarcoma-specific molecules using marine compounds. The marine environment has emerged as a significant reservoir of anticancer agents with unique mechanisms of action. Altogether, our findings have demonstrated that these compounds are both non-toxic and highly effective in impeding the growth of osteosarcoma tumors. Consequently, the continuation of preclinical and clinical studies is imperative to ascertain the precise role of this novel class of compounds in the treatment of cancer, particularly osteosarcoma.

When employing *in silico* methods, it is imperative to recognize that the tools utilized are merely models and, as such, their efficacy is contingent upon the quality of the underlying data and ideas. Consequently, a fundamental principle necessitates the ongoing experimental validation and refinement of these models, a task best accomplished through the collaborative efforts of an interdisciplinary team.

In light of this perspective, we anticipate that the the results of our study will be critically evaluated and implemented within both medical and experimental contexts, paving the way for future scientific advancements in the field.

REFERENCES

1. Lindsey BA, Markel JE, Kleinerman ES. Osteosarcoma Overview. Rheumatology and Therapy [Internet]. 2016 Dec 8;4(1):25–43.
2. Gill J, Ahluwalia MK, Geller D, Gorlick R. New targets and approaches in osteosarcoma. Pharmacology & Therapeutics. 2013 Jan ;137(1) :89–99.
3. Wachtel M, Schäfer BW. Targets for cancer therapy in childhood sarcomas. Cancer Treatment Reviews. 2010 Jun ;36(4) :318–27.59.
4. Ottaviani G, Jaffe N. The epidemiology of osteosarcoma. In: Pediatric and adolescent osteosarcoma. Springer ; 2009. p. 3–13
5. Smith MA, Seibel NL, Altekruse SF, Ries LAG, Melbert DL, O'Leary M, et al. Outcomes for Children and Adolescents with Cancer: Challenges for the Twenty-First Century. Journal of Clinical Oncology [Internet]. 2010 May 20 [cited 2020 Oct 22];28(15):2625–34.
6. Jaffe N, Puri A, Gelderblom H. Osteosarcoma: Evolution of Treatment Paradigms. Sarcoma [Internet]. 2013 [cited 2019 Nov 21] ;2013 :1–7.
7. Aljubran AH, Griffin A, Pintilie M, Blackstein M. Osteosarcoma in adolescents and adults: survival analysis with and without lung metastases. Annals of Oncology. 2009 Jun ;20(6) :1136–41.
8. Ma X, Xu W, Jin X, Mu H, Wang Z, Hua Y, et al. Telocinobufagin inhibits osteosarcoma growth and metastasis by inhibiting the JAK2/STAT3 signaling pathway. 2023 Jan 1 ;942 :175529–9.
9. Broadhead ML, Clark JCM, Myers DE, Dass CR, Choong PFM. The Molecular Pathogenesis of Osteosarcoma: A Review. Sarcoma [Internet]. 2011 [cited 2019 Dec 2] ;2011 :1–12.
10. Gelberg K, Fitzgerald E, Hwang S, Dubrow R. Growth and development and other risk factors for osteosarcoma in children and young adults. International Journal of Epidemiology. 1997 Apr 1 ;26(2) :272–8.
11. Russo S, Scotto di Carlo F, Gianfrancesco F. The Osteoclast Traces the Route to Bone Tumors and Metastases. Frontiers in Cell and Developmental Biology [Internet]. 2022 May 13 [cited 2023 May 4];10.
12. Lauvrak SU, Munthe E, Kresse SH, Stratford EW, Namløs HM, Meza-Zepeda LA, et al. Functional characterisation of osteosarcoma cell lines and identification of mRNAs and miRNAs associated with aggressive cancer phenotypes. British Journal of Cancer [Internet]. 2013 Sep 24 ;109(8) :2228–36.
13. Hanel W, Moll UM. Links between mutant p53 and genomic instability. Journal of Cellular Biochemistry [Internet]. 2012 Jan 5 ;113(2) :433–9.
14. Egas-Bejar D, Anderson PM, Agarwal R, Corrales-Medina F, Devarajan E, Huh WW, et al. Theranostic Profiling for Actionable Aberrations in Advanced High-Risk Osteosarcoma with Aggressive Biology Reveals High Molecular Diversity: The Human Fingerprint Hypothesis. Oncoscience [Internet]. 2014 Mar 12 [cited 2022 Feb 2];1(2):167–79.
15. Smeland S, Müller C, Alvegard TA, Wiklund T, Wiebe T, Björk O, et al. Scandinavian Sarcoma Group Osteosarcoma Study SSG VIII. European Journal of Cancer. 2003 Mar;39(4):488–94.
16. Picci P. Osteosarcoma (Osteogenic sarcoma). Orphanet Journal of Rare Diseases. 2007 Jan 23 ;2(1).
17. Moore DD, Luu HH. Osteosarcoma. Cancer Treatment and Research. 2014 ;65–92.
18. Harris MA, Hawkins CJ. Recent and Ongoing Research into Metastatic Osteosarcoma Treatments. International Journal of Molecular Sciences. 2022 Mar 30 ;23(7) :3817.
19. ildirim O, Al Khatalin M, Kargin OA, Camurdan VB. MRI for evaluation of preoperative chemotherapy in osteosarcoma. Radiography [Internet]. 2022 Aug 1 [cited 2022 May 9];28(3):593–604.
20. Bertrand TE, Cruz A, Binitie O, Cheong D, Letson GD. Do Surgical Margins Affect Local Recurrence and Survival in Extremity, Nonmetastatic, High-grade Osteosarcoma? Clinical Orthopaedics and Related Research®. 2015 May 27 ;474(3) :677–83.

21. Xiang H, Yang Q, Gao YS, Zhu D, Pan SS, Xu T, et al. Cocrystal Strategy toward Multifunctional 3D-Printing Scaffolds Enables NIR-Activated Photonic Osteosarcoma Hyperthermia and Enhanced Bone Defect Regeneration. 2020 Jun 1 ;30(25) :1909938–8.
22. Miwa S, Shirai T, Yamamoto N, Hayashi K, Takeuchi A, Igarashi K, et al. Current and Emerging Targets in Immunotherapy for Osteosarcoma. Journal of Oncology. 2019 Jan 1; 2019:1–8.
23. Zhang X, Wei H, Dong C, Wang J, Zhang T, Huang L, et al. 3D printed hydrogel/bioceramics core/shell scaffold with NIR-II triggered drug release for chemo-photothermal therapy of bone tumors and enhanced bone repair. 2023 Feb 1 ;461 :141855–5.
24. Anjum K, Abbas SQ, Shah SAA, Akhter N, Batool S, Hassan SS ul. Marine Sponges as a Drug Treasure. Biomolecules & Therapeutics [Internet]. 2016 Jul 1 ;24(4) :347–62.
25. Dou X, Dong B. Origins and Bioactivities of Natural Compounds Derived from Marine Ascidians and Their Symbionts. Marine Drugs. 2019 Nov 28 ;17(12) :670.
26. Zhao C, Shen A, Zhang L, Lin K, Wang X. Borocarbonitrides nanosheets engineered 3D-printed scaffolds for integrated strategy of osteosarcoma therapy and bone regeneration. Chemical Engineering Journal. 2020 Dec ;401 :125989.
27. Meyers PA, Healey JH, Chou AJ, Wexler LH, Merola PR, Morris CD, et al. Addition of pamidronate to chemotherapy for the treatment of osteosarcoma. Cancer. 2010 Nov 8;117(8):1736–44.
28. Luetke A, Meyers PA, Lewis I, Juergens H. Osteosarcoma treatment – Where do we stand? A state of the art review. Cancer Treatment Reviews. 2014 May;40(4):523–32.
29. Denduluri S.K, et al., Molecular pathogenesis and therapeutic strategies of human osteosarcoma. Journal of biomedical research. 2016 Jan 30 ;5–18.
30. Saraf AJ, Fenger JM, Roberts RD. Osteosarcoma: Accelerating Progress Makes for a Hopeful Future. Frontiers in Oncology. 2018 Jan 26 ;8.
31. Surgical options for children with osteosarcoma. The Lancet Oncology [Internet]. 2005 Feb 1 [cited 2021 Jul 29];6(2):85–92.
32. Mirabello L, Troisi RJ, Savage SA. Osteosarcoma incidence and survival rates from 1973 to 2004. Cancer. 2009 Apr 1 ;115(7) :1531–43.
33. Sheng G, Gao Y, Yang Y, Wu H. Osteosarcoma and Metastasis. Frontiers in Oncology [Internet]. 2021 Dec 10;11:780264.
34. Rodan GA, Heath JK, Yoon K, Noda M, Rodan SB. Diversity of the osteoblastic phenotype. Ciba Foundation Symposium [Internet]. 1988 [cited 2023 May 31]; 136:78–91.
35. Agarwal M. OSTEOSARCOMA [Internet]. 1st ed. Smiljanic T, editor. InTech: Ivana Zec; [cited 2023 Mar 19]. (https://z-lib.is/book/osteosarcoma)
36. Savvidou OD, Koutsouradis P, Chloros GD, Papanastasiou I, Sarlikiotis T, Kaspiris A, et al. Bone tumours around the elbow: a rare entity. EFORT Open Reviews. 2019 Apr ;4(4) :133–42.
37. Horner, M.J., Ries, L.A., Krapcho, M., et al. (2009) SEER Cancer Statistics Review, 1975-2006. National Cancer Institute, Bethesda.
38. Bielack SS, Kempf-Bielack B, Delling G, Exner GU, Flege S, Helmke K, et al. Prognostic Factors in High-Grade Osteosarcoma of the Extremities or Trunk: An Analysis of 1,702 Patients Treated on Neoadjuvant Cooperative Osteosarcoma Study Group Protocols. Journal of Clinical Oncology. 2002 Feb 1;20(3):776–90.
39. Shen Y, Li J, Peng D, Liao L, Chen X, Zhong W, et al. Chondroitin Polymerizing Factor (CHPF) promotes cell proliferation and tumor growth in human osteosarcoma by inhibiting SKP2's ubiquitination while activating the AKT pathway. 2022 Aug 1.

40. Gaebler M, Silvestri A, Haybaeck J, Reichardt P, Lowery CD, Stancato LF, et al. Three-Dimensional Patient-Derived In Vitro Sarcoma Models: Promising Tools for Improving Clinical Tumor Management. Frontiers in Oncology [Internet]. 2017 [cited 2023 May 31] ;7 :203.
41. Pavlou M, Shah M, Gikas P, Briggs T, Roberts SJ, Cheema U. Osteomimetic matrix components alter cell migration and drug response in a 3D tumour-engineered osteosarcoma model. Acta Biomaterialia. 2019 Sep ;96 :247–57.
42. Yang B, Yin J, Chen Y, Pan S, Yao H, Gao Y, et al. 2D-Black-Phosphorus-Reinforced 3D-Printed Scaffolds: A Stepwise Countermeasure for Osteosarcoma. Advanced Materials (Deerfield Beach, Fla) [Internet]. 2018 Mar 1 [cited 2023 May 31] ;30(10).
43. Durfee RA, Mohammed M, Luu HH. Review of Osteosarcoma and Current Management. Rheumatology and Therapy [Internet]. 2016 Oct 19 ;3(2) :221–43.
44. Murray E, Provvedini D, Curran D, Catherwood B, Sussman H, Manolagas S. Characterization of a human osteoblastic osteosarcoma cell line (SAOS-2) with high bone alkaline phosphatase activity. Journal of Bone and Mineral Research. 2009 Dec 3 ;2(3) :231–8.
45. Czekanska EM, Stoddart MJ, Richards RG, Hayes JS. In search of an osteoblast cell model for in vitro research. European Cells & Materials [Internet]. 2012 Jul 9 [cited 2021 Sep 5] ;24 :1–17.
46. Lian JB, Stein GS. Development of the osteoblast phenotype: molecular mechanisms mediating osteoblast growth and differentiation. The Iowa Orthopaedic Journal [Internet]. 1995 [cited 2023 May 31] ;15 :118–40.
47. Mutsaers AJ, Walkley CR. Cells of origin in osteosarcoma: Mesenchymal stem cells or osteoblast committed cells? Bone. 2014 May; 62:56–63.
48. Jaffe N, Bruland OS, Bielack S, editors. Pediatric and Adolescent Osteosarcoma. Cancer Treatment and Research. Boston, MA : Springer US ; 2010.
49. Hausser HJ, Brenner RE. Phenotypic instability of Saos-2 cells in long-term culture. 2005 Jul 22;333(1):216–22.
50. Xie D, Wang Z, Li J, Guo D, Lu A, Liang C. Targeted Delivery of Chemotherapeutic Agents for Osteosarcoma Treatment. Frontiers in Oncology. 2022 Mar 4;12.
51. Fogh J, Fogh JM, Orfeo T. One Hundred and Twenty-Seven Cultured Human Tumor Cell Lines Producing Tumors in Nude Mice. JNCI : Journal of the National Cancer Institute [Internet]. 1977 Jul 1 ;59(1) :221–6.
52. Wilkesmann S, Fellenberg J, Nawaz Q, Reible B, Moghaddam A, Boccaccini AR, et al. Primary osteoblasts, osteoblast precursor cells or osteoblast-like cell lines: Which human cell types are (most) suitable for characterizing 45S5-bioactive glass? Journal of Biomedical Materials Research Part A. 2019 Dec 4;108(3):663–74
53. Rodan SB, Imai Y, Thiede MA, Wesolowski G, Thompson D, Bar-Shavit Z, et al. Characterization of a human osteosarcoma cell line (Saos-2) with osteoblastic properties. Cancer Research [Internet]. 1987 Sep 15;47(18):4961–6.
54. Mahonen A, Pirskanen A, Keinänen R, Mäenpää PH. Effect of 1,25(OH)2D3 on its receptor mRNA levels and osteocalcin synthesis in human osteosarcoma cells. Biochimica et Biophysica Acta (BBA) - Gene Structure and Expression. 1990 Jan;1048(1):30–7.
55. Clover J, Gowen M. Are MG-63 and HOS TE85 human osteosarcoma cell lines representative models of the osteoblastic phenotype? Bone. 1994 Nov ;15(6) :585–91.
56. Wunder JS, Gokgoz N, Parkes R, Bull SB, Eskandarian S, Davis AM, et al. TP53 Mutations and Outcome in Osteosarcoma: A Prospective, Multicenter Study. Journal of Clinical Oncology. 2005 Mar 1;23(7):1483–90.
57. Perry JA, Kiezun A, Tonzi P, Van Allen EM, Carter SL, Baca SC, et al. Complementary genomic approaches highlight the PI3K/mTOR pathway as a common vulnerability in osteosarcoma. Proceedings of the National Academy of Sciences of the United States of America [Internet]. 2014 Dec 23 ;111(51) : E5564-5573.

58. Sadykova LR, Ntekim AI, Muyangwa-Semenova M, Rutland CS, Jeyapalan JN, Blatt N, et al. Epidemiology and Risk Factors of Osteosarcoma. Cancer Investigation. 2020 May 27 ;38(5) :259–69.
59. Kubota D, Kenta Mukaihara, Yoshida A, Tsuda H, Kawai A, Kondo T. Proteomics study of open biopsy samples identifies peroxiredoxin 2 as a predictive biomarker of response to induction chemotherapy in osteosarcoma. 2013 Oct 8 ;91 :393–404.
60. Huang J, Xie F, Tan X, Xing W, Zheng Y, Zeng C. Treatment of Osteosarcoma of the Talus With a 3D-Printed Talar Prosthesis. The Journal of Foot and Ankle Surgery. 2021 Jan ;60(1) :194–8.
61. Choi JH, Ro JY. The 2020 WHO Classification of Tumors of Soft Tissue: Selected Changes and New Entities. Advances in Anatomic Pathology. 2020 Sep 24 ;28(1) :44–58.
62. Misaghi A, Goldin A, Awad M, Kulidjian AA. Osteosarcoma: a comprehensive review. SICOT-J [Internet]. 2018 ;4(12) :12.
63. Cherrier B, Gouin F, Heymann MF, Jean Paul Thiery, Françoise Rédini, Heymann D, et al. A New Experimental Rat Model of Osteosarcoma Established by Intrafemoral Tumor Cell Inoculation, Useful for Biology and Therapy Investigations. 2005 May 1 ;26(3) :121–30.
64. Klein MJ, Siegal GP. Osteosarcoma. American Journal of Clinical Pathology. 2006 Apr ;125(4) :555–81
65. Pilavaki P, Gahanbani Ardakani A, Gikas P, Constantinidou A. Osteosarcoma : Current Concepts and Evolutions in Management Principles. Journal of Clinical Medicine. 2023 Apr 9 ;12(8) :2785.
66. Le Vu B, de Vathaire F, Shamsaldin A, Hawkins MM, Grimaud E, Hardiman C, et al. Radiation dose, chemotherapy and risk of osteosarcoma after solid tumours during childhood. International Journal of Cancer. 1998 Jul 29 ;77(3) :370–7.
67. Arlen M, Higinbotham NL, Huvos AG, Marcove RC, Miller T, Shah IC. Radiation-induced sarcoma of bone. Cancer. 1971 ;28(5) :1087–99.
68. Rickel K, Fang F, Tao J. Molecular genetics of osteosarcoma. Bone [Internet]. 2017 Sep 1 ;102 :69–79.
69. Ferguson JL, Turner SP. Bone Cancer: Diagnosis and Treatment Principles. American Family Physician [Internet]. 2018 Aug 15;98(4):205–13.
70. Hansen MF, Nellissery MJ, Bhatia P. Common mechanisms of osteosarcoma and Paget's disease. Journal of Bone and Mineral Research: The Official Journal of the American Society for Bone and Mineral Research [Internet]. 1999 Oct 1 ;14 Suppl 2 :39–44.
71. Geller DS, Gorlick R. Osteosarcoma: a review of diagnosis, management, and treatment strategies. Clinical Advances in Hematology & Oncology : H&O [Internet]. 2010 Oct 1 ;8(10) :705–18.
72. Y. Savitskaya, Rico-Martínez G, Linares-González Lm, Ea DC, René Téllez-Gastelum, Alfonso Benito Alfaro-Rodríguez, et al. Serum tumor markers in pediatric osteosarcoma: a summary review. 2012 Mar 23 [cited 2023 May 31]
73. Limmahakhun S, Pothacharoen P, Theera-Umpon N, Arpornchayanon O, Leerapun T, Luevitoonvechkij S, et al. Relationships between serum biomarker levels and clinical presentation of human osteosarcomas. Asian Pacific journal of cancer prevention: APJCP [Internet]. 2011 [cited 2023 May 31];12(7):1717–22.
74. Bacci G, Longhi A, Ferrari S, Briccoli A, Donati D, De Paolis M, et al. Prognostic Significance of Serum Lactate Dehydrogenase in Osteosarcoma of the Extremity: Experience at Rizzoli on 1421 Patients Treated over the Last 30 Years. Tumori Journal. 2004 Sep ;90(5) :478–84.
75. Yang Y, Han L, He Z, Li X, Yang S, Yang J, et al. Advances in limb salvage treatment of osteosarcoma. Journal of Bone Oncology. 2018 Mar; 10:36–40.
76. Jawad MU, Scully SP. In Brief: Classifications in Brief. Clinical Orthopaedics & Related Research. 2010 Jul;468(7):2000–2.

77. Wolf RE, Enneking WF. The staging and surgery of musculoskeletal neoplasms. The Orthopedic Clinics of North America [Internet]. 1996 Jul 1 [cited 2023 May 31];27(3):473–81.
78. Jafari F, Javdansirat S, Sanaie S, Naseri A, Shamekh A, Rostamzadeh D, et al. Osteosarcoma: A comprehensive review of management and treatment strategies. Annals of Diagnostic Pathology. 2020 Dec; 49:151654.
79. Bielack S, Carrle D, Casali PG. Osteosarcoma: ESMO Clinical Recommendations for diagnosis, treatment and follow-up. Annals of Oncology. 2009 May;20: iv137–9.
80. Tran Trung D, Quang SNT, Trung HP, Tu NV, Sy Quyen NV, Duc TT, et al. Partial replacement of pelvis with the hip joint in osteosarcoma treatment: A case report. Annals of Medicine and Surgery. 2021 Oct ;70 :102812.
81. Tiwari A. Current concepts in surgical treatment of osteosarcoma. Journal of Clinical Orthopaedics and Trauma [Internet]. 2012 Jun [cited 2019 Nov 6];3(1):4–9.
82. Allison DC, Carney SC, Ahlmann ER, Andrew Eugene Hendifar, Chawla SP, Fedenko A, et al. A Meta-Analysis of Osteosarcoma Outcomes in the Modern Medical Era. Sarcoma. 2012 Mar 18 ;2012 :1–10.
83. Marcove RC, Miké V, Hajek JV, Levin AG, Hutter RV. Osteogenic sarcoma under the age of twenty-one. A review of one hundred and forty-five operative cases. The Journal of Bone and Joint Surgery American Volume [Internet]. 1970 Apr 1 [cited 2023 May 31] ;52(3) :411–23.
84. Ueda T, Kawa A, editors. osteosarcoma [Internet]. 1st ed. Springer; [cited 2023 Apr 8]. Available from: DOI 10.1007/978-4-431-55696-1
85. Ritter J, Bielack SS. Osteosarcoma. Annals of Oncology. 2010 Oct 1;21: vii320–5.
86. Luetke A, Meyers PA, Lewis I, Juergens H. Osteosarcoma treatment – Where do we stand? A state of the art review. Cancer Treatment Reviews. 2014 May;40(4):523–32.
87. Vijayamurugan N, Bakhshi S. Review of management issues in relapsed osteosarcoma. Expert Review of Anticancer Therapy. 2013 Nov 26 ;14(2) :151–61.
88. Burns J, Wilding CP, L Jones R, H Huang P. Proteomic research in sarcomas – current status and future opportunities. Seminars in Cancer Biology [Internet]. 2020 Apr 1 [cited 2022 May 7] ;61 :56–70.
89. Lorusso D, Pignata S. Role of adjuvant chemotherapy in early-stage endometrioid and clear-cell ovarian cancer. Annals of Oncology. 2017 Dec ;28(12) :2909–11.
90. Jaffe N, Frei E, Traggis D, Bishop Y. Adjuvant Methotrexate and Citrovorum-Factor Treatment of Osteogenic Sarcoma. New England Journal of Medicine. 1974 Nov 7 ;291(19) :994–7.
91. Isakoff MS, Bielack SS, Meltzer P, Gorlick R. Osteosarcoma: Current Treatment and a Collaborative Pathway to Success. Journal of Clinical Oncology [Internet]. 2015 Sep 20 [cited 2021 Feb 24] ;33(27) :3029–35.
92. Eary JF, Mankoff DA. Tumor metabolic rates in sarcoma using FDG PET. Journal of Nuclear Medicine: Official Publication, Society of Nuclear Medicine [Internet]. 1998 Feb 1 [cited 2023 May 31];39(2):250–4.
93. Amjad MT, Kasi A. Cancer Chemotherapy [Internet]. PubMed. Treasure Island (FL): StatPearls Publishing; 2020.
94. Link MP, Goorin AM, Miser AW, Green AA, Pratt CB, Belasco JB, et al. The Effect of Adjuvant Chemotherapy on Relapse-Free Survival in Patients with Osteosarcoma of the Extremity. New England Journal of Medicine. 1986 Jun 19 ;314(25) :1600–6.
95. Yu Z, Xiao Z, Shuai X, Tian J. Local delivery of sunitinib and Ce6 via redox-responsive zwitterionic hydrogels effectively prevents osteosarcoma recurrence. Journal of Materials Chemistry B [Internet]. 2020 Aug 5 [cited 2023 May 31] ;8(30) :6418–28.
96. Chou AJ, Merola PR, Wexler LH, Gorlick RG, Vyas YM, Healey JH, et al. Treatment of osteosarcoma at first recurrence after contemporary therapy. Cancer. 2005 Nov 15 ;104(10) :2214–21.

97. Picci P, Bacci G, Campanacci M, Gasparini M, Pilotti S, Cerasoli S, et al. Histologic evaluation of necrosis in osteosarcoma induced by chemotherapy regional mapping of viable and nonviable tumor. Cancer. 1985 Oct 1;56(7):1515–21.
98. Friebele JC, Peck J, Pan X, Abdel-Rasoul M, Mayerson JL. Osteosarcoma: A Meta-Analysis and Review of the Literature. American Journal of Orthopedics (Belle Mead, NJ) [Internet]. 2015 Dec 1;44(12):547–53.
99. Daw NC, Chou AJ, Jaffe N, Rao BN, Billups CA, Rodriguez-Galindo C, et al. Recurrent osteosarcoma with a single pulmonary metastasis: a multi-institutional review. British Journal of Cancer [Internet]. 2015 Jan 1 [cited 2023 Feb 17] ;112(2) :278–82.
100. Kempf-Bielack B, Bielack SS, Jürgens H, Branscheid D, Berdel WE, Exner GU, et al. Osteosarcoma Relapse After Combined Modality Therapy: An Analysis of Unselected Patients in the Cooperative Osteosarcoma Study Group (COSS). Journal of Clinical Oncology. 2005 Jan 20;23(3):559–68.
101. Ferrari S, Mercuri M, Bacci G, Bielack SS, Jürgens H. Comment on "Prognostic Factors in High-Grade Osteosarcoma of the Extremities or Trunk: An Analysis of 1,702 Patients Treated on Neoadjuvant Cooperative Osteosarcoma Study Group Protocols." Journal of Clinical Oncology. 2002 Jun 15 ;20(12) :2910–1.
102. Xin S, Wei G. Prognostic factors in osteosarcoma: A study level meta-analysis and systematic review of current practice. Journal of Bone Oncology. 2020 Apr ;21 :100281.
103. Smith JG, Heelan RT, Huvos AG, Caparros B, Rosen G, Urmacher C, et al. Radiographic changes in primary osteogenic sarcoma following intensive chemotherapy. Radiological-pathological correlation in 63 patients. 1982 May 1;143(2):355–60.
104. Zhang Y, Wang F, Li M, Yu Z, Qi R, Ding J, et al. Self-Stabilized Hyaluronate Nanogel for Intracellular Codelivery of Doxorubicin and Cisplatin to Osteosarcoma. Advanced Science. 2018 Feb 15 ;5(5) :1700821.
105. Schwartz CL, Wexler LH, Krailo MD, Teot LA, Devidas M, Steinherz LJ, et al. Intensified Chemotherapy with Dexrazoxane Cardioprotection in Newly Diagnosed Nonmetastatic Osteosarcoma: A Report from the Children's Oncology Group. Pediatric Blood & Cancer [Internet]. 2016 Jan 1 [cited 2023 May 31] ;63(1) :54–61.
106. Shaojie D, Chen Y, Yu L, Lin K, Wang X. Magnetic Hyperthermia–Synergistic H 2 O 2 Self-Sufficient Catalytic Suppression of Osteosarcoma with Enhanced Bone-Regeneration Bioactivity by 3D-Printing Composite Scaffolds. 2020 Jan 1 ;30(4) :1907071–1.
107. Eilber F, Giuliano A, Eckardt J, Patterson K, Moseley S, Goodnight, J. Adjuvant chemotherapy for osteosarcoma: a randomized prospective trial. Journal of Clinical Oncology: Official Journal of the American Society of Clinical Oncology [Internet]. 1987 [cited 2021 May 4] ;5(1) :21–6.
108. Hong A, Millington S, Ahern V, McCowage G, Boyle RP, Martin H.N. Tattersall, et al. Limb preservation surgery with extracorporeal irradiation in the management of malignant bone tumor: the oncological outcomes of 101 patients. 2013 Oct 1;24(10):2676–80.
109. Wang F, Pang JD, Huang LL, Wang R, Li D, Sun K, et al. Nanoscale polysaccharide derivative as an AEG-1 siRNA carrier for effective osteosarcoma therapy. International Journal of Nanomedicine. 2018 Feb; Volume 13:857–75.
110. Wang SY, Hu HZ, Qing XC, Zhang ZC, Shao ZW. Recent advances of drug delivery nanocarriers in osteosarcoma treatment. Journal of Cancer. 2020 ;11(1) :69–82.
111. Di Sanzo M, Cipolloni L, Borro M, La Russa R, Santurro A, Scopetti M, et al. Clinical Applications of Personalized Medicine: A New Paradigm and Challenge. Current Pharmaceutical Biotechnology. 2017 Apr 16 ;18(3) :194–203.
112. Anjum K, Abbas SQ, Shah SA, Akhter N, Batool S, Hassan SS. Marine Sponges as a Drug Treasure. Biomol Ther (Seoul). 2016 Jul 1;24(4):347-62.

113. Heidi R Bokesch, Lewis K Pannell, Tawnya C McKee, Michael R Boyd, Coscinamides A, B and C, three new bis indole alkaloids from the marine sponge Coscinoderma sp., Tetrahedron Letters, Volume 41, Issue 33, 2000, Pages 6305-6308, ISSN 0040-4039.
114. Loaëc N, Attanasio E, Villiers B, Durieu E, Tahtouh T, Cam M, Davis RA, Alencar A, Roué M, Bourguet-Kondracki M-L, Proksch P, Limanton E, Guiheneuf S, Carreaux F, Bazureau J-P, Klautau M, Meijer L. Marine-Derived 2-Aminoimidazolone Alkaloids. Leucettamine B-Related Polyandrocarpamines Inhibit Mammalian and Protozoan DYRK & CLK Kinases. Marine Drugs. 2017; 15(10):316.
115. Francesco Cafieri, Ernesto Fattorusso, Alfonso Mangoni, Orazio Taglialatela-Scafati, Dispacamides, anti-histamine alkaloids from Caribbean Agelas sponges, Tetrahedron Letters, Volume 37, Issue 20, 1996, Pages 3587-3590, ISSN 0040-4039.
116. SpongeMaps, sponge taxonomy, sponge identification [Internet]. spongemaps. [cited 2023 May 31].
117. Dou X, Dong B. Origins and Bioactivities of Natural Compounds Derived from Marine Ascidians and Their Symbionts. Marine Drugs. 2019; 17(12):670.
118. Shenkar, N.; Gittenberger, A.; Lambert, G.; Rius, M.; Moreira da Rocha, R.; Swalla, B.J.; Turon, X. (2023). Ascidiacea World Database. Accessed at www.marinespecies.org/ascidiacea on 2023-04-26.
119. Tae Hyung Won, Ju-eun Jeon, So-Hyoung Lee, Boon Jo Rho, Ki-Bong Oh, Jongheon Shin, Beta-carboline alkaloids derived from the ascidian Synoicum sp., Bioorganic & Medicinal Chemistry, Volume 20, Issue 13, 2012, Pages 4082-4087, ISSN 0968-0896.
120. Rohan A Davis, William Aalbersberg, Semisi Meo, Rosana Moreira da Rocha, Chris M Ireland, The isolation and synthesis of polyandrocarpamines A and B. Two new 2-aminoimidazolone compounds from the Fijian ascidian, Polyandrocarpa sp., Tetrahedron, Volume 58, Issue 16, 2002, Pages 3263-3269, ISSN 0040-4020.
121. WoRMS - World Register of Marine Species [Internet]. Marinespecies.org. 2019. Available from: https://www.marinespecies.org/
122. Stanzione F, Giangreco I, Cole JC. Use of molecular docking computational tools in drug discovery. Progress in Medicinal Chemistry. 2021 ;273–343.
123. Jia CY, Li JY, Hao GF, Yang GF. A drug-likeness toolbox facilitates ADMET study in drug discovery. Drug Discovery Today. 2019 Nov.
124. Daina A, Michielin O, Zoete V. SwissADME: a Free web Tool to Evaluate pharmacokinetics, drug-likeness and Medicinal Chemistry Friendliness of Small Molecules. Scientific Reports [Internet]. 2017 Mar 3 ;7(1).
125. Lipinski CA. Lead- and drug-like compounds: the rule-of-five revolution. Drug Discovery Today: Technologies. 2004 Dec;1(4):337–41.
126. Lagorce D, Douguet D, Miteva MA, Villoutreix BO. Computational analysis of calculated physicochemical and ADMET properties of protein-protein interaction inhibitors. Scientific Reports. 2017 Apr 11 ;7(1).
127. Durán-Iturbide NA, Díaz-Eufracio BI, Medina-Franco JL. *In Silico* ADME/Tox Profiling of Natural Products: A Focus on BIOFACQUIM. ACS Omega. 2020 Jun 25 ;5(26) :16076–84.
128. Wang Z, Yang H, Wu Z, Wang T, Li W, Tang Y, et al. *In Silico* Prediction of Blood-Brain Barrier Permeability of Compounds by Machine Learning and Resampling Methods. ChemMedChem. 2018 Sep 21 ;13(20) :2189–201.
129. Vilar S, Chakrabarti M, Costanzi S. Prediction of passive blood–brain partitioning: Straightforward and effective classification models based on *in silico* derived physicochemical descriptors. Journal of Molecular Graphics and Modelling [Internet]. 2010 Jun [cited 2020 Feb 3];28(8):899–903.
130. Zhang Z, Tang W. Drug metabolism in drug discovery and development. Acta Pharmaceutica Sinica B. 2018 Sep ;8(5) :721–32.
131. Dresser GK, Spence JD, Bailey DG. Pharmacokinetic-pharmacodynamic consequences and clinical relevance of cytochrome P450 3A4 inhibition. Clinical pharmacokinetics [Internet]. 2000 ;38(1) :41–57.

132. Beck TC, Beck KR, Morningstar J, Benjamin MM, Norris RA. Descriptors of Cytochrome Inhibitors and Useful Machine Learning Based Methods for the Design of Safer Drugs. Pharmaceuticals. 2021 May 17;14(5):472.
133. Issa NT, Wathieu H, Ojo A, Byers SW, Dakshanamurthy S. Drug Metabolism in Preclinical Drug Development: A Survey of the Discovery Process, Toxicology, and Computational Tools. Current Drug Metabolism [Internet]. 2017 Jul 21 [cited 2019 Oct 31];18(6).
134. Pires DEV, Blundell TL, Ascher DB. pkCSM: Predicting Small-Molecule Pharmacokinetic and Toxicity Properties Using Graph-Based Signatures. Journal of Medicinal Chemistry [Internet]. 2015 Apr 22 ;58(9) :4066–72.
135. Smith DA, Beaumont K, Maurer TS, Di L. Clearance in Drug Design. Journal of Medicinal Chemistry. 2018 Oct 3 ;62(5) :2245–55.
136. Smith DA, Beaumont K, Maurer TS, Di L. Relevance of Half-Life in Drug Design. Journal of medicinal chemistry. 2018 ;61(10) :4273–82.
137. Sato T, Yuki H, Ogura K, Honma T. Construction of an integrated database for hERG blocking small molecules. Song C, editor. PLOS ONE. 2018 Jul 6 ;13(7) : e0199348.
138. He S, Ye T, Wang R, Zhang C, Zhang X, Sun G, et al. An *In Silico* Model for Predicting Drug-Induced Hepatotoxicity. 2019 Apr 17 ;20(8) :1897–7.
139. Lagunin AA, Dubovskaja VI, Rudik AV, Pogodin PV, Druzhilovskiy DS, Gloriozova TA, et al. CLC-Pred: A freely available web-service for *in silico* prediction of human cell line cytotoxicity for drug-like compounds. Rishi A, editor. PLOS ONE. 2018 Jan 25;13(1): e0191838.
140. von Mering C, Jensen LJ, Kuhn M, Chaffron S, Doerks T, Kruger B, et al. STRING 7--recent developments in the integration and prediction of protein interactions. Nucleic Acids Research. 2007 Jan 3;35(Database): D358–62.
141. Ooi HS, Schneider G, Chan YL, Lim TT, Eisenhaber B, Eisenhaber F. Databases of protein-protein interactions and complexes. Methods in Molecular Biology (Clifton, NJ) [Internet]. 2010 [cited 2022 Mar 9]; 609:145–59.
142. Szklarczyk D, Gable AL, Lyon D, Junge A, Wyder S, Huerta-Cepas J, et al. STRING v11: protein–protein association networks with increased coverage, supporting functional discovery in genome-wide experimental datasets. Nucleic Acids Research. 2019 Jan 8;47(Database issue): D607–13.
143. von Mering C. STRING: known and predicted protein-protein associations, integrated and transferred across organisms. Nucleic Acids Research. 2004 Dec 17;33(Database issue): D433–7.
144. Jensen LJ, Kuhn M, Stark M, Chaffron S, Creevey C, Muller J, et al. STRING 8--a global view on proteins and their functional interactions in 630 organisms. Nucleic Acids Research. 2009 Jan 1;37(Database): D412–6.
145. Renaud J, Bischoff S, Buhl T, Philipp Floersheim, Fournier B, Halleux C, et al. Estrogen Receptor Modulators: Identification and Structure−Activity Relationships of Potent ERα-Selective Tetrahydroisoquinoline Ligands. Journal of Medicinal Chemistry. 2003 Jun 10;46(14):2945–57.
146. Pakdel F. Molecular Pathways of Estrogen Receptor Action. International Journal of Molecular Sciences. 2018 Aug 31;19(9):2591.
147. Halloran D, Durbano HW, Nohe A. Bone Morphogenetic Protein-2 in Development and Bone Homeostasis. Journal of Developmental Biology. 2020 Sep 13 ;8(3) :19.
148. Maria Gabriella Brasca, Mantegani S, Amboldi N, Bindi S, Dannica Caronni, Casale E, et al. Discovery of NMS-E973 as novel, selective and potent inhibitor of heat shock protein 90 (Hsp90). 2013 Nov 15 ;21(22) :7047–63.
149. Miura T, Fukami TA, Hasegawa K, Ono N, Suda A, Shindo H, et al. Lead generation of heat shock protein 90 inhibitors by a combination of fragment-based approach, virtual screening, and structure-based drug design. 2011 Oct 1;21(19):5778–83.
150. Brough PA, Aherne W, Barril X, Borgognoni J, Boxall K, Cansfield JE, et al. 4,5-Diarylisoxazole Hsp90 Chaperone Inhibitors: Potential Therapeutic Agents for the Treatment of Cancer. Journal of Medicinal Chemistry. 2007 Nov 20 ;51(2) :196–218.

151. Andrew James Woodhead, Angove HC, Carr M, Gianni Chessari, Congreve M, Coyle JT, et al. Discovery of (2,4-Dihydroxy-5-isopropylphenyl)-[5-(4-methylpiperazin-1-ylmethyl)-1,3-dihydroisoindol-2-yl] methanone(AT13387), a Novel Inhibitor of the Molecular Chaperone Hsp90 by Fragment Based Drug Design. 2010 Jul 28;53(16):5956–69.

152. Wan X, Zhang W, Li L, Xie Y, Li W, Huang N. A new target for an old drug: identifying mitoxantrone as a nanomolar inhibitor of PIM1 kinase via kinome-wide selectivity modeling. 2013 Mar 15 ;56(6) :2619–29.

153. Kumar A, Valsan Mandiyan, Suzuki Y, Zhang C, Rice J, Tsai JC, et al. Crystal Structures of Proto-oncogene Kinase Pim1: A Target of Aberrant Somatic Hypermutations in Diffuse Large Cell Lymphoma. Journal of Molecular Biology. 2005 Apr 1 ;348(1) :183–93.

154. Bullock AN, Debreczeni JE, Amos A, Knapp S, Turk BE. Structure and Substrate Specificity of the Pim-1 Kinase. Journal of Biological Chemistry. 2005 Dec 16 ;280(50) :41675–82.

155. Dowling DP, Gantt SL, Gattis SG, Fierke CA, Christianson DW. Structural Studies of Human Histone Deacetylase 8 and Its Site-Specific Variants Complexed with Substrate and Inhibitors†, ‡. Biochemistry [Internet]. 2008 Dec 23 ;47(51) :13554–63.

156. Vannini A, Volpari C, Gallinari P, Jones P, Mattu M, Carfí A, et al. Substrate binding to histone deacetylases as shown by the crystal structure of the HDAC8–substrate complex. EMBO reports. 2007 Aug 10 ;8(9) :879–84.

157. Hu E, Chen Z, Fredrickson T, Zhu Y, Kirkpatrick R, Zhang GF, et al. Cloning and characterization of a novel human class I histone deacetylase that functions as a transcription repressor. The Journal of Biological Chemistry [Internet]. 2000 May 19 [cited 2022 Jul 19];275(20):15254–64.

158. Balasubramanian S, Ramos J, Luo W, Sirisawad M, Verner E, Buggy JJ. A novel histone deacetylase 8 (HDAC8)-specific inhibitor PCI-34051 induces apoptosis in T-cell lymphomas. Leukemia [Internet]. 2008 Feb 7 [cited 2019 Oct 22] ;22(5) :1026–34.

APPENDIXES

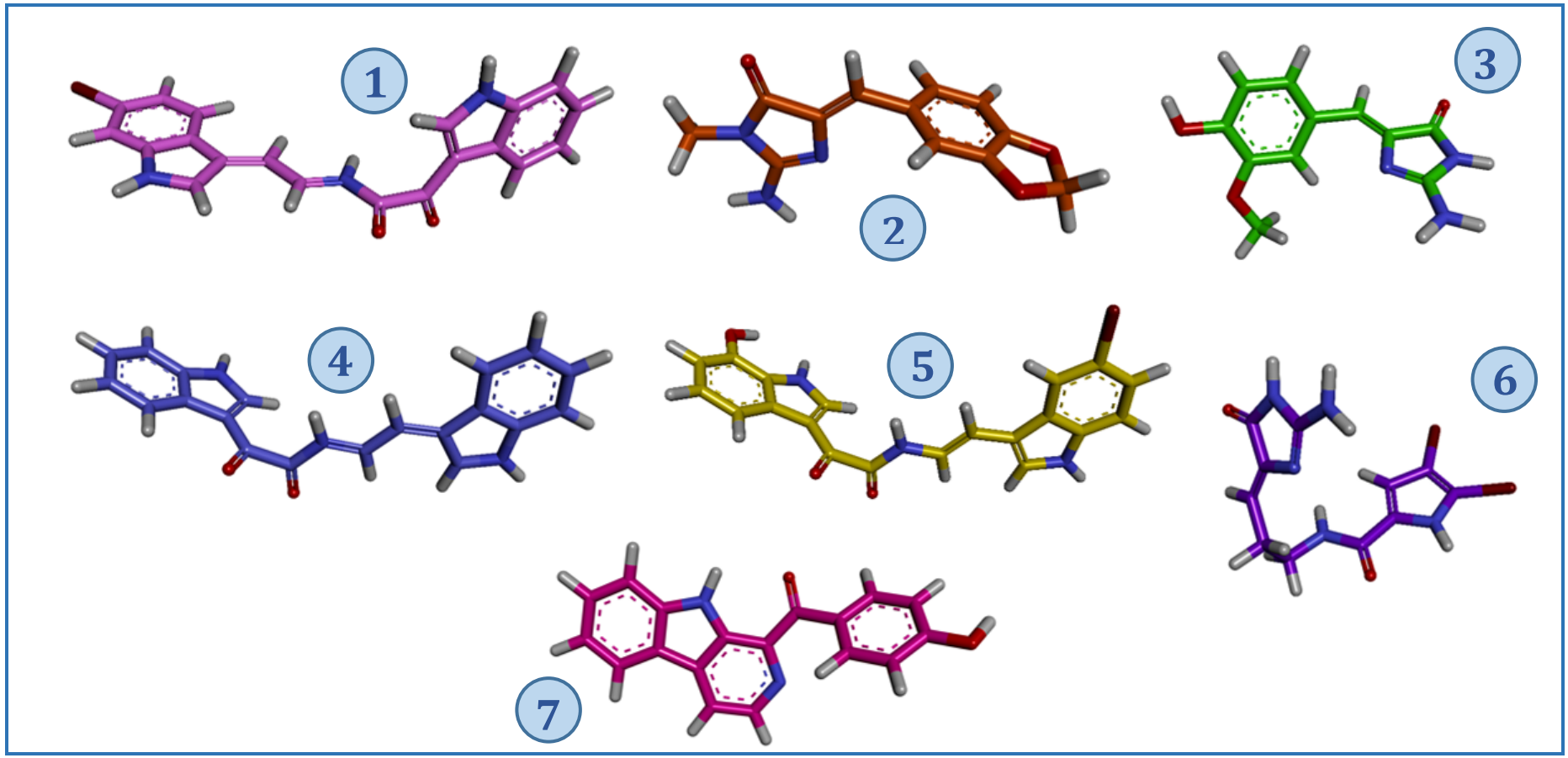

Appendix 01 : 3D structural representation of the seven alkaloidic componds obtained from marin sources with potontiel inhibition of human osteosarcoma targets, (1) Coscinamide A **(mol1)** represented in light purple, (2) Leucettamine B **(mol2)** represented in orange, (3) Polyandrocarpamine A **(mol3)**represented in green, (4) Coscinamide B **(mol4)** represented in blue (5) Coscinamide C **(mol5)** represented in yellow, (6) Dispacamide **(mol6)** represented in dark purple, (7) Eudistomin Y1**(mol7)** represented in dark pink

Appendix 02 table representing the different active sites of the five studied human osteosarcoma targets using **UNIPLOT database** and **Discovery Studio visualizer**

Target	Active Sites	Amino Acids of the Active Sites
1uom	Active site	Met343, Leu346, Thr347, Ala350, Asp351, Glu353, Trp383, Leu387, Arg394, Ile424, Gly521, His524, Leu525, Leu539
4qa3	Substrat-binding site	His2 ys4 lys33 tyr100 asp101 Tyr111 Gly140, trp141 his143 his142 gly151 Phe152 asp176 asp178 his180 asp183 phe208 pro209 asp267 phe306
	BC1	Pro273, Met274, Tyr306
4bqg	ATP-binding site	Leu48, Asn51, Ser52, Ala55, Lys58, Asp93, Gly97, Met98, Leu107, Phe138, Trp162, Thr184
4i41	ATP-binding site	Leu44, Phe49, Ala65, E89, Leu120, Glu121, Pro123, Asp128, Lys169, Asn172, and Asp186
	substrate-binding pocket	Phe130, Asp131, Ile133, Thr134, Asp167, Asp170, Glu171, Thr204, Asp234, Asp239, Pro241, Glu243, Glu247, and Arg256
5i3r	AC1	Gly60, Ser63, Val65, Ala77, Met130, Glu131, Tyr132, Cys133, Arg134, Gly136, Gln137, Glu184, Asn185, Cys197, Asp198
	AC2	Ala321, Asp322
	AC4	His49, Gln50, Thr70
	ATP Binding Site	Ile98, Met99, Lys100, Glu101, Leu102, Ser103, Gly104, His105, Lys106

AC : active site

Appendix 03: ADMET stand ranges

	Stand ranges	
Physicochemical Properties		
Molecular weight (g/mol)	≤ 500	Lipinski et al., 2012
Rotatable bonds	<10	Lipinski et al., 2012
H-bond acceptors	≤10	Lipinski et al., 2012
H-bond donors	<5	Lipinski et al., 2012
Molar Refractivity	40≤ MR ≤ 130	Lipinski et al., 2012
TPSA (Å²)	>70	Lipinski et al., 2012
Absorption		
Buffer solubility (mg/L)	Higher better	Issa et al., 2017
Caco-2 cell permeability (nm/sec)	>20	Issa et al., 2017
Human intestinal absorption (HIA%)	Superior than 96%	Lee et al., 2003
Distribution		
BBB penetration (C.brain/C.blood)	LogBBB > 0.3	Vilar et al., 2010
Plasma protein binding (%)	High (80-100%) Midium (50-80%) Low (<50%)	Lagorce et al., 2017
Skin Permeability (logKp, cm/hour)	Bad ≥-3	Khan et al., 2015
Métabolism		
CYP3A4 inhibition	Yes (bad) / or No	Dresser et al., 2000
CYP3A4 substrate	Yes (good) / or No	Dresser et al., 2000
Elimination		
T $_{1/2}$ (Hour)	0.5h< T $_{1/2}$ <3h	Smith et a., 2018
CL (mL/min/kg)	< 5 mL/min/kg	Smith et a., 2019
Toxicity		
Ames test (mutagenesis)	Mutagen (bad)/ or No	Pires et al., 2015
Human Hepatotoxicity	Yes (bad) / or No	He et al., 2019
Skin sensitisation	Yes (bad) / or No	Pires et al., 2015
Carcinogens	Yes (bad) / or No	Pires et al., 2015
LD50 (mg/kg)	Low toxicity > 500 mg/kg	Beck et al., 2021
Fish aquatic toxicity	Yes (bad) / or No	Pires et al., 2015
hERG inhibition	Risky (bad) / or No	Sato et a., 2018

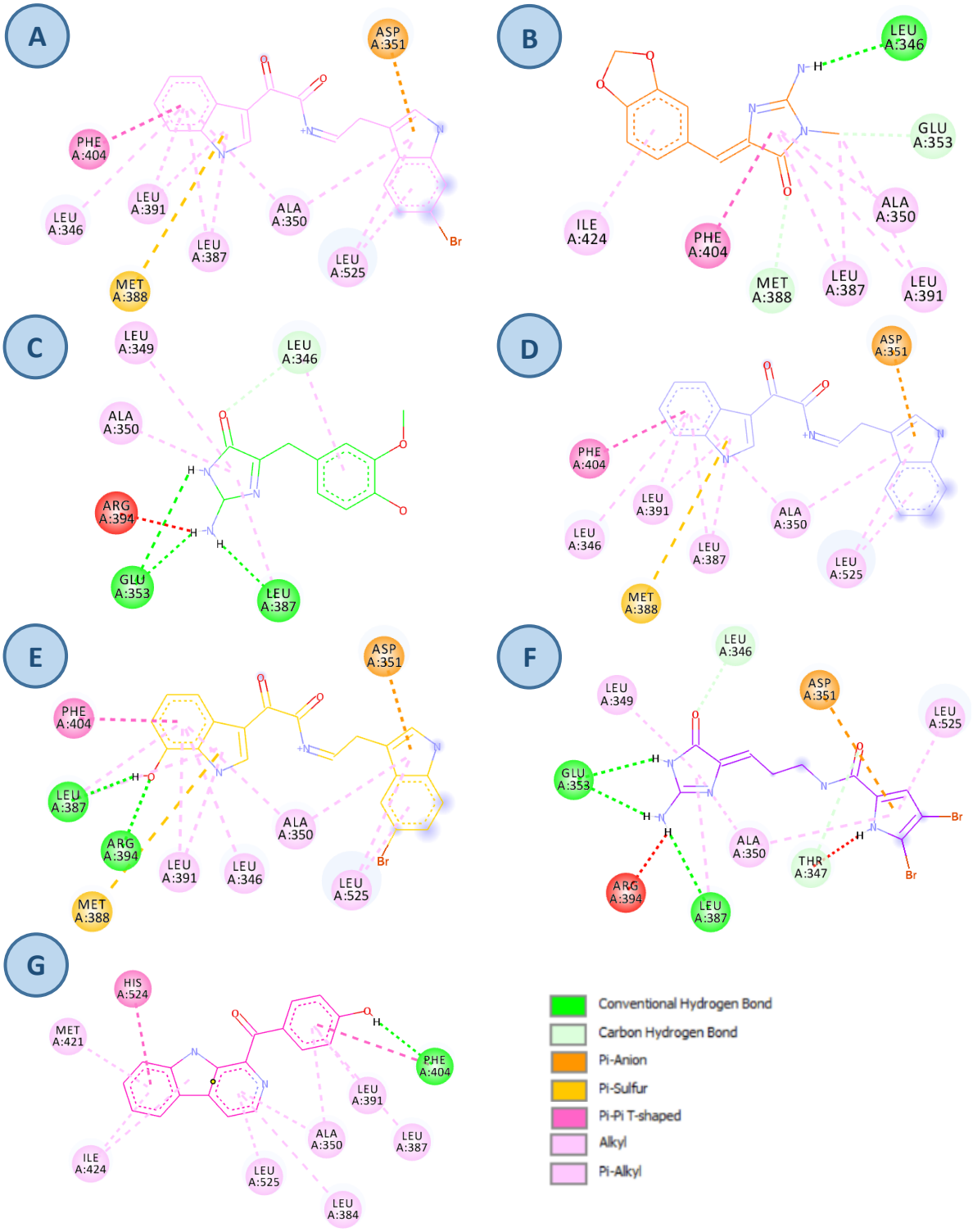

Appendix 04: A 2D diagram represents the interactions between the residues near the active site of the Estrogen Receptor (**PDB ID: 1uom**) and our seven ligands (marin alkaloids). A: 2D interaction between **Mol1** (in light purple) and **1uom** binding site; B: 2D interaction between **Mol2** (in orange) and the **1uom** binding site; C: 2D interaction between **Mol3** (in green) and **1uom** binding site; D: 2D interaction between **Mol4** (in blue) and **1uom** binding site; E: 2D interaction between **Mol5** (in yellow) and **1uom** binding site; F: 2D interaction between **Mol6** (in dark purple) and **1uom** binding site; G: 2D interaction between **Mol7** (in pink) and **1uom** binding site.

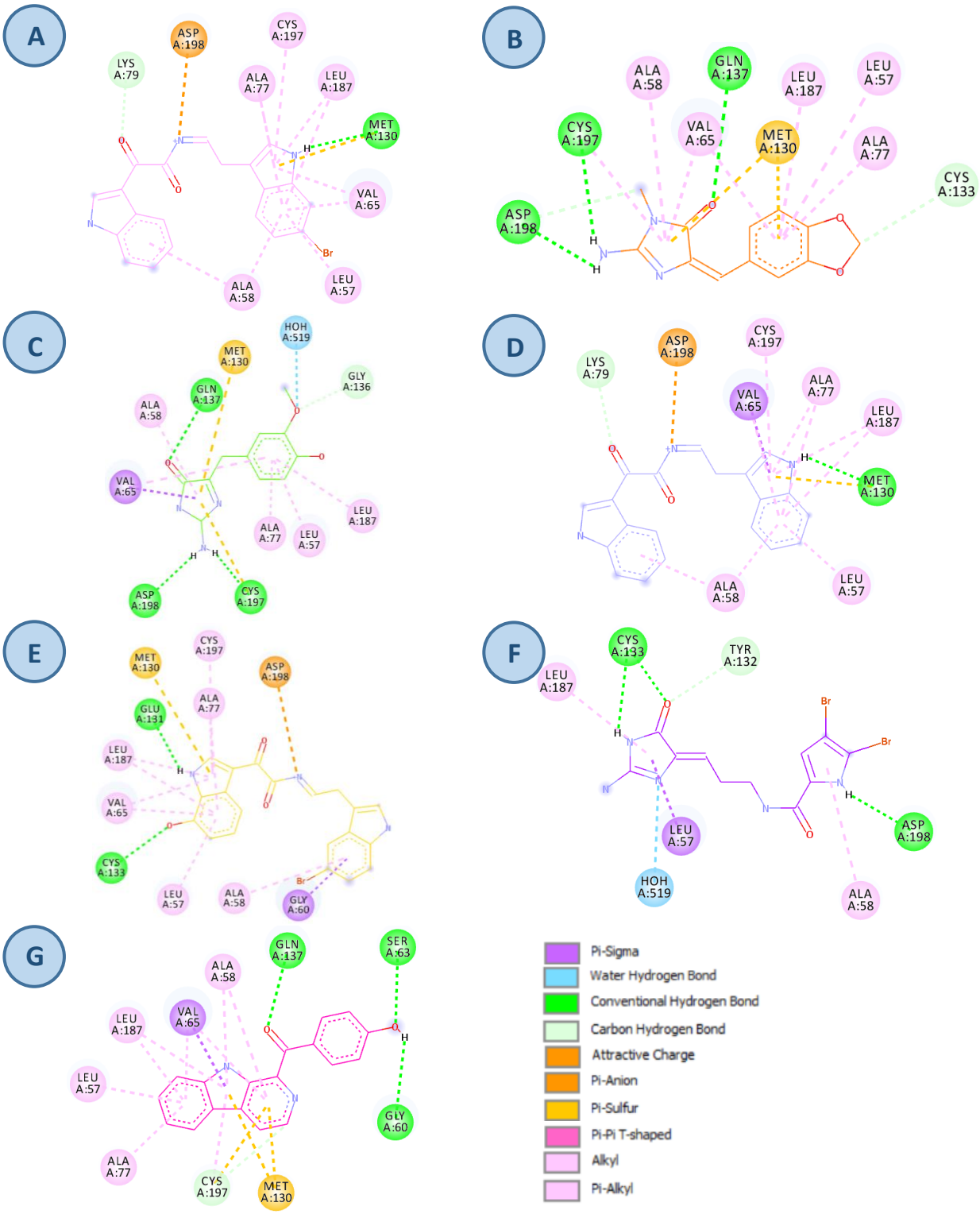

Appendix 05: 2D diagram represents the interactions between the residues near the active site of the BMP-2-inducible protein kinase **(PDB ID: 5i3r)** and our seven ligands (marin alkaloids). A: 2D interaction between **Mol1** (in light purple) and **5i3r** binding site; B: 2D interaction between **Mol2** (in orange) and the **5i3r** binding site; C: 2D interaction between **Mol3** (in green) and **5i3r** binding site; D: 2D interaction between **Mol4** (in blue) and **5i3r** binding site; E: 2D interaction between **Mol5** (in yellow) and **5i3r** binding site; F: 2D interaction between **Mol6** (in dark purple) and **5i3r** binding site; G: 2D interaction between **Mol7** (in pink) and **5i3r** binding site.

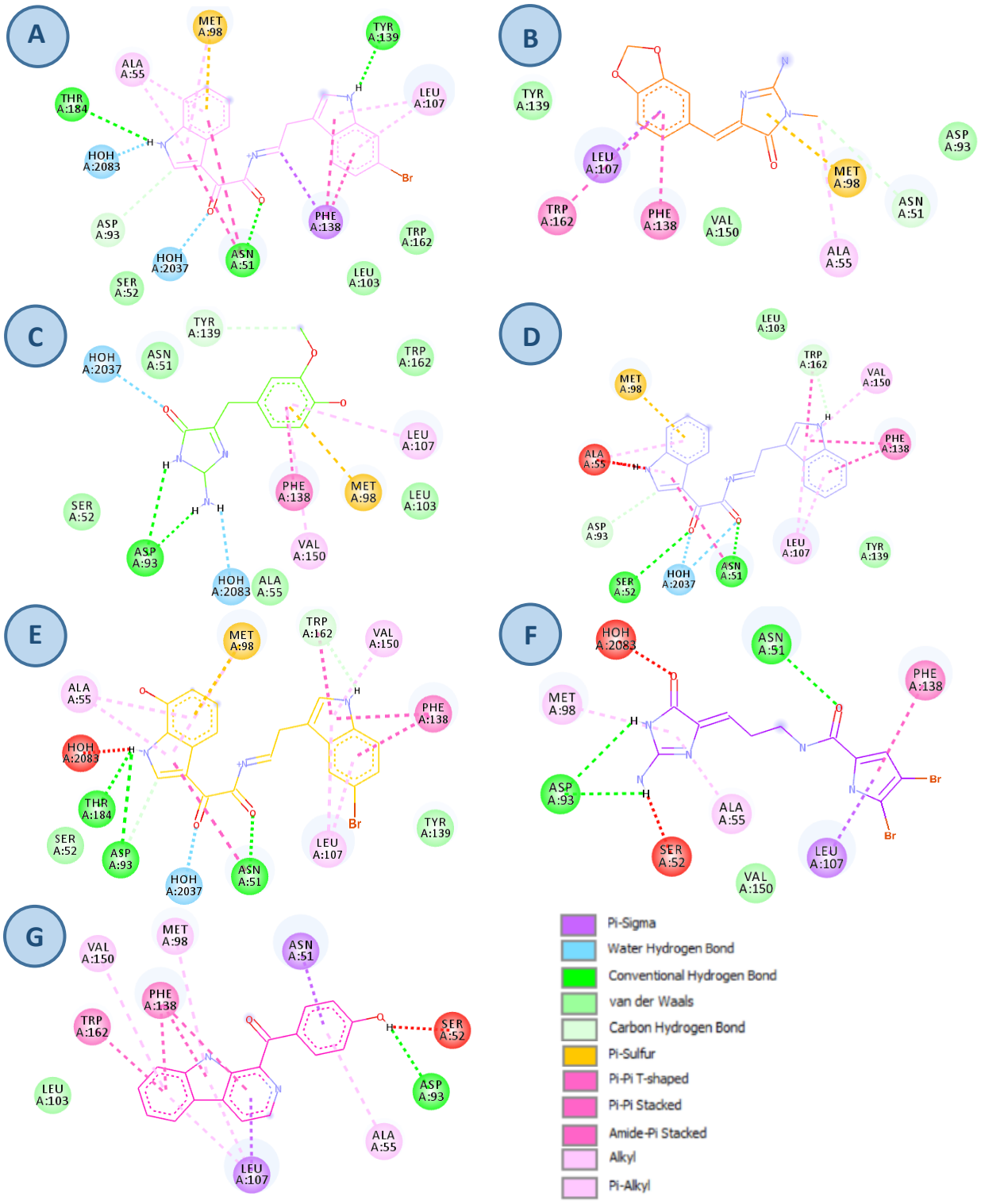

Appendix 06: 2D diagram represents the interactions between the residues near the active site of the Heat Shock Protein 90 **(PDB ID: 4bqg)** and our seven ligands (marin alkaloids). A: 2D interaction between **Mol1** (in light purple) and **4bqg** binding site; B: 2D interaction between **Mol2** (in orange) and the **4bqg** binding site; C: 2D interaction between **Mol3** (in green) and **4bqg** binding site; D: 2D interaction between **Mol4** (in blue) and **4bqg** binding site; E: 2D interaction between **Mol5** (in yellow) and **4bqg** binding site; F: 2D interaction between **Mol6** (in dark purple) and **4bqg** binding site; G: 2D interaction between **Mol7** (in pink) and **4bqg** binding site.

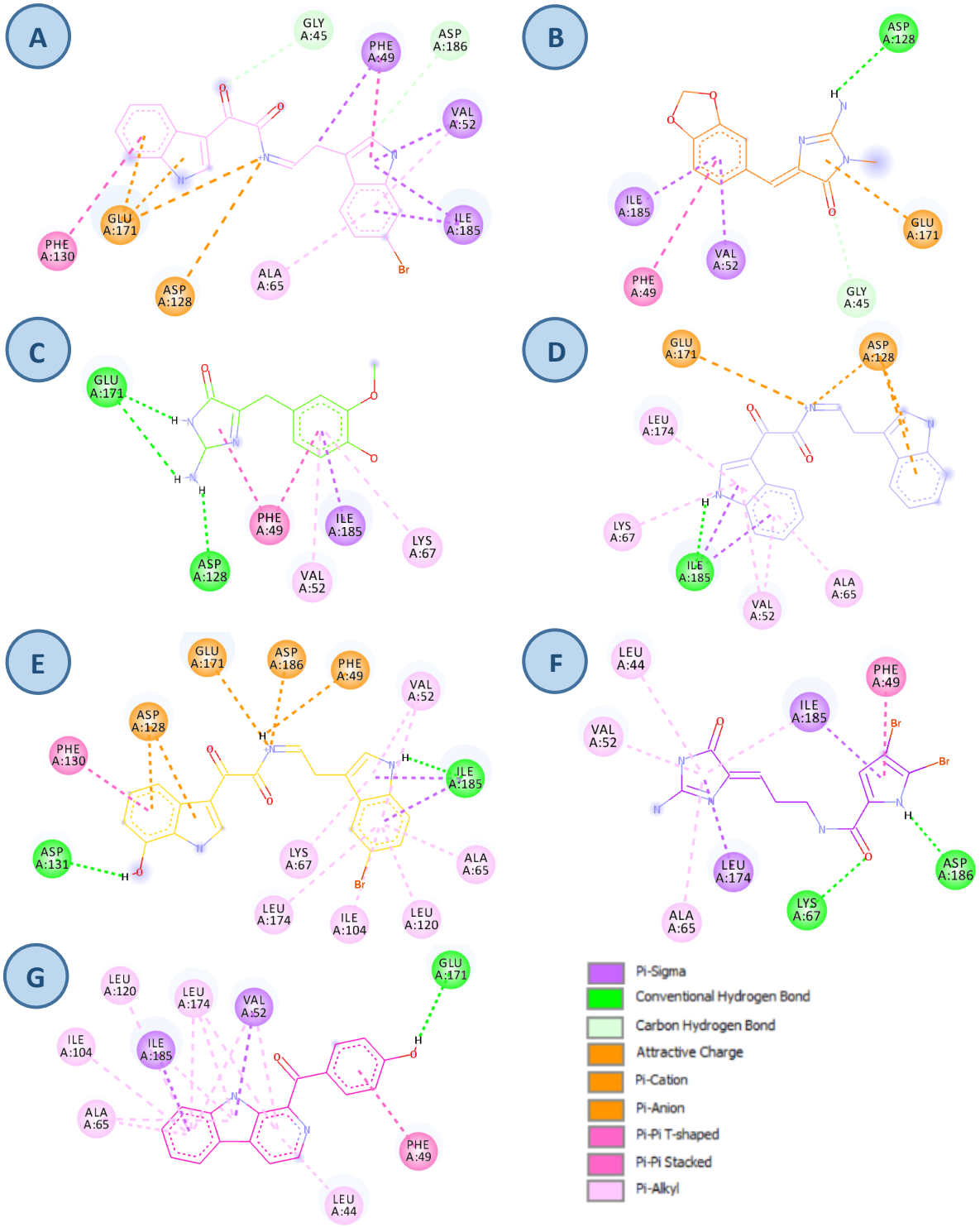

Appendix 07: 2D diagram represents the interactions between the residues near the active site of the Serine/threonine-protein kinase pim-1 **(PDB ID: 4i41)** and our seven ligands (marin alkaloids). A: 2D interaction between **Mol1** (in light purple) and **4i41** binding site; B: 2D interaction between **Mol2** (in orange) and the **4i41** binding site; C: 2D interaction between **Mol3** (in green) and **4i41** binding site; D: 2D interaction between **Mol4** (in blue) and **4i41** binding site; E: 2D interaction between **Mol5** (in yellow) and **4i41** binding site; F: 2D interaction between **Mol6** (in dark purple) and **4i41** binding site; G: 2D interaction between **Mol7** (in pink) and **4i41** binding site.

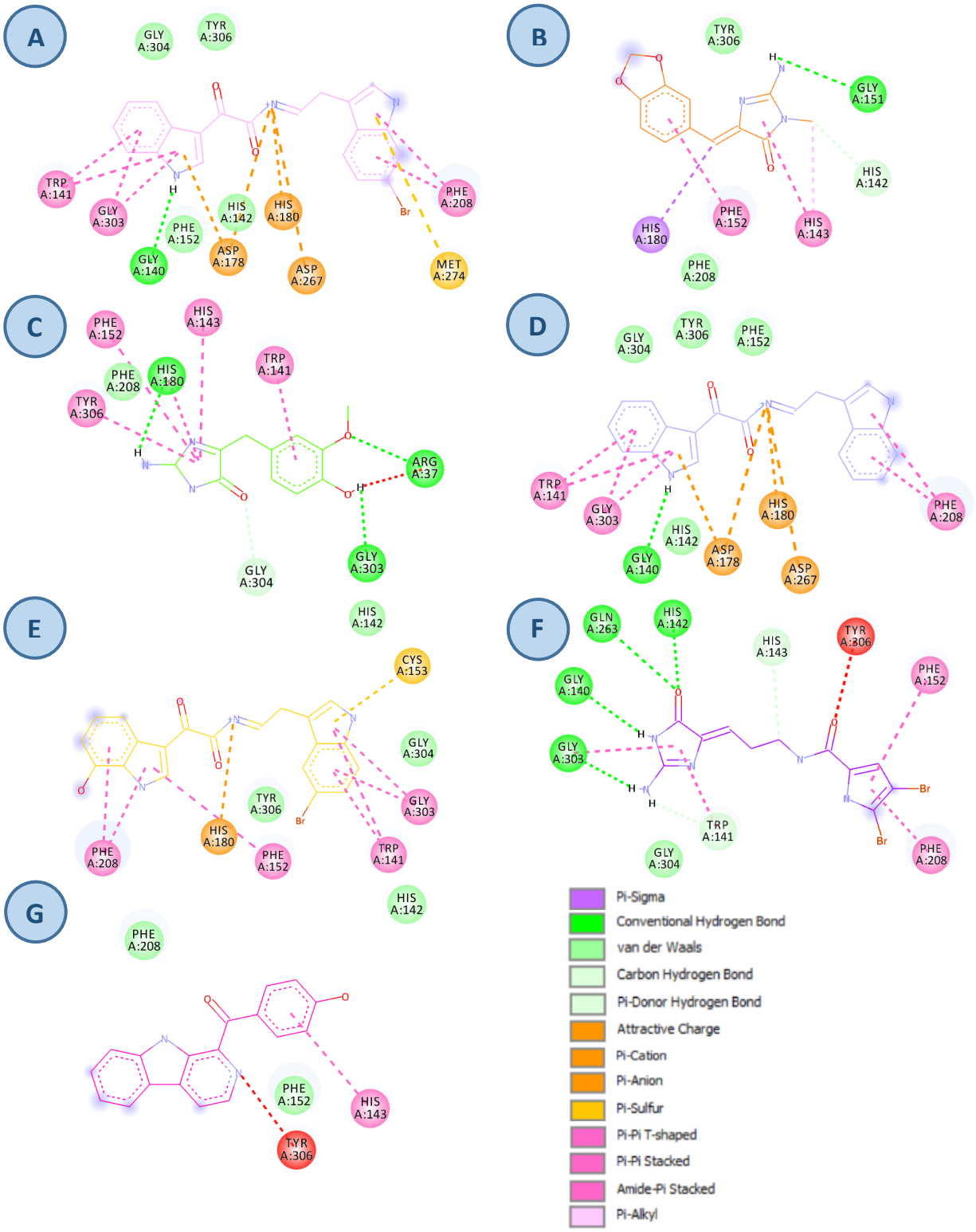

Appendix 08: 2D diagram represents the interactions between the residues near the active site of the Histone deacetylase 8 **(PDB ID: 4QA3)** and our seven ligands (marin alkaloids). A: 2D interaction between **Mol1** (in light purple) and **4QA3** binding site; B: 2D interaction between **Mol2** (in orange) and the **4QA3** site; C: 2D interaction between **Mol3** (in green) and **4QA3** binding site; D: 2D interaction between **Mol4** (in blue) and **4QA3** binding site; E: 2D interaction between **Mol5** (in yellow) and **4QA3** binding site; F: 2D interaction between **Mol6** (in dark purple) and **4QA3** binding site; G: 2D interaction between **Mol7** (in pink) and **4QA3** binding site.